The Role of *Iron Regulated 2* and *Iron Regulated Transporter 1* in Nickel Hyperaccumulation Traits in *Senecio coronatus*

Angus Mackay

MCKANG006

Dissertation presented for the degree of Master of Science in the Department of Molecular and Cellular Biology, at the University of Cape Town

July 2017

Supervisor: Dr. Robert Ingle

Declaration

1. I know that plagiarism is wrong. Plagiarism is to use another's work and pretend that it is one's own.

2. I have used the Harvard convention for citation and referencing. Each contribution to, and quotation in, this report from the work(s) of other people has been attributed, and has been cited and referenced.

3. This report is my own work.

4. I have not allowed, and will not allow, anyone to copy my work with the intention of passing it off as his or her own work.

Signed by candidate

Signature Removed

Signature

Angus Mackay

Date 21/07/2017

Acknowledgements

First and foremost, I would like to thank my supervisor Dr. Robert Ingle. His guidance and knowledge were the basis for all work accomplished. His patience when helping me write my thesis was endless.

I greatly appreciate all of the support I received from my family and particularly the involvement of my mother Angela.

I acknowledge our collaborator, Sylvain Merlot and colleagues at the Institut des Sciences du Végétal, France who assisted in our study. His cooperation and helpfulness was greatly appreciated.

Dr. Lara Donaldson assisted me wherever she could and it is appreciated. She assisted in giving feedback about my thesis.

The assistance of Dr. Keren Cooper was essential for the fluorescence microscopy done in this project, managing and instructing in the use of equipment.

The other students in my lab also assisted me by providing *Arabidopsis* resources. Tia Hendry, Lee Cacket and Grant Mc Gowan are foremost among these.

Other students and laboratories also assisted me during my experimental work. Corrie Gunter and the Ed Rybicki research group shared reagents. The Nicci Illing lab and Janet Hapgood lab were generous in their loaning of equipment.

I would also like to thank my girlfriend, Lauren, for her endless love and support during this process.

List of Abbreviations

Ade	Adenine
ADH	Alcohol Dehydrogenase
BF	Bright Field
bp	Base Pair(s)
°C	degree Celsius
Ca	Calcium
Cd	Cadmium
cDNA	Complementary Deoxyribonucleic Acid
CDS	Coding DNA Sequence
cfu	Colony Forming Units
CM/CSM	Complete Media/Complete Synthetic Media
Co	Cobalt
Col-0	*Arabidopsis thaliana* ecotype Columbia
Cr	Chromium
Cu	Copper
DAS	Dense Alignment Surface
DNA	Deoxyribonucleic Acid
dNTP	Deoxynucleosidetriphosphate
EDTA	Ethylenediaminetetraacetic Acid
eFP	Electronic Fluorescent Pictograph
Fe	Iron
For	Forward
g	Gram(s)
GFP	Green Fluorescent Protein
His	Histidine
int	Internal
K	Potassium
kan	Kanamycin
kb	Kilobase(s)
L	Litre(s)
LB	Luria Bertani
M	Molar
MES	Morpholineethanesulfonic Acid
Mg	Magnesium
MHz	Megahertz
MM	Minimal Media
mRNA	Messenger Ribonucleic Acid
N	Nitrogen
ng	Nanogram(s)
Ni	Nickel
$NiCl_2$	Nickel(II) chloride
nm	Nanometer(s)
OD	Optical Density
ORFs	Open Reading Frames
PBS	Phosphate-Buffered Saline
PCR	Polymerase Chain Reaction
pDR195 GTW	Gateway compatible variant of *pDR195*
PEG	Polyethylene Glycol
pH	Potential of Hydrogen
PMA	Phorbol 12-myristate 13-acetate
qPCR	Quantitative PCR
rev	Reverse

rif	Rifampicin
RNA	Ribonucleic acid
RNA-Seq	RNA sequencing
ROS	Reactive Oxygen Species
rpm	Revolutions per Minute
RT-PCR	Real-Time PCR
s	Second(s)
seq	Sequencing
TAE	Tris, acetic acid and EDTA
TE	Tris and EDTA
TEL	Tris, EDTA and Lithium
T_m	Melting Temperature
Trp	Tryptophan
µ	micro
U	Unit(s)
ura	Uracil
UTR	Untranslated Region
UV	Ultraviolet
V	Volt
v/v	Volume per Volume
w/v	Weight per Volume
YEPD/YPD	Yeast Extract Peptone Dextrose
YFP	Yellow Fluorescent Protein
YNB	Yeast Nutrient Broth
Zn	Zinc

Abstract

Metal hyperaccumulating plants accumulate exceptionally high concentrations of metal ions in their above ground tissues and are defined as containing 1000 µg/g dry mass Co, Cu, Cr, Pb, Zn or Ni. This is remarkable because plants typically only require small amounts of these metals for survival, such as 0.004 µg/g Ni and 15-20 µg/g Zn. Scientific investigation has sought to understand the mechanisms underpinning hyperaccumulation in order to apply them in the phyto-technological processes of phytoremediation (removal of metal pollutants from the environment) and phytomining. However, little is known about the molecular mechanisms underlying Ni hyperaccumulation despite the fact that Ni hyperaccumulators account for almost three quarters of all known hyperaccumulating species. A comparative RNA-Seq experiment carried out on Ni accumulating and non-accumulating populations of the South African Ni hyperaccumulator *Senecio coronatus* (Asteraceae) identified a number of putative transport proteins that are constitutively upregulated in the hyperaccumulator plants. This MSc project focused on two of these, *iron regulated 2* (*ScIREG2*) and *iron regulated transporter 1* (*ScIRT1*), and aimed to validate the RNA-Seq derived nucleotide sequences, test for Ni transport activity and determine their sub-cellular localisation.

Full-length *ScIREG2* and *ScIRT1* protein coding sequences were obtained using RT-PCR and conformed to the predicted sequences derived from the RNA-Seq data. Heterologous expression of *ScIRT1* in yeast consistently conferred an increased Ni resistance phenotype to yeast across a variety of experimental conditions, suggesting that this protein is capable of transporting Ni, and may function as a Ni export protein in yeast. In contrast, the results obtained from heterologous expression of *ScIREG2* were variable and thus inconclusive. An attempt was made to determine the subcellular localization of ScIRT1 using transient expression of an ScIRT1-YFP fusion protein in onion cells. While inconclusive, a YFP signal was detected in these cells, and appeared to localise to the plasma membrane. The work conducted serves as a pilot study to optimize the experimental systems necessary to identify Ni transporters from *S. coronatus*. These experimental systems can now be applied to characterise the remaining transport proteins identified in the RNA-Seq analysis.

Table of Contents

List of Figures

List of Tables

1. Introduction

1.1 Overview

Metal hyperaccumulating plants are capable of taking up and accumulating transition metals (such as Ni, Zn, Cd or Cu) in their above ground tissues at concentrations of 1000 µg/g dry matter, which can be four orders of magnitude greater than the amount observed in non-accumulator relatives (Baker & Brookes, 1989; Baker et al., 2000). This is in contrast with metal hypertolerant plants which do not suppress or enhance metal uptake but are capable of surviving on metal rich soils by excluding metals from the xylem, maintaining a consistently low concentration in their aerial tissues (Baker & Brookes, 1989). Metal hyperaccumulation is also relatively rare, being observed in approximately 500 species across diverse taxa indicating that it has evolved independently numerous times. Research has been conducted into metal hyperaccumulators, with the aim of understanding the molecular mechanisms which underlie this extreme phenotypic trait, and the potential biotechnological applications of hyperaccumulator plants.

1.2 Hyperaccumulation of Heavy Metals

The nutrients necessary for plant survival can be categorized into macronutrients, necessary for energy production, and micronutrients which are required in small amounts at junctions in metabolism (Epstein, 1965; Whitney & Rolfes, 2007; Barker & Pilbeam, 2015). A nutrient is considered essential when the plant or organism is incapable of producing it through its own metabolism and therefore, must be acquired from the external environment (Whitney & Rolfes, 2005). The transition metals sequestered by hyperaccumulator plants are usually essential micronutrients such as Ni, an essential cofactor for the enzyme urease (Seregin & Kozhevnikova, 2006) and Zn, which is an essential component of many enzymes in plants (Tsonev & Lidon, 2012). For plant survival, 0.004 µg Ni and 15-20 µg Zn are required per gram of tissue (Beckett & Davis, 1977). These differences in basal metal concentration and the comparative phytotoxicity of each metal affect the internal metal concentration required for a plant to be described as a metal hyperaccumulator. For example, while the threshold for Zn hyperaccumulation is 1% on a dry biomass basis, for Ni it is 0.1%, and for the non-essential Cd 0.01% (Beckett & Davis, 1977; Krämer, 2010).

Intracellular Ni concentrations are finely regulated by non-accumulator plant species because of the deleterious effects caused by excessive amounts of Ni. It interferes with the acquisition of other essential metals such as Fe and leads to the production of Reactive Oxygen Species (ROS) causing oxidative stress. These reactive and dangerous compounds pose a threat to the cellular machinery and cause damage to membranes, proteins and DNA (Navari-Izzo et al., 1998; Navari-Izzo et al., 1999; Quartacci et al., 2001). To avoid this, the uptake of Ni is tightly controlled by the roots in non-accumulators. The transport of Ni throughout the plant is also limited, resulting in metals being sequestered and stored in the root tissue to protect the vulnerable aerial tissues from high Ni concentrations (Hall, 2002). Considering these toxic effects, it is remarkable that Ni hyperaccumulators are defined as possessing 250-fold increase in internal Ni concentration (>1000 mg $Ni.kg^{-1}$ dry biomass) (Krämer, 2010).

The majority of identified hyperaccumulator species are hyperaccumulators of Ni (73% i.e. 390 out of 533 species) (Krämer, 2010). Ni hyperaccumulating plants are strongly associated with serpentine soils which are derived from ultramafic rock, have a low Ca-Mg ratio, low levels of the essential nutrients N, P and K, and contain particularly high concentrations of Ni, Fe, Cr and Co (Chiarucci & Baker, 2007). The relative prevalence of Ni hyperaccumulator species appears to be as a result global ubiquity of serpentine soils favouring the evolution of this adaptation (Baker & Brookes, 1989).

1.3 The Evolution of Metal Hyperaccumulation in Plants

Various hypotheses have attempted to explain the adaptive advantage and selective pressures that may have led to the evolution of metal hyperaccumulation traits. The theory of elemental defence states that hyperaccumulator plants make use of high concentrations of heavy metals to protect themselves from herbivore and/or pathogen attack (Hörger et al., 2013). Some feeding preference studies have suggested that herbivores show a preference for plant matter with typically low concentrations of Zn and Ni as opposed to equivalent tissue from hyperaccumulator plants (Hörger et al., 2013). However, Noret et al. (2007) demonstrated in a large scale field experiment that the defence of the hyperaccumulator, *Noccaea caerulescens* against herbivorous attack was attributable to the secondary metabolite glucosinolate and not accumulated Zn. Boyd & Martens (1998) also discovered evidence which suggests that the metal concentrations accumulated by hyperaccumulators for various metals is excessive for the defence benefit achieved.

Another hypothesis attempting to explain the origin of metal hyperaccumulation traits is elemental allelopathy, which suggests that hyperaccumulators interfere with the germination of competitor species using metals (Rascio & Navari-Izzo, 2011). The theory claims that heavy metal hyperaccumulators generate a 'toxic zone' in their vicinity containing high concentrations of biologically available heavy metals which deters competitors and favours the metal hyperaccumulator and its descendants. Zhang et al. (2007) demonstrated experimentally that while the addition of Ni hyperaccumulator *Alyssum murale* tissue does elevate the concentration of Ni present in topsoil, this Ni was quickly bound to iron and manganese oxides present, making it biologically unavailable. This increase in Ni concentration was shown not to affect the germination of herbaceous species, thus providing evidence against the notion of a toxic zone and the elemental defence hypothesis.

1.4 Motivation for Studying Hyperaccumulation

The study of metal hyperaccumulating plants proposes an elegant solution to the problems associated with conventional mining practices through the development of phytoextraction technologies. Phytoremediation is a phytoextraction process that has been proposed as a means for removing heavy metal pollution from the environment using metal hyperaccumulating plants (Padmavathiamma & Li, 2007; Zhao & McGrath, 2009). There is also interest in phytomining, which involves applying metal hyperaccumulating plants to mine precious metals for commercial purposes by generating metal hyperaccumulator biomass and burning it to produce bio-ore (Anderson et al., 1999; Brooks et al., 1998). These proposals are appealing because they would enable the commercial use of land that has metal concentrations too low to mine in the conventional manner. However, the application of these technologies relies on further tests of hyperaccumulator plants in field conditions to better understand the site-specific conditions necessary to effectively utilize these processes (Padmavathiamma & Li, 2007). In particular, the rhizosphere and microbial conditions necessary for optimal metal hyperaccumulator growth need to be characterised so agricultural techniques can be developed to specifically accommodate for metal hyperaccumulator plants and to improve the generated biomass and volume of accumulated metals (Rascio & Navari-Izzo, 2011). It has also been proposed that bio-fortification strategies can be used to improve the nutritional quality of food crops and this may be informed through the study of metal hyperaccumulating plants (Ellis & Salt, 2003; Zhao et al., 2009). This is possible because hyperaccumulator plants may serve as a case study for the better understanding of metal homeostasis in plants. Progress can be made to applying metal hyperaccumulator plants to these technological processes by better understanding the molecular mechanisms involved in metal uptake and distribution.

1.5 The Molecular Mechanisms of Hyperaccumulation

The scientific investigation of the molecular mechanism of heavy metal hyperaccumulating plants has historically focused on two members of the *Brassicaceae* family, the Zn/Cd hyperaccumulators *Noccaea (*formerly *Thlaspi) caerulescens* and *Arabidopsis halleri*. The investigation of these plants has been facilitated by their relatively close evolutionary relationship with the model plant, *Arabidopsis thaliana* which has enabled the use of molecular and genomic tools available for this species. The study of these organisms has resulted in the formulation of a model explaining the molecular and genetic basis for Zn/Cd hyperaccumulation traits. Microarray analyses of *A. halleri* and *N. caerulescens* using *A. thaliana* specific gene chips has indicated that these organisms express genes encoding metal transport and metal binding proteins at constitutively higher levels than those exhibited by the non-accumulator *A. thaliana* (Becher et al., 2004; Weber et al., 2004; van der Mortel & Aarts, 2006)**.** This observation suggests that metal hyperaccumulation traits might arise from mutations that alter the regulation of genes involved in metal homeostasis (Verbruggen et al., 2009). This is opposed to the notion that the evolution of novel genes is required to confer metal hyperaccumulation traits. Since the alternative regulation of existing genes can occur as a result of simple changes by mutation relative to the evolution of entirely novel genes this may explain the independent evolution of metal hyperaccumulation traits across diverse taxa (Hanikenne et al., 2008).

A well characterised Zn/Cd transporter from *A. halleri*, *HMA4* is a typical example of such a metal transport protein implicated in Zn/Cd hyperaccumulation. HMA4 is expressed in the vascular tissue of the roots, stems and leaves, localising to the plasma membranes. Its occurrence and activity has implicated it in xylem loading of Zn/Cd in the roots (Courbot et al., 2007; Mills et al., 2005). The non-accumulator *A. thaliana* possesses a single copy of *HMA4* which encodes a transport protein functionally equivalent to that of the homolog in *A. halleri* (Hussain et al., 2004). Talke et al. (2006) identified one of the key factors in the Zn/Cd hyperaccumulation traits in *A. halleri* to be the relative transcript abundance of *AhHMA4* compared to that of *AtHMA4* (between 6 and 53-fold higher), using microarray analysis. The increase in *HMA4* mRNA levels in *A. halleri* versus *A. thaliana* has been attributed to a combination of mutations in the genome, which have caused enhancements in the activity of the promoter of *AhHMA4*, and gene duplication events which resulted in three functionally equivalent copies being present in tandem in the *A. halleri* genome (Hanikenne et al., 2008).

Further investigations into the hyperaccumulation traits in *A. halleri* reveal that the roots also have increased metal uptake as a result of a metal "starvation" state setup by *HMA4* and other transport proteins causing efficient translocation of Zn/Cd from the roots to the aerial tissues (Hanikenne et al., 2008)**.** This starvation state in the roots causes upregulation of the genes responsible for Zn/Cd uptake which are *ZNT1* and *ZNT2* in *N. caerulescens* (Assunção et al., 2001) and *ZIP6* and *ZIP9* in *A. halleri* (Assunção et al., 2010). Therefore, the activity of HMA4 causes larger quantities of metal to be taken up despite of its molecular function being xylem loading. The heterologous expression of *AhHMA4* in *A. thaliana* has been demonstrated to not be sufficient to cause the complete Zn/Cd hyperaccumulation phenotype alone (Hanikenne et al., 2008). Therefore, other factors likely enabling the vacuolar sequestration of metals, are involved in causing the Zn/Cd hyperaccumulation phenotype in *A. halleri* (Talke et al., 2006)**.**

The capacity to sequester metals in *N. caerulescens* and *A. halleri* has also been attributed to the activity of the secondary metabolite nicotianamine (Talke et al., 2006; Weber et al., 2004). This metal chelator has been demonstrated to occur in abundance in these hyperaccumulators compared to the non-accumulator, *A. thaliana* (Vacchina et al., 2003). The sequestration of Zn/Cd in above-ground tissues is therefore achieved by localizing it to

heavy metal complexes, chaperoned by ligands like nicotianamine, in cell walls and vacuoles which are metabolically inactive. This protects the vulnerable cellular machinery from the effects of metal toxicity**.**

While understanding the molecular basis of Zn/Cd hyperaccumulation is informative, its application is limited because Zn/Cd hyperaccumulators represent less than 4% of total hyperaccumulator species and the genes identified encode transporters which are specific to Zn and Cd. Therefore, the molecular mechanisms underpinning the metal hyperaccumulation traits in the majority of hyperaccumulator species have yet to be discovered. The development of phytoextraction technologies would therefore benefit greatly from the study of Ni hyperaccumulators, which represent a 73% majority of hyperaccumulator species.

1.6 The Investigation of Ni Hyperaccumulation in Plants

In contrast, the molecular basis for Ni hyperaccumulation in plants is not yet well characterised. However, it is considered likely that the system would be similar to that employed by Zn/Cd hyperaccumulators involving the constitutive overexpression of existing metal transport proteins rather than the evolution of novel hyperaccumulation specific genes. The sequestration of Ni in the aerial tissues of hyperaccumulators has been linked to increased levels of Ni-binding ligands including citrate, malate, and in particular nicotianamine and histidine (Krämer et al., 1996; Vacchina et al., 2003). An enhanced Ni tolerance phenotype was conferred to transgenic *A. thaliana* by creating a 15-fold increase in shoot free histidine levels. This was achieved by expressing the rate limiting enzyme in histidine biosynthesis, ATP-phosphoribosyl transferase, from the Ni hyperaccumulator *Alyssum lesbiacum* (Ingle et al., 2005). However, the molecular players involved in Ni transport in hyperaccumulators have yet to be identified or understood.

An appropriate experimental procedure is needed to identify Ni transport proteins efficiently and definitively in Ni hyperaccumulators. Various studies of metal transport proteins in the past have employed the technique of heterologous expression in yeast as an effective method of identifying proteins capable of transporting specific metals by assaying the sensitivity of the transgenic yeast to the metal of interest (Korshunova, et al., 1999; Mills et al., 2005; Pence et al., 2000). Yeast are eukaryotic and therefore serve as a better cellular model for the activity of proteins from plants relative to bacteria. They are also convenient to transform and culture. Characterization of metal transport proteins in the literature also typically includes evidence of the subcellular localisation of the protein in addition to its capabilities as a metal transporter because the localisation in the cell often informs on the transporter's function.

Few Ni transport proteins have been characterised from plants, but studies using *A. thalian*a and yeast expression systems have resulted in the discovery of several proteins capable of transporting this metal ion. Schaaf et al. (2006) conducted experimental investigations into *AtIREG2* and demonstrated that its expression in both wild type and *cot1* Ni sensitive yeast conferred increased resistance to the effects of Ni toxicity. Furthermore, *A. thaliana* plants overexpressing *AtIREG2* were also shown to have increased tolerance to Ni. Fluorescence microscopy demonstrated that AtIREG2 localized to the tonoplast in root cells suggesting its role in sequestration of Ni into the vacuole. *AtIREG1* displays high sequence identity to *AtIREG2* and Morrissey et al. (2009) observed that the *A. thaliana ireg1 ireg2* double mutant exhibited increased sensitivity to Ni. However, the contribution of *IREG1* to Ni resistance appears to be minor as no phenotype was observed in the single *ireg1* mutant, in contrast to the *ireg2* mutant which displays marked reduction in resistance to exogenous Ni (Morrissey et al., 2009).

IRT1, the major route of Fe^{2+} uptake in *A. thaliana* roots (Vert et al., 2002), has also been implicated in Ni transport. Transgenic yeast expressing *AtIRT1* were found to have enhanced Ni uptake by Nishida et al. (2011). The authors acquired *A. thaliana irt1* T-DNA insertion mutants and exposed these plants and a Col-0 control to 25 µM $NiCl_2$ in hydroponic solution and induced the expression of *IRT1* by limiting available Fe. Atomic absorption spectrophotometry of root tissue then determined that the *irt1* mutant line did not accumulate Ni in the presence or absence of Fe while the Col-0 control experienced a 3.1-fold increase in Ni concentrations under Fe deficiency. Dimethylglyoxime staining of Ni and radiolabelling of Ni directly confirmed that the root tissue of the *irt1* mutant plants accumulate lower Ni concentrations than the *AtIRT1* expressing control. These observations directly implicated *AtIRT1* in Ni uptake in *A. thaliana*.

Research has been conducted into Ni hyperaccumulators from the *Noccaea* genus of the *Brassicaceae* in an attempt to identify genes encoding Ni transport proteins which may be more informative of the genes responsible for Ni hyperaccumulation traits in hyperaccumulators as opposed to the Ni transporters from the non-accumulator, *A. thaliana*. The study of *Noccaea japonicum* and *N. caerulescens* has resulted in the discovery of *NjZNT1*, *NjZNT2* and *NcNRAMP3* as putative Ni transporters. Mizuno et al. (2005) found enhanced resistance to Ni in yeast expressing the *ZIP* homologs, *NjZNT1* and *NjZNT2*. Experiments conducted by the group in 2007 found the observed enhanced resistance to Ni to be attributable to either the genes encoding proteins functional in Ni efflux or the proteins being functional in influx of other metals causing competitive inhibition of Ni uptake. Wei et al. (2009) demonstrated yeast expressing *TcNRAMP3* had enhanced Ni resistance and reduced intracellular concentrations of Ni suggesting it encodes a protein functional in the exclusion of Ni. However, when they overexpressed *TcNRAMP3* in *Nicotiana tabacum*, Ni resistance was not improved.

Merlot et al. (2014) made use of advances in next generation sequencing technology to identify highly upregulated genes in the New Caledonian Ni hyperaccumulator species *Psychotria gabriellae*. The authors performed a *de novo* transcriptome assembly in an attempt to identify genes with Ni transport activity. They made use of Blast2GO software to annotate Gene Ontology of generated contigs in an attempt to identify contigs that were annotated as transporters. They further filtered the 1436 identified contigs with transporter activity by identifying homology to characterised transporter gene families from *A. thaliana* such as *IREG*, *NRAMP* and *ZIP*. This methodology identified *PgIREG1*, *PgNRAMP1* and *PgNRAMP2* as candidate genes for encoding Ni transport proteins in *Psychotria gabriellae*. Experimental analysis demonstrated that heterologous expression of *PgIREG1* in yeast confers Ni tolerance. *PgIREG1* found was found to localize to vesicular structures in the cytoplasm and potentially the tonoplast, using fluorescence microscopy of transgenic *A. thaliana*. *PgNRAMP1* and *PgNRAMP2* were also expressed in yeast and found to result in a Ni sensitivity phenotype. However, no evidence of elevated intracellular Ni concentrations was observed in the yeast transformed with *PgNRAMP1* and *PgNRAMP2*. This indicates that these proteins may not be functioning to transport Ni directly and the observed sensitivity was as a result of the indirect activity of these proteins.

Merlot et al. (2014) made use of transcriptomic analysis and bioinformatics on a hyperaccumulator species to identify Ni transport proteins based on Gene Ontology and homology. However, an alternative approach is to perform a comparative transcriptomic study of a hyperaccumulator and a non-accumulator. A study of this nature would enable the detection of genes that are differentially expressed between these plants, including transporters. In order to make use of next generation sequencing technology to perform a comparative transcriptomic study to identify genes involved in Ni hyperaccumulation, the hyperaccumulator and non-accumulator compared should

ideally differ as little as possible. This is to reduce the background of differentially expressed genes which are not involved in the hyperaccumulation phenotype. Comparisons of transcriptomes between species diverged across evolutionary time such as *N. caerulescens* and *A. halleri* to *A. thaliana* will identify many differences in expression merely as a result of speciation in response to selective pressures unrelated to metal hyperaccumulation traits. This was demonstrated by Weber et al. (2004) who compared *A. thaliana* and *A. halleri* and identified that almost 50% of the 8000 features on their microarray had a >2-fold variation in intensity. For these reasons, the use of a single plant species displaying Ni hyperaccumulator and non-accumulator phenotypes is desirable for transcriptomic analysis to specifically identify transporter genes differentially expressed in hyperaccumulators.

Ni hyperaccumulor species are typically endemic to serpentine soils and are obligate hyperaccumulators (Pollard et al., 2014), however some are facultative hyperaccumulators that also occur on non-serpentine soils. For example, *Rinoarea bengalensis* is a Ni hyperaccumulating species which accumulates more than 3000 mg Ni kg^{-1} dry mass on serpentine soil and 1 to 300 mg Ni kg^{1} on soils with less available Ni (Brookes & Wither., 1977). The majority of facultative hyperaccumulators always accumulate Ni when growing on serpentine soils, but this is not the case for all. The Turkish Ni hyperaccumulator *Alyssum sibiricum*, has been shown to possess populations which do not accumulate Ni when grown on serpentine soil despite clearly being a Ni hyperaccumulator species demonstrating typical hyperaccumulator Ni concentrations when occurring in similar conditions. This observation suggests that metal hyperaccumulation is not a species-wide trait in every instance (Reeves & Adıgüzel, 2004).

1.7 *Senecio coronatus* as a Model for Ni Hyperaccumulation

The endemic Southern African Ni hyperaccumulator *Senecio coronatus* (Asteraceae) also exhibits marked intraspecific variation in hyperaccumulation. The shoot Ni contents of *S. coronatus* have been investigated at four serpentine soil sites at ultramafic outcrops of the Barberton Greenstone Belt in South Africa where the soil contains >1000 mg kg^{-1} dry weight Ni (Morrey et al., 1989). This investigation has demonstrated that this species consists of hyperaccumulating and non-accumulating populations because some populations were observed to accumulate 12000 and 8800 mg Ni kg^{-1} dry weight while others contain only 130 and 120 mg kg^{-1} dry weight Ni (Boyd et al., 2008). The presence of other Ni hyperaccumulator species at the sites cohabiting with the non-accumulator populations (such as *Berkheya coddii* and *Berkheya rehmani*) suggests that the variation in Ni sequestration in the subpopulations of *S. coronatus* is as a result of genetic factors and not environmental factors.

An attempt was made to test whether the facultative Ni hyperaccumulation traits observed in *S. coronatus* had a genetic basis and were not due to differences in the environment. Meier et al. (2017) performed a survey of *S. coronatus* populations at 12 sites within its range. They found that at no site were both hyperaccumulating and non-accumulating plants present, and that there was no correlation between soil Ni concentration (or pH) and the shoot Ni content. These observations suggest that the intraspecific variation of *S. coronatus* Ni hyperaccumulation traits has a genetic basis and is not caused by environmental factors. Confirmation of this was achieved by conducting a soil swap experiment, by growing individuals from hyperaccumulating subpopulations in the soil of plants from a non-accumulating subpopulation and *vice versa*. After growth in these conditions the dry weight of Ni was determined using ICP-MS and it was found that the swapping of soil did not affect the Ni accumulation phenotype of the subpopulations (Meier et al., 2017).

1.8 Transcriptomic Analysis of *Senecio coronatus* and Identification of *IREG2* and *IRT1*

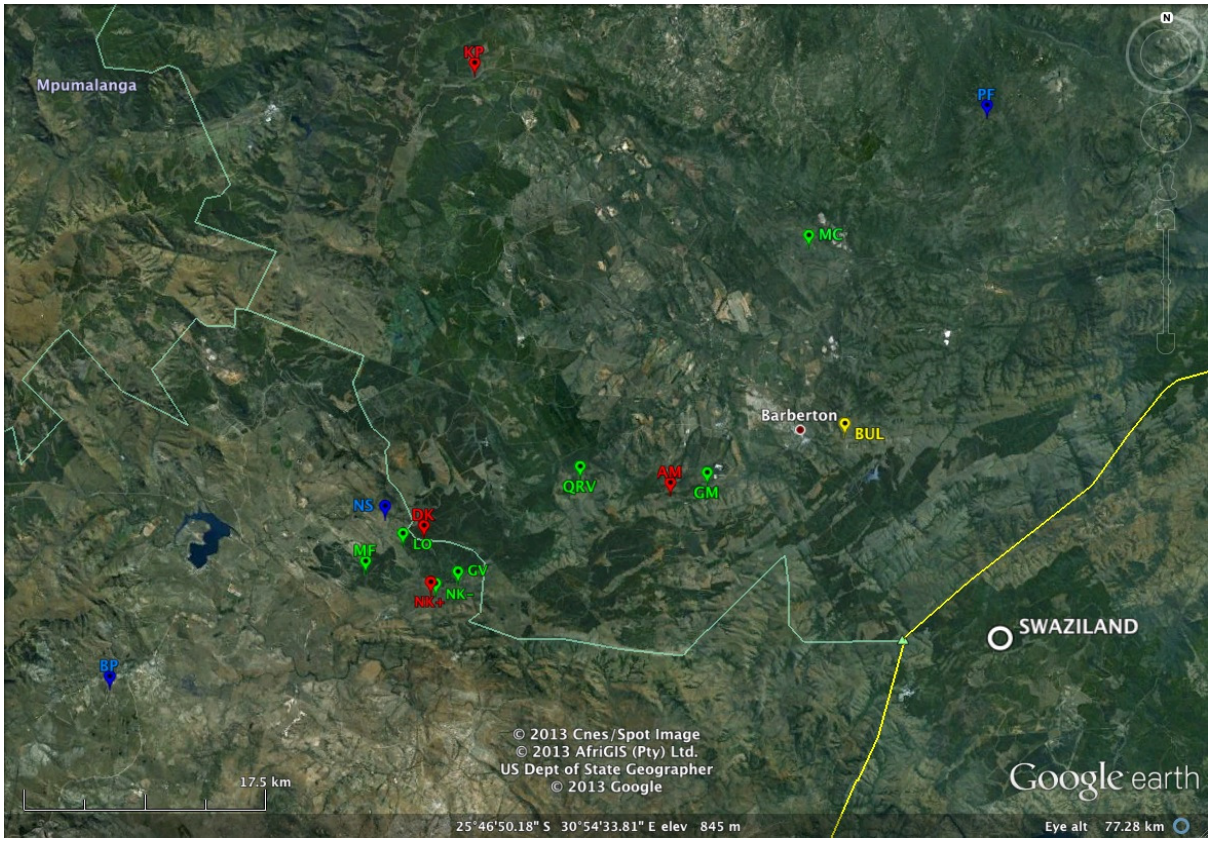

Figure 1**| Distribution of *Senecio coronatus* sample collection sites in the Barberton Greenstone Belt region in South Africa.** Global location of collection sites is indicated by proximity to the country Swaziland from Google Earth Images. Three different *S. coronatus* ecotypes were collected on 15 different sites (only 14 sites are shown due to scaling, the Komati site is located approximately 160 km West of Badplaas). *S. coronatus* was sampled to include phenotypes showing Ni hyperaccumulating (red), Ni hypertolerant non-accumulating (green) and Ni non-accumulating (blue) occurrence on normal soil.

A comparative RNA-Seq analysis was conducted by Meier et al. (2017). *S. coronatus* Ni hyperaccumulating and non-accumulating subpopulations growing on serpentine soil were collected from 15 different locations within its range (shown in Figure 1). RNA-Seq was used to compare the transcriptomes of two representative hyperaccumulators to two non-accumulators. Statistically significantly upregulated genes in the roots and in the shoots of the hyperaccumulators were identified. Functional enrichment analysis of GO terms associated with the identified upregulated genes showed enrichment for Fe transport and Ni transport. This suggests that *A. thaliana* transport proteins have functional, upregulated homologs in *S. coronatus*. It was theorized by Meier et al. (2017), that Ni hyperaccumulation may have evolved in this lineage through mutation of the Fe uptake network, resulting in an overexpression and abundance of key transport proteins that were then able to uptake Ni from the soil.

The RNA-Seq data was used to identify candidate genes that may encode Ni transport proteins. In total, 394 root and 399 shoot genes were identified as upregulated in hyperaccumulating subpopulations. Twenty-two candidate transporters were identified by selecting those upregulated transcripts that were annotated as homologs of known transport proteins by BLASTX analysis. These 22 identified candidate genes were selected for further experimental

analysis to determine their function in Ni hyperaccumulation traits in *S. coronatus*. Two of the most promising Ni transporter candidates identified in this way from the RNA-Seq data were, *ScIREG2* and *ScIRT1*. Both genes have well characterised *A. thaliana* homologs which have been experimentally proven to be instrumental in Ni homeostasis (Nishida et al., 2011; Schaaf et al., 2006). It is hypothesized that the *S. coronatus* homologs of these genes encode proteins that are functional in Ni transport and their overexpression in hyperaccumulators contributes to the hyperaccumulation phenotype.

1.9 Project Aims and Objectives

The identification of *ScIREG2* and *ScIRT1* as candidate Ni transport proteins for *S. coronatus* formed the basis for this Masters project. This project aimed to clone and amplify *ScIREG2* and *ScIRT1* to experimentally validate the predicted nucleotide sequences derived from the RNA-Seq data for these two genes. Once the sequences were validated, the project aimed to determine if the proteins encoded by these genes of interest could catalyse the transport of Ni *in vivo* using a yeast expression system. Finally, an attempt was made to determine the subcellular localisation of these two proteins by generation of C-terminal YFP fusion proteins.

2. Materials and Methods

2.1 *Senecio coronatus* Plants

Senecio coronatus plants of both sub-populations were taken from the Barberton Greenstone Belt region in Mpumalanga South Africa by Robert Ingle (University of Cape Town). The plants were potted and transported to the University of Cape Town where they were kept and maintained in the University of Cape Town Botany greenhouse under ambient light for the duration of the project.

2.2 Bioinformatic Analysis of *IREG2* and *IRT1* Sequences

Gene sequences for *S. coronatus IREG* and *IRT1* were acquired during the *de novo* transcriptome assembly previously carried out for *S. coronatus* (Meier et al. 2017). Putative transmembrane domains were then predicted by inputting the full-length amino acid sequence of each gene into the 'Dense Alignment Surface' Transmembrane Prediction Server (http://www.sbc.su.se/~miklos/DAS/).

Phylogenetic analysis was performed for the genes of interest to provide evidence for correct annotation by acquiring complete amino acid sequences for genes showing the top BLASTp hits from the Viridiplantae database in the National Centre for Biological Information database (https://www.ncbi.nlm.nih.gov/). The complete amino acid sequences were then put into Mega7 software in FASTA format and relevant sequences were then aligned using ClustalW multiple sequence alignment. The multiple sequence alignment was then used to generate a phylogenetic tree to compare relatedness of the sequences using a Neighbour Joining Tree. The tree was generated with a bootstrap value of 1000 to give an indication of the probability of phylogenetic relationship and the resulting tree was rooted to the more distantly related version of the gene.

The accuracy of bioinformatic subcellular localisation predictor tools was assessed by accessing the precompiled results for many of these tools for the *A. thaliana* homologous genes from The Subcellular Proteomic Database (SUBA4). The generated results were then compared to the experimentally determined subcellular localisation to calculate the frequency that the correct localisation is predicted.

2.3 Genomic DNA Isolation

Genomic DNA was isolated using a modified version of the Dellaporta method (Dellaporta et al., 1983). Zero-point-five g of leaf tissue was flash frozen in liquid nitrogen and ground to a fine powder using a chilled mortar and pestle. 1.4 mL of extraction buffer (Dellaporta et al., 1983) was added to the powder and the mixture was incubated at 65°C for 10 minutes. 500 µL of 5 M Potassium Acetate was added and the mixture was shaken. The extraction was kept at 4°C for 20 minutes then centrifuged for 20 minutes at 25,000 RCF. The supernatant of the extraction was then transferred to a fresh microfuge tube and 1 mL isopropanol was added. It was then incubated at -20°C for 30 minutes and the DNA was pelleted by centrifuging at 20,000 RCF for 15 minutes. The supernatant was gently poured off to preserve the pellet and it was air dried for 15 minutes. The pellet was resuspended in 70 µL 50 mM Tris-HCl, 1 mM EDTA pH8. The leftover debris was then removed by centrifuging at 25,000 RCF for 5 minutes. The supernatant was transferred to a fresh 1.5 mL microfuge tube and 7.5 µL of 3 M NaAc pH 5.2 and 50 µL isopropanol was added. It was mixed and chilled on ice for 15 minutes then centrifuged at 20,000 RCF for 10 minutes then washed with 500 µL

of 80% (v/v) ethanol and thoroughly air dried. The pellet was then resuspended in 10 µL TE buffer (50 mM Tris-HCl, 1 mM EDTA pH 8) and stored at -20°C.

An aliquot of *A. thaliana* Columbia genomic DNA was received from Tia Henry (University of Cape Town).

2.4 *Arabidopsis thaliana* Plant Culture

A. thaliana (Col-0 ecotype) seeds were provided by Lara Donaldson and Lee Cacket (University of Cape Town). Sterile seeds were grown in petri dishes on Plant Nutrient media (5 mM KNO_3, 2 mM $MgSO_4.7H_2O$, 2 mM $Ca(NO_3)_2.4H_2O$, 0.05 mM FeNaEDTA, 1x micronutrients, 2.5 mM KPO_4 buffer, pH 5.5) (Haughn and Somerville, 1987) with 0.6% (w/v) agar. Fifty seeds were sown on each petri dish. Plates were then placed in a growth room (100 mM photons.m-2.s-1; 16 hr light/8 hr dark; 22°C; 50-60% relative humidity) for two weeks. Plants grown on PN media for two weeks were transferred to Plant Nutrient media without FeNaEDTA and grown for a further two weeks prior to harvesting of tissue in order to induce *AtIREG2* expression.

2.5 RNA Extraction

The Chomczynski & Mackey (1995) RNA extraction protocol was used. Plant tissue was harvested and immediately flash frozen in liquid nitrogen. One mL TRIzol Reagent (100 mM NaAc pH 5.2, 800 mM guanidine thiocyanate, 400 mM ammonium thiocyanate, 5% glycerol (v/v) and 38% phenol (v/v) pH 4) was added per 100 mg plant tissue. The mixture was then homogenized by subjecting it to 5 minutes of intense shaking in a paint shaker using three small ball bearings. The homogenized tissue was incubated at room temperature for 5 minutes and 200 µL chloroform was added and samples were inverted to mix them. The samples were then kept at room temperature for 3 minutes and centrifuged at 20,000 RCF for 15 minutes at 4°C. The aqueous phase was then pipetted out carefully into a fresh microfuge tube. RNA was then isolated from the aqueous phase by adding 500 µL isopropanol and centrifuging at 20,000 RCF for 10 minutes at 4°C. The RNA pellet was then washed by resuspending it in 1 mL 75% (v/v) ethanol and centrifuging it at 20,000 RCF for 5 minutes at 4°C. The supernatant was then carefully removed and the pellet was air dried 5-10 minutes. The pellet was then resuspended in 87.5 µL RNAse free water and was incubated at 60°C for 10 minutes. The RNA was stored at -80°C.

2.5.1 DNase Treatment of RNA Samples

Ten µL RDD buffer and 2.5 µL DNase I (Qiagen) were added to the 1.5 mL microfuge tube containing the 87.5 µL RNA solution and incubated at 25°C 10 minutes. The RNA was then purified using a Qiagen RNeasy Mini Kit as per the manufacturer's guidelines.

2.5.2 cDNA Synthesis

Up to 5 µg total RNA, 250 ng hexamer primers, 1 µL dNTP mix and distilled H_2O were added to a final volume of 13 µL. The reaction was heated to 65°C for 5 minutes and returned to 4°C for 1 minute. The liquid was briefly spun down by pulse centrifugation and 1 µL SuperScript III Reverse transcriptase (Invitrogen) was added with 1 µL 0.1M DTT and 4 µL 5x Invitrogen First-Strand Buffer. The solution was then mixed by gentle pipetting it and subjecting it to a thermocycle of 25°C for 5 minutes, 50°C for 60 minutes and 70°C for 15 minutes (heat inactivation).

2.6 Polymerase Chain Reaction

DNA and cDNA was amplified using the polymerase chain reaction (PCR) using Supertherm DNA polymerase (Separations). Small amounts of starting template DNA (<500 ng) were introduced to a 20 µL reaction mixture (1.5 mM $MgCl_2$, 1x Supertherm PCR Buffer, 0.4 µM of forward and reverse primer (Table 1), 0.2 mM dNTPs, 0.5 U Supertherm DNA *Taq* polymerase) and subjected to thermocycling with an initial 5 minute denaturation step of 94°C followed by 35 cycles of 15 seconds of 94°C, 30 seconds of the appropriate primer annealing temperature, and 2 minutes of 72°C after which a final 7 minute elongation step takes place. The thermocycling was conducted in a Gene Amp PCR System 2700 (Applied Biosystems). This method is used primarily for characterization purposes.

For cloning purposes, where low error rates are required high fidelity PCR was performed using Q5 or Thermo Scientific high-fidelity DNA polymerase. The manufacturer's suggested cycling parameters were used with the primer pairs annealing temperature (T_A).

2.6.1 Table 1 | Primers used for DNA amplification throughout project.

Oligonucleotides synthesized and used in pairs for cloning or for sequencing purposes.

Gene Amplification		
Name	Sequence	T_A
***IRT1* FOR**	ACGGATCCATGGCTTCAAGTTCAAAAAATGTCA	55^{O}C
***IRT1* ECO rev**	ACGAATTCTTAAGCCCATTTTGCCATC	55^{O}C
***IRT1* YFP rev2**	ACGAATTCGCAGCCCATTTTGCCATCAG	55^{O}C
***IREG* FOR SALI**	ACTGTCGACATGGAGGAGGGGTATTATTATGCA	50^{O}C
***IREG* FOR NOTI**	ATGCGGCCGCTCAAAGAAACAGGGCAAGCA	50^{O}C
***IREG* BAM for**	ACTGGATCCATGGAGGAGGGGTATTATTATGCA	50^{O}C
***IREG* SEQ int**	TAAACTCCAGAATCCGTAGAATCGA	seq[1]
***IREG* YFP rev2**	ATGAATTCGCAAGAAACAGGGCAAGCA	50^{O}C
***pDR195* GTW for**	CATTCAAAAGAAAGAAAAAAAATATA	50^{O}C
***pDR195* GTW rev**	CTTTAAAATTTGTATACACTTATTTTT	50^{O}C
***pDR* AMP for**	ATGAGTATTCAACATTTCCGTGTC	50^{O}C
***pDR* AMP rev**	TTACCAATGCTTAATCAGTGAGGC	50^{O}C
***A.IREG* BAM for**	ACACGGATCCATGGAGGAGGAAACAGAAACTAG	50^{O}C
***A.IREG* ECO rev**	ACGAATTCTCATGAAGCAAAAAAGTTGTTCAATA	50^{O}C
***A.IREG* NOTI rev**	ACACGCGGCCGCTCATGAAGCAAAAAAGTTGTTCAATA	50^{O}C
***A.IREG* INT for**	TAAGCTACTGTCTCCGGTTA	seq
***A.IREG* INT rev**	TGATTCCTCTGCCTATACCA	seq
YFP rev	CGTAGCCGAAGGTGGTCA	seq
M13 for	GTTTTCCCAGTCACGACGTTGTA	seq
M13 rev	AGCGGATAACAATTTCACACAGGA	seq

2.7 DNA Electrophoresis

DNA was analysed using TAE gel electrophoresis. Gels comprised 1% w/v agarose, 0.016 µg/mL Ethidium Bromide dissolved in 1x TAE buffer (10 mM Tris, 1 mM EDTA, 0.11% v/v glacial acetic acid) and were subjected to an 80-volt

[1] Sequencing reaction

electrical current for 45 minutes. On all gels one or two of the lanes included a 1 kb Fermentas O' GeneRuler DNA ladder for sizing of fragments. Gels were then visualized in a Syngene Gbox with a Cybertech 220 V 50 MHz Camera with optics.

2.7.1 Gel Extraction of DNA Bands

Amplified products necessary for further use in cloning or sequencing were extracted from agarose gels by visualizing on a long wave length (365 nm) transilluminator and cut out manually using a sterilized scalpel blade. The gel slice was then immersed in an equivalent volume of column binding solution (Wizard Plus DNA Purification System, Promega Corporation) and the DNA was purified as per the manufacturer's protocol.

2.8 Digestion of DNA using Restriction Enzymes

A volume of 500 µg of plasmid or PCR product was added to a 20 µL solution with appropriate buffers (Fermentas Yellow, Orange, Red) (New England Biolabs Cutsmart) at manufacturer's recommended concentrations and 1 µL (5 - 10 Units) desired restriction enzyme. The reaction was then incubated at 37°C for 3-4 hours and the DNA was purified as stated above or run out on an agarose gel for characterisation purposes. Double restriction enzyme digests were also performed in this way by adding a second restriction enzyme to this solution with care being taken to select the optimum reaction buffer for both restriction enzymes as defined by the manufacturer. The restriction enzyme digestion was then heat inactivated by incubating the reaction at the manufacturer's (Fermentas lnternational, Ontario, Canada) recommended inactivation temperature and duration. Alternatively, the DNA was column purified out of the restriction enzyme reaction using Wizard Plus DNA Purification System, Promega Corporation.

2.9 Ligation of Digested Ends

Double digested vector and insert DNA (ng) was mixed in a 200 µL tube where the amounts of DNA added were determined by the equation:

$$\frac{\text{Amount of vector (ng) X size of insert (Kb)}}{\text{Size of vector (Kb)}} = \text{Amount of insert (ng)}$$

Amount of vector was typically 200 ng and Fermentas T4 DNA ligase buffer was added to a final concentration of 1x and 5 U of T4 DNA Ligase enzyme. The insert: vector molar ratio used in all ligations was 3:1. The reaction volume was made up to 20 µL with H_2O and incubated at 37°C for 4 to 6 hours.

2.10 *Escherichia coli* Culture

Liquid or agar (1.5% w/v) Luria-Bertani media (1% w/v tryptone, 0,5% w/v yeast extract, 0,5% w/v NaCl) was used to grow *E. coli* DH5α and Life Technologies *E. coli* Oneshot cultures. In some cases, corresponding antibiotics were included in the growth medium at appropriate concentrations to select for cells containing plasmids of interest. The cultures were incubated at 37°C for over 12 hours and liquid cultures were also subjected to moderate shaking for the duration of the incubation.

2.11 *E. coli* Competent Cell Preparation

E. coli DH5α frozen glycerol stock was streaked out onto an LB plate with no antibiotic selection using sterile technique and the plate was incubated overnight at 37°C. A single colony was then inoculated into 10 mL LB liquid media and incubated at 37°C overnight with shaking. One L of LB liquid media was then inoculated with the 10 mL starter culture and the OD_{600} was checked every hour until the absorbance was between 0.35 and 0.4 then the culture was chilled to 4°C and kept cold for the remainder of the process. The full volume of the culture was then spun down in a centrifuge at 5,000 RCF for 3 minutes. The growth medium was poured off and the cell pellet was gently resuspended in 20 mL ice cold 50 mM $CaCl_2$. The cells were kept at 4°C for 20 minutes and centrifuged at 5,000 RCF for 3 minutes, the $CaCl_2$ was poured off and the cells were resuspended in 2.5 mL 50 mM $CaCl_2$, 10% (v/v) glycerol. The competent cells were pipetted into 100 µL aliquots, flash frozen in liquid nitrogen and stored at -80°C.

2.12 *E. coli* Transformation

One-hundred µL competent *E. coli* DH5α or Oneshot cells were thawed on ice for 5 minutes and 2 µl of DNA ligation was added. The cells and DNA were mixed and incubated in ice for 20 minutes. The transformation was then heat-shocked at 42°C for 50 seconds and returned to ice for 2 minutes. The transformation was then resuspended in 900 µL LB and incubated for 2 hours at 37°C with moderate shaking. The transformation was then spun at 3,000 RCF for 5 minutes and the media was poured off. The cells were resuspended in 100 µL TE buffer and spread plated onto LB plates with appropriate antibiotic selection. The plates were incubated at 37°C overnight (12 hours) and then stored at 4°C to avoid growth of contaminants.

2.12.1 Glycerol Stock Preparation

For bacteria and yeast 875 µL of liquid culture was added to 125 µL 80% glycerol in a 1.5 mL microfuge tube, thoroughly mixed, flash frozen in liquid nitrogen and stored at -80°C.

2.13 Plasmid Miniprep

Overnight cultures were spun down at 10,000 RCF for 1 minute and pellets resuspended in 600 µL H_2O and an Invitrogen PureLink Quick Plasmid Miniprep Kit was used to extract plasmid DNA as per manufacturer's instructions.

2.14 Colony PCR

DNA amplification by PCR was conducted as a method to identify transformed colonies. An inoculating loop was used to pick a small, barely visible cluster of *E. coli* cells from the transformation plate and used as template in the PCR reaction.

2.15 DNA Sequencing

DNA was sequenced at the Stellebosch Central Analytical Facility on an Applied Biosystems ABL3730 DNA analyser. Results of the sequencing reaction were then analysed on Chromas Pro (Technelysium Pty Limited) and compared to RNA seq data (Meier et al. 2017) using BioEdit (Ibis Biosciences).

2.16 Gateway Cloning

Vectors used:

Entry Vector *pENTR1A*

Gateway entry vector designed to have inserts cloned in using multiple cloning sites and is ready to transfer the inserts to destination expression vectors by Gateway cloning using *attL* sites. A kanamycin selection marker is present for selection in bacteria.

Destination Vectors

- *pDR195 GTW*
  Gateway destination vector designed to constitutively express the insert in yeast. Makes use of *attR* sites to receive insert from entry vector in the correct position. Contains *ccdB* suicide gene to ensure only desired Gateway clones are capable of surviving. Propagation of the empty vector before Gateway cloning was done in Life Technologies *E. coli* Oneshot cells which are unaffected by the *ccdB* suicide gene. Makes use of ampicillin for selection purposes in bacteria and *URA3* (uracil biosynthesis gene) for positive selection in yeast.
- *pEarlyGate101*
  Gateway destination vector designed to fuse the insert to YFP by reading through to an in-frame YFP sequence. Makes use of *attR* sites to receive insert from entry vector in the correct position. Contains *ccdB* suicide gene to ensure only desired Gateway clones are capable of surviving. Propagation of the empty vector before Gateway cloning was done in Life Technologies *E. coli* Oneshot cells which are unaffected by the *ccdB* suicide gene. Makes use of kanamycin for selection purposes.

A volume containing 150 ng entry clone (*pENTR1A* containing gene of interest), 150 ng/µL destination vector (*pDR195 GTW* or *pEarlyGate101*) was added to a 200 µL tube and the volume was made up to 8 µL with TE buffer (10 mM Tris-HCl pH 8, 1 mM EDTA). Life Technologies LR Clonase II enzyme was thawed on ice for 2 minutes and suspension of the enzyme was ensured using vortexing. Two µL of the enzyme was added to the tube and was mixed in thoroughly by briefly vortexing. The reaction was incubated at 25°C for an hour or at 4°C overnight. A 1 µL volume of Proteinase K was added to terminate the reaction by being incubated with the reaction at 37°C for 10 minutes. An amount of 2-5 µL of the Gateway reaction was then used to transform competent *E. coli* cells.

Gateway cloning from *pENTR1A* into *pEarlyGate101* was problematic due to both vectors making use of kanamycin resistance for selection making it impossible to distinguish entry clones from Gateway clones. To solve this problem, *pENTR1A* containing genes of interest for Gateway cloning into *pEarlyGate101*, was restriction enzyme digested before entering the gateway cloning reaction. The enzyme used was *Nhe*I because it only cuts the vector once a sufficient distance away from the *attL* sites and not in the genes of interest. In this case an additional transformation control was included with only digested entry vector used to transform competent cells to give an indication of the background of intact entry clones after digestion in the gateway clone transformation.

2.17 *Saccharomyces cerevisiae* Culture

S. cerevisiae zrt1zrt2 mutant strains were cultured in various solid and liquid media for experimental and bulking purposes. Both strains were received from collaborator Sylvain Merlot (Institut des Sciences du Végétal, France) and were revived using YEPD (yeast extract peptone dextrose) complete media (0.3% w/v yeast extract, 1% w/v peptone,

1% w/v dextrose, 2% w/v agar). The cultures were incubated at 30°C for approximately 48 hours or longer if required and liquid cultures were subjected to moderate intensity shaking for the duration.

2.18 Yeast Competent Cell Preparation

A single colony of *S. cerevisiae zrt1zrt2* strain was inoculated into 100 mL YEPD and incubated at 30°C with shaking until and OD_{600} greater than 0.6 was reached. The culture was then pelleted by centrifugation at 3,000 RCF for 5 minutes, the growth media was removed and the pellet resuspended in 10 mL TEL buffer (0.1 M LiOAc, 10 mM Tris-HCl pH 8, 1 mM EDTA) and shaken for approximately 12 hours at 30°C. The suspension was then centrifuged at 3,000 RCF, the buffer was poured off and the pelleted cells were resuspended in 1 mL TEL buffer and separated into 100 µL aliquots and stored at 4°C. Competent cells were not stored for longer than a month before being used.

2.18.1 Yeast Transformation

Fifty µg Salmon sperm DNA and 1 µg desired plasmid DNA for transformation were added to a competent cell aliquot. The mixture was then incubated at room temperature for 30 minutes and 700 µL 40% PEG - TEL (20% w/v PEG 4000/3350, 0.1 M LiOAc, 10 mM Tris-HCl pH8, 1 mM EDTA) was then added thoroughly mixed into the suspension. The transformation was then incubated for 60 minutes at room temperature then heat shocked for 10 minutes at 42°C and centrifuged at 3,000 RCF for 3 minutes. The PEG - TEL was decanted and the pelleted cells were resuspended in TE buffer (10 mM Tris-HCl pH 8, 1 mM EDTA) and spread plated on appropriate selective plates.

2.19 Selective Culturing of Yeast

Yeast nutrient broth complete supplement media -uracil (YNB CSM-ura) was used to selectively culture strains containing the *pDR195* vector by uracil synthetic drop-out complementation. A 10x YNB CSM -uracil stock was made by filter sterilizing (0.2 µm filter) 5 g dextrose, 6.7 g yeast nitrogen bases without amino acids (Sigma Aldrich, Y0626) and 1.92 g complete supplement media -uracil (Sigma Aldrich, Y1501) dissolved in 100 mL H_2O and storing at 4°C. To make liquid YNB CSM-ura, 90 mL H_2O was autoclaved and 10 mL 10xYNB CSM-ura was added under sterile conditions. To make YNB CSM-ura plates 2 g agar (2% w/v) was added to 90 mL H_2O, then autoclaved and 10 mL 10x YNB CSM-ura was then added before pouring the plates.

Yeast nutrient broth minimal media -uracil (YNB MM-ura) was also used to selectively culture yeast strains containing the *pDR195* vector by uracil synthetic drop-out complementation. This approach was used to limit the concentration of potential Ni-binding ligands e.g. histidine in the media. A 10x YNB MM-uracil stock was made in the same way as 10x YNB CSM-uracil but no complete supplement media (Sigma Aldrich, Y1505) was included. A 100x adenine tryptophan stock was made by filter sterilizing (0.2 µm filter) 90 mg adenine and 380 mg tryptophan in 50 mL H_2O and storing at 4°C. To make liquid YNB MM-ura, 89mL H_2O was autoclaved and 10 mL 10x YNB MM-ura was added under sterile conditions as well as 1 mL 100x adenine tryptophan stock. To make YNB MM-ura plates 2 g agar was added to 89 mL H2O, then autoclaved and 10 mL 10x YNB MM-ura as well as 1 mL 100x adenine tryptophan stock was added before pouring the plates.

Ni enriched synthetic drop-out plates were synthesized for use in a Ni sensitivity assay. Plates were made up in the same way as complete and minimal media but pH was adjusted to 5.0 using 20mM Morpholineethanesulfonic acid

(MES) – KOH. A 20 mL 200 mM $NiCl_2$ was made up and filter sterilized (0.2 µm filter) and the appropriate volume of the stock was added to the agar before pouring to give the desired final concentration of Nickel in the plate. A series of plates with increasing metal concentrations was synthesized in this way for use in a Ni sensitivity assay.

2.20 Yeast Colony PCR- Sodium Hydroxide Method

Single yeast transformant colonies were picked and transferred into 20 µL 40 mM NaOH which was then heated to 95°C for 45 minutes. Two µL of the resultant solution was then used as a template in a PCR for confirmation of presence of genes of interest.

2.21 Ni Sensitivity Assay

2.21.1 Resuspension of Yeast Culture at OD = 1

Uracil deficient selective yeast liquid cultures were made for each strain required for the Ni sensitivity assay. After a 48-hour incubation the overnight cultures were pipetted into 2 mL microfuge tubes, the tubes were centrifuged at 10,000 RCF for 1 minute, the growth medium was decanted and more of the overnight culture was added to the tube until the entire overnight culture had been pelleted. The pellet was then resuspended in 500 µL autoclaved H_20. The OD_{600} of the resuspension was then taken using a spectrophotometer (Novaspec II, Pharmacia Biotech) and was diluted to an OD of 1.

2.21.2 Plating of Ni Sensitivity Assay

Five µL of OD = 1 resuspension, 1 in 10, 1 in 100, 1 in 500 and 1 in 1000 dilution for each strain were spot inoculated onto the metal enriched plates for the Ni sensitivity assay. The plates were then incubated at 30°C and the growth phenotype of yeast strains was captured by photographing after 24, 48 and 92 hours. Imaging of growth during Ni sensitivity assay as done using a Syngene Gbox with a Cybertech 220 V 50 MHz Camera with optics using an upper white light.

2.22 Subcellular Localisation of ScIREG-YFP and ScIRT1-YFP by Fluorescence Microscopy

2.22.1 *Agrobacterium tumefaciens* Growth and Competent Cell Preparation

A. tumefaciens GV3101 strain was selectively cultured on LB plates with 150 µg/mL rifampicin and 15 µg/mL gentamycin selection. The plates were incubated with minimal light at 30°C for around 48 hours. YEP liquid media (1% w/v peptone, 1% w/v yeast extract, 0.5% w/v NaCl) was used to culture colonies from these plates using 100 µg/mL rifampicin for over 12 hours at 30°C. To obtain cells in the optimum phase of growth, 2 mL of the overnight culture was inoculated into 50 mL YEP media with the same selection and was incubated until the culture reached an OD_{600} greater than 0.5. The culture was then centrifuged at 5,000 RCF for 5 minutes and the pellet was resuspended in near freezing 20 mM $CaCl_2$. The suspension was aliquoted into 100 µL volumes and flash frozen using liquid nitrogen and stored at -80°C.

2.22.2 *A. tumefaciens* Transformation

A. tumefaciens was transformed using the *pEarlyGate101* vector containing genes of interest. 100 µl competent cells was mixed with 25 µL of appropriate plasmid and heat shocked at 37°C for 5 minutes. Nine-hundred µL of YEP media was added and the cells were incubated (with shaking) at 30°C for 6 hours. The transformed cells were then plated out on LB plates (1.5% w/v agar) containing 150 µg/mL rifampicin and 15 µg/mL gentamicin and 50 µg/mL kanamycin to select for the *pEarlyGate101* vector, and incubated at 30°C for 2-3 days until colonies appeared. Transformants were screened by colony PCR.

2.22.3 Preparation of *Agrobacterium* Inoculum

A. tumefaciens harbouring the *pEarlyGate101* vector containing *ScIRT1* was revived from glycerol stock and grown overnight at 30°C in 0.5 L YEP media supplemented with 150 µg/mL rifampicin and 15 µg/mL gentamicin and 50 µg/mL kanamycin to an OD_{600} between 1.5 and 2.0. The culture was then centrifuged at 5,000 RCF for 10 minutes and resuspended in 20 mL infiltration liquid (41.65 mM D-glucose, 100 mM $CaCl_2$, 100 mM MES-KOH pH 5.) stock solution, 0.011 mM BAP, 0.01% v/v Silwet L-77, 0.05 mM $MgCl_2$, 12.5 mM AS, dH_2O) and this resuspension was repeated three times.

2.22.4 Onion Cell Transformation

Red onions (*Allium cepa* L) were pretreated for *Agrobacterium* injection by being incubated at 30°C in complete darkness for 72 hours. A volume of 200 µL agroinfiltration liquid OD_{600} = 0.1 was injected with a small syringe into a pretreated red onion between the adaxial epidermis and mesophyll of the bulb and the agroinfiltration was left at 30°C for 72 hours (Xu et al., 2014). During injection, an effort was made to form an 'agroinfiltration bubble' between cell layers full of agroinfiltration liquid.

2.22.5 Onion Cell Staining

After 72-hour incubation transformation incubation the onions were dissected into thin single cell layers and wet mounts were created on glass slides for visualization. 500 µL 1 µL/mL Hoechts stain was then applied to the wet mounts for 15 minutes. The stain was then washed three times using PBS (137 mM/L NaCl, 2.7 mM/L KCl, 10mM/L Na2HPO4, 1.8 mM/L KH2PO4). A cover slip was placed over the wet mounts and the slides were set.

2.22.6 Fluorescent Microscopy Visualization

The wet mounts were visualized on a darkfield fluorescence microscope (Nikon Eclipse T*i*-E, Department of Molecular and Cell Biology, University of Cape Town) and digital photographs were taken. A YFP filter (barrier to wavelengths outside of 510 -570 nm), UV filter, bright field and 10x objective was used to visualize the samples and NIS Elements Advanced Research software was used to operate the microscope.

3. Results and Discussion

3.1 Overview

An experimental investigation into the candidate *Senecio coronatus* metal transporters *IREG2* and *IRT1* was conducted. The first aim was cloning and amplification of the genes of interest for confirmation of the predicted nucleotide sequences derived from a previous RNA-Seq experiment (Meier et al., 2017). This was done using conventional RT-PCR and cloning the resulting products into the commercial entry vector *pENTR1A*.

The second aim of the project was to investigate whether the *S. coronatus* IRT1 and IREG2 proteins are able to catalyse the transport of Ni *in vivo*. This was achieved by determining whether heterologous expression of these proteins in yeast was sufficient to alter the sensitivity of the resulting transgenic yeast to exogenous Ni. This technique has been widely used to characterize the substrate specificity of many metal transport proteins (Nishida et al., 2011; Oomen et al., 2009; Schaaf et al., 2006). The yeast strains used in the metal sensitivity assays are often mutated in their own metal transport proteins making the effect of heterologous expression of a transport protein easier to detect. In these experiments, the yeast *zrt1zrt2* mutant was utilized in order to test whether ScIREG2 and ScIRT1 could transport Ni, by analysing the sensitivity of the transgenic yeast to a range of Ni concentrations. If the protein encoded by the transgene acted as metal importer in yeast this would result in increased intracellular metal concentrations leading to increased toxicity and hence reduced growth. Conversely, if it acted as an exporter (either to the vacuole or across the plasma membrane) then the opposite would apply, and increased resistance to the metal ion would be observed.

The final objective for this project was to determine the subcellular localisation of the proteins encoded by *ScIREG2* and *ScIRT1*. This information was anticipated to be useful evidence in describing the cellular functions of these genes or supporting evidence of their transporter capabilities generated through Ni sensitivity assays because metal transporters are typically associated with specific cellular membranes. In the literature, characterization of metal transporters often includes experimental evidence for subcellular localisation in addition to metal sensitivity assays (Ma et al., 2005; Merlot et al., 2014; Schaaf et al., 2006). In this Masters project, subcellular localisation of the proteins encoded by the genes of interest was investigated using transient expression of C-terminal yellow fluorescent protein (YFP) fusion proteins and fluorescence microscopy was used to visualize the location of the protein directly when expressed in plant cells.

3.2 Cloning of Full-Length *ScIRT1* and *ScIREG2* from *Senecio coronatus* cDNA

The first aim of validating the predicted nucleotide sequences from the RNA-Seq transcriptome assembly for *ScIREG2* and *ScIRT1* was undertaken by attempting to clone the full-length sequences from *S. coronatus* cDNA extracted from root tissues. By cloning these ORFs into a gateway compatible entry vector (*pENTR1A*), the resulting vectors could then be made use of in downstream expression and localisation experiments. The restriction enzymes *Sal*I and *Not*I were selected for insertion of the 1500 base pair *ScIREG2* product into *pENTR1A*, and *Bam*HI and *Eco*RI for insertion of the 1047 base pair *ScIRT1* product. The necessary restriction enzyme sites were incorporated into the PCR primers (Table 1 | Primers).

3.2.1 PCR Amplification of *ScIREG2* and *ScIRT1*

PCR amplification of full-length *ScIRT1* and *ScIREG2* open reading frames from *S. coronatus* root cDNA was performed using a high-fidelity DNA polymerase and yielded products of the predicted size for both genes (1500 base pairs and 1047 base pairs), confirming that both genes are indeed expressed in root tissue. (Figure 2 & Figure 3)

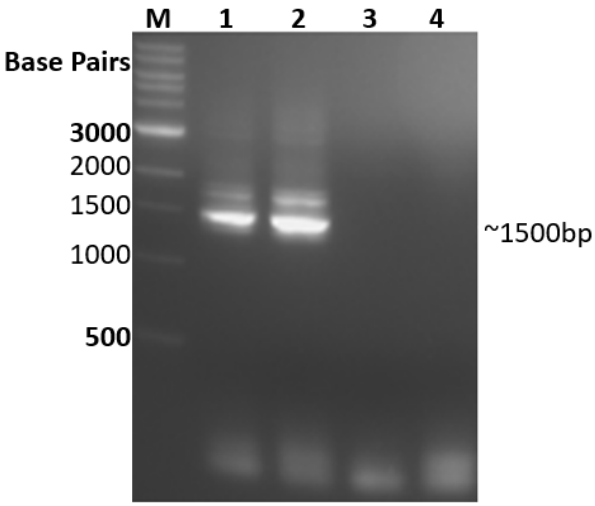

Figure 2**| Amplification of *ScIREG2* from *S. coronatus* cDNA using high fidelity polymerase.** Lanes 1 and 2 contain products of a PCR amplification of *S. coronatus* cDNA using the *ScIREG2* specific primers: *IREG FOR NOTI* and *IREG FOR SALI*, and Phusion Hi-Fi Hotstart polymerase. Lanes **3** and **4** contain the negative PCR controls for lanes 1 and 2 with the appropriate primers and a water template. Products were visualized on a 1% agarose gel and sized with New England Biolabs 1kb DNA Ladder.

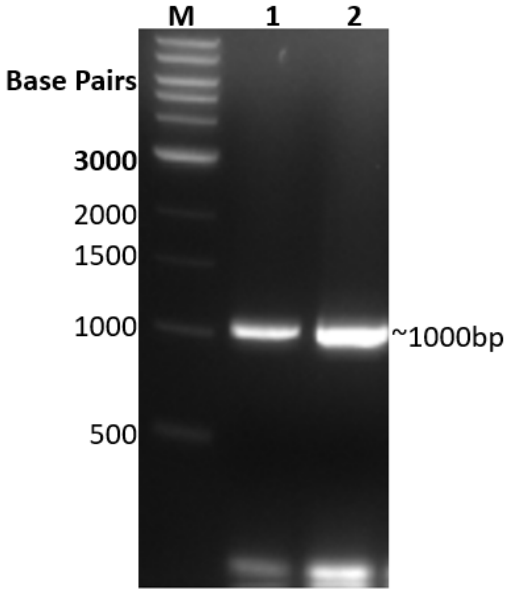

Figure 3**| Amplification of *ScIRT1* from *S. coronatus* cDNA using high fidelity polymerase.** Lanes **1** and **2** contain products of a PCR amplification of *S. coronatus* cDNA using the *ScIRT1* specific primers: *IRT1 FOR* and *IRT1 ECO rev*, and Phusion Hi-Fi Hotstart polymerase. Products were visualized on a 1% agarose gel and sized with New England Biolabs 1kb DNA Ladder.

Several diagnostic restriction enzyme digests of *pENTR1A* were set-up to confirm the identity of the vector, and to

prepare the necessary vector backbone for cloning of the *ScIRT1* and *ScIREG2* inserts (Figure 4). A comparison can be made to the vector map (Appendix, Supplementary Figure 1).

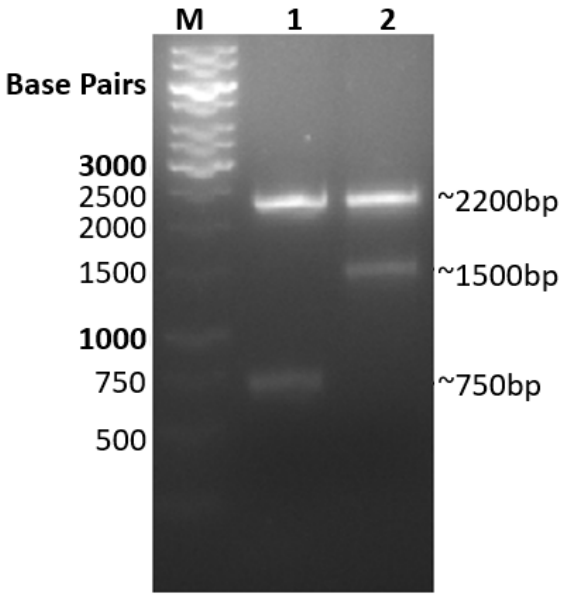

Figure 4**| Confirmation of identity of *pENTR1A* Entry Vector and generation of backbone for cloning.** Double digest of 500 ng purified *pENTR1A* vector with *Xho*I and *Bam*HI (Lane **1**) or *Not*I and *Sal*I (Lane **2**). Products were visualized on a 1% agarose gel and sized with Thermo Scientific O'GeneRuler 1kb DNA Ladder.

The digestion of *pENTR1A* with *Xho*I and *Bam*HI in lane 1 yielded the predicted bands of 2.2 and 0.7 kb, confirming the identity of the vector. The digestion of *pENTR1A* with *Not*I and *Sal*I in lane 2 yielded the predicted 2.2 kb *pENTR1A* vector backbone (used for cloning of *ScIREG2*) and 1.5 kb insert. A similar digest with *Bam*HI and *Eco*RI was used to generate the vector backbone for ligation of the *ScIRT1* PCR product (data not shown). PCR products were digested with the appropriate enzymes and ligation reactions set up. These ligation reactions were then used to transform competent *E. coli* cells.

3.2.2 Identification of *ScIREG2* Transformants

Single putative transformant colonies from selective media were used directly as templates in a colony PCR using *ScIREG2* specific primers to test for the presence of the insert (Figure 5).

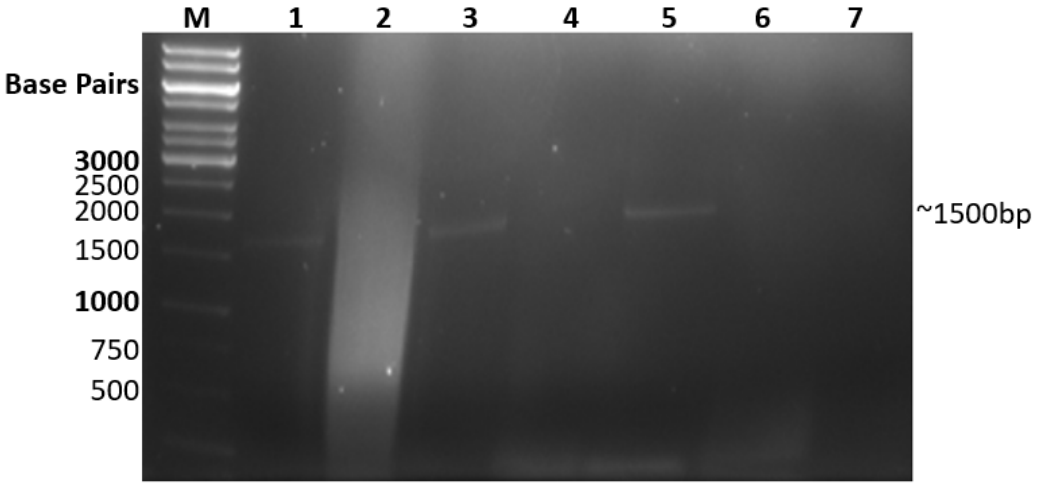

Figure 5**|Colony PCR of *E. coli* colonies transformed with *ScIREG2* and *pENTR1A* ligation.** Lanes **1 to 6** contain PCR amplification of *E. coli pENTR1A:ScIREG2* transformation colonies using the *ScIREG2* specific primers: *IREG FOR NOTI* and *IREG FOR SALI*, and Supertherm polymerase. Lane **7** contains the negative PCR control for lanes 1 to 6 with the appropriate primers and a water template. Products were visualized on a 1% agarose gel and sized with Thermo Scientific O'GeneRuler 1kb DNA Ladder.

Lanes 1, 3 and 5 corresponding to colonies 1, 3 and 5 amplified a single specific product at approximately 1500 base pairs which is the expected size for amplification of *ScIREG2*, and suggests that they contain the ligated *pENTR1A:ScIREG2* construct. To confirm this, plasmids were digested with *Sal*I and *Not*I (the restriction enzymes used to clone in the insert) in order to release the insert from the backbone (Figure 6).

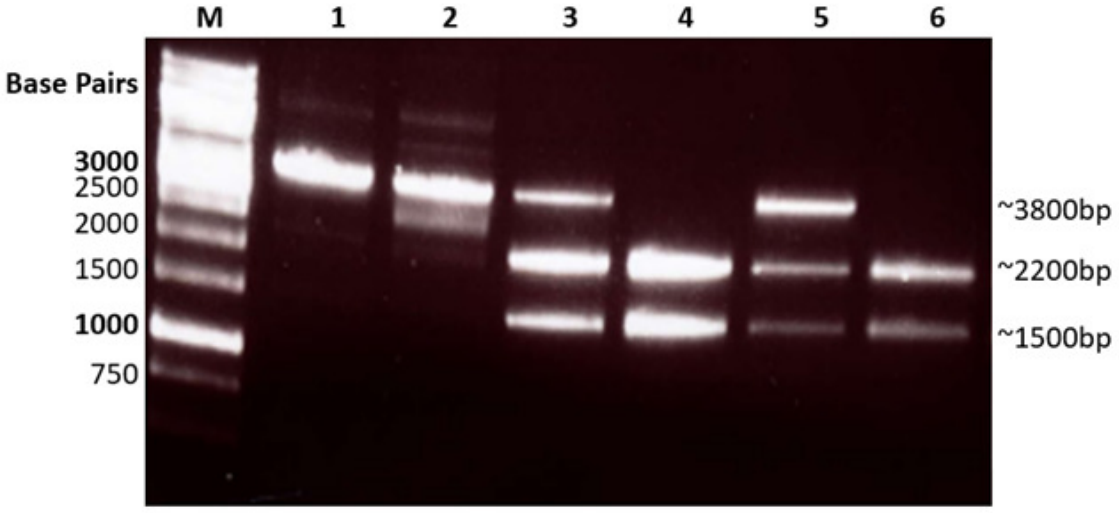

Figure 6**|Double digest of 500 ng plasmid DNA extracted from *E. coli* colonies transformed with *ScIREG2* and *pENTR1A* ligation.** Lanes **1 to 6** contain purified plasmid extracted from *E. coli* transformed with *ScIREG2* and *pENTR1A* ligation and subjected to restriction enzyme double digestion with *SalI* and *Not*I. Products were visualized on a 1% agarose gel and sized with Thermo Scientific O'GeneRuler 1kb DNA Ladder.

Double digestion of extracted plasmids resulted in three strongly visible bands. The size of the bands corresponds to the 2267 base pair *pENTR1A* backbone, the 1500 base pair gene of interest (*ScIREG2*) and the 3767 base pair

linearised complete vector. The fact the band at 3.8 kilobases is similar to the expected size of the sum of the insert and the vector length indicates that the double digestion did not fully digest all the extracted plasmid present in lanes 3 and 5. Possible reasons for this could be that insufficient time was given for the restriction enzymes to act upon the DNA or an excess of DNA was added. Lanes 4 and 6 have bands present at approximately 2200 and 1500 base pairs which is exactly the result expected for digestion of *pENTR1A:ScIREG2* with *Sal*I and *Not*I. However, the colonies associated with these extracts did not amplify the gene of interest during colony PCR. In view of this, the *pENTR1A:ScIREG2* plasmid from lane 3 (corresponding to colony 3) was selected for DNA sequencing because it gave a positive result in the colony PCR and an insert band of the correct size in the double digestion.

3.2.3 *pENTR1A:ScIREG2* Sequencing

The plasmid was sequenced to confirm the presence of *ScIREG2* to ensure that no mutations had been introduced into *ScIREG2* by the DNA polymerase, particularly those that could cause a frame shift. The vector was sequenced using forward and reverse primers designed to anneal to the *pENTR1A* vector on either side of the multiple cloning site (*M13*). The length of *ScIREG2* being 1500 base pairs resulted in poor quality sequencing reads towards the middle of the gene from both directions. In view of this, an additional internal gene specific sequencing primer was designed and used to generate a good quality sequencing read of this region of the gene (*IREG SEQ int*). The compiled sequence from the three reads was compared to the *ScIREG2* sequences generated from the Meier et al. (2017) RNA-Seq experiment in a ClustalW multiple sequence alignment (Figure 7). The *ScIREG2* sequences from the RNA-Seq data originated from two distinct *S. coronatus* populations A (hyperaccumulator population in Agnes Mine) and C (hyperaccumulator population in Kaapsehoop). The gene sequences for these populations were generated for different individuals within these populations. A small amount of variation in nucleotide and amino acid sequence was evident within these populations.

A)

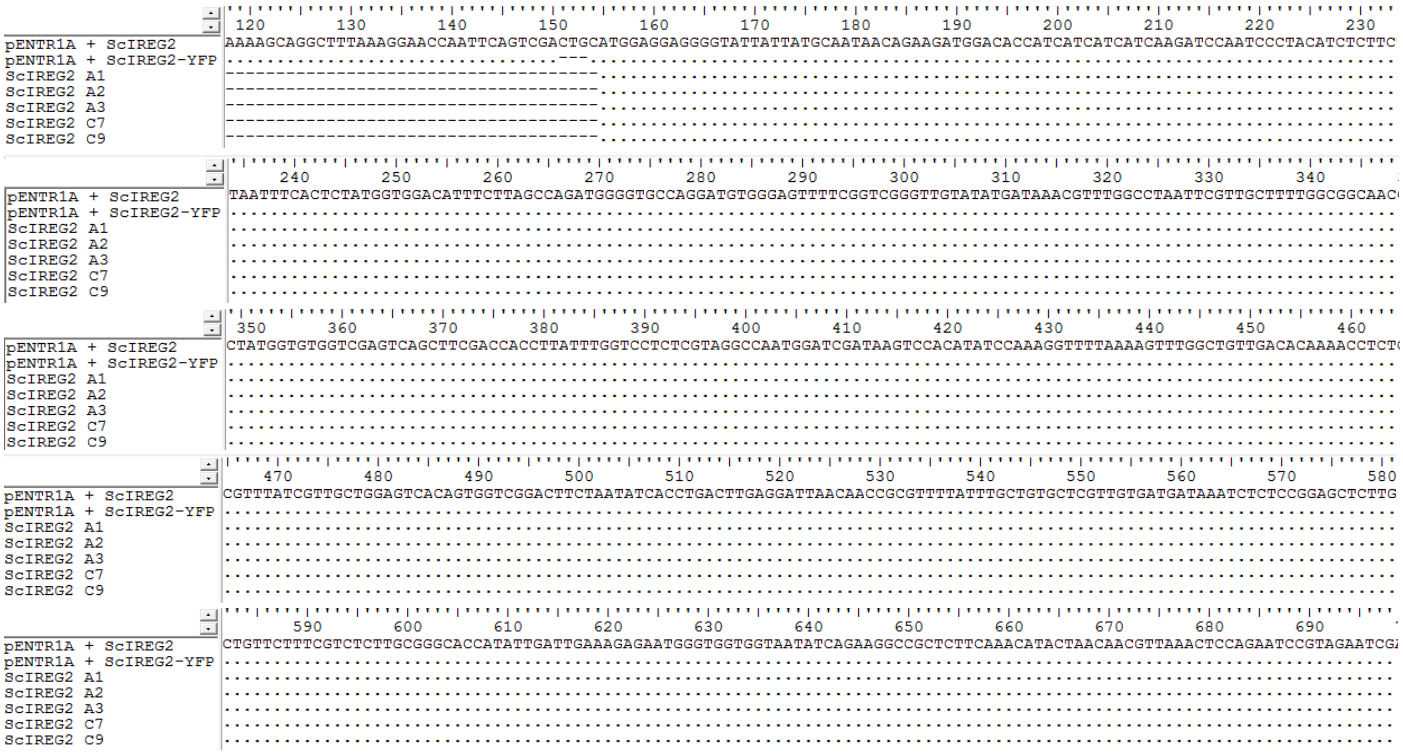

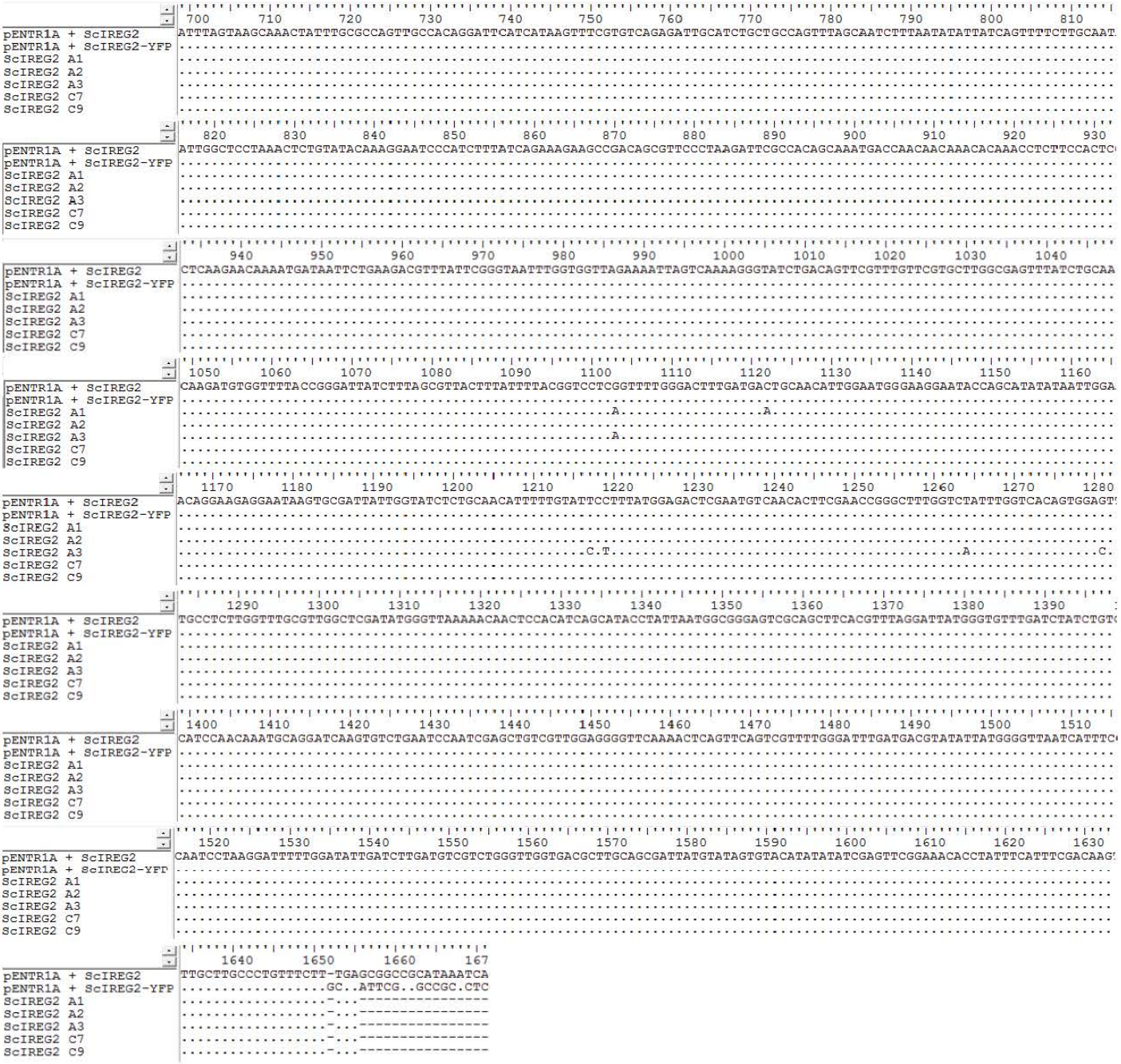
pENTR1A + ScIREG2
pENTR1A + ScIREG2-YFP
ScIREG2 A1
ScIREG2 A2
ScIREG2 A3
ScIREG2 C7
ScIREG2 C9

B)


pENTR1A + ScIREG2
ScIREG2 A1
ScIREG2 A2
ScIREG2 A3
ScIREG2 C7
ScIREG2 C9

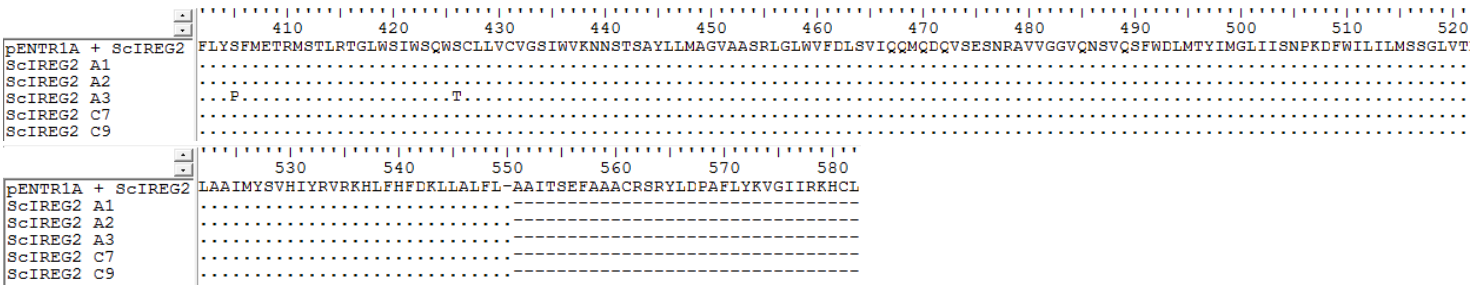

Figure 7**|ClustalW nucleotide (A) and amino acid (B) multiple sequence alignment in BioEdit of cloned *ScIREG2* to full gene sequences generated from *de novo* transcriptome assembly.**

The sequence of this clone perfectly matched the nucleotide sequences from *S. coronatus* individuals A2, C7 and C9. The sequence has a small number of base pair substitutions when compared to the A1 and A3 populations. These substitutions are non-synonymous and result in the serine 317 becoming glycine, asparagine 323 becoming threonine, proline 355 becoming serine and threonine 376 becoming serine. The fact that there was a perfect match to known sequences of *ScIREG2* from A2, C7 and C9 confirms the sequence of *ScIREG2* predicted by the RNA-Seq experiment, and this construct was now available for gateway cloning into the expression vectors for expression analysis.

3.2.4 Identification of *ScIRT1* Transformants

The *ScIRT1* and *pENTR1A* ligation was transformed into competent *E. coli* DH5α and the resultant plasmid DNA was extracted from colonies capable of surviving on selective media. The plasmids were then digested using *Bam*HI and *Eco*RI (the restriction sites used to clone the insert) to determine if the insert was present (Figure 8).

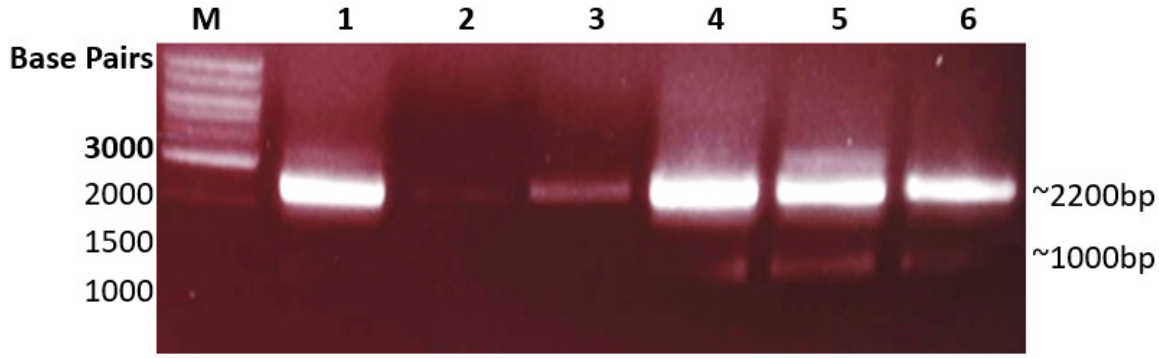

Figure 8**| Double digest of extracted 500 ng *pENTR1A:ScIRT1* from *E. coli.*** Lanes **1 to 8** contain extracted plasmid from *E. coli* transformed with *IRT1* and *pENTR1A* ligation mix subjected to complete digestion with *Bam*HI and *Eco*RI. Products were visualized on a 1% agarose gel and sized with New England Biolabs 1kb DNA Ladder.

Double digestion of the extracted plasmid generated a strong band for all the samples at approximately 2200 base pairs which is the expected size for the vector backbone. A smaller, fainter band is visible in extracts 4, 5 and 6 at approximately 1000 base pairs corresponding to the expected 1047 base pair size of the *ScIRT1* insert. The plasmid digested in lane 5 was selected for DNA sequencing.

3.2.5 *pENTR1A:ScIRT1* Sequencing

Similar to the *ScIREG2* sequencing performed in section 3.2.3, the *ScIRT1* sequencing reads generated with the *M13* primers was compared to the *ScIRT1* sequences generated from the Meier et al. (2017) RNA-Seq experiment in a ClustalW multiple sequence alignment (Figure 9). *ScIRT1* is shorter than *ScIREG2* so an internal sequencing read was found to be unnecessary. The *ScIRT1* sequences were compared to the same individuals from populations A and C as *ScIREG2* from the RNA-Seq data. An additional sequence was available for individual C8 for *ScIRT1*.

A)

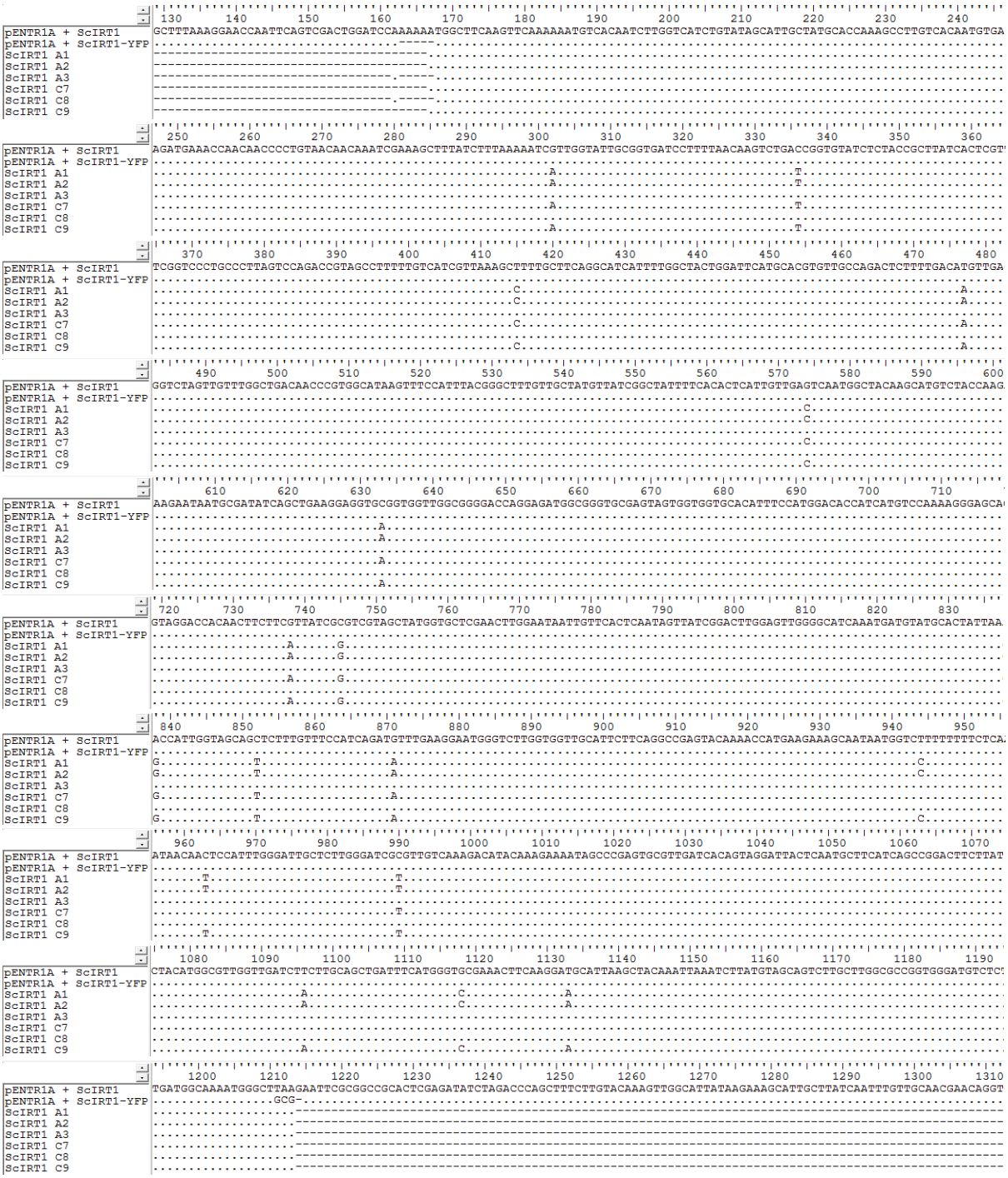

B)

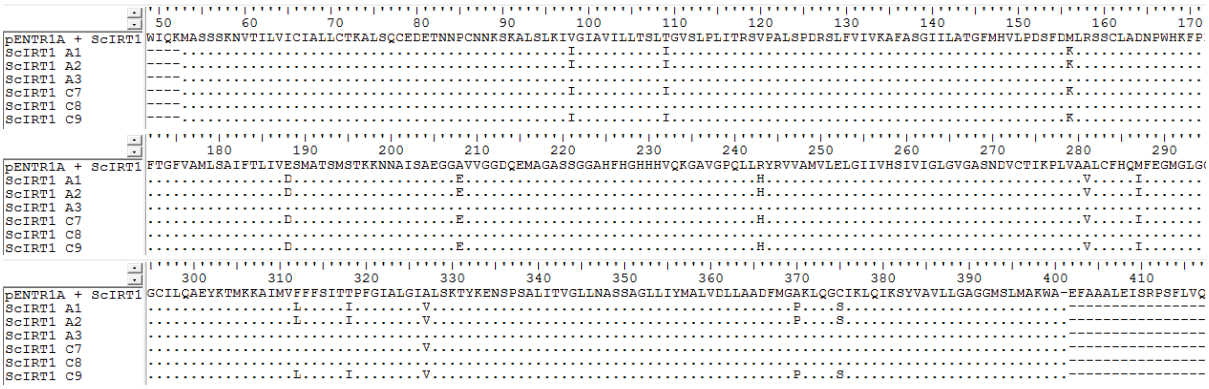

Figure 9**|ClustalW nucleotide (A) and amino acid (B) multiple sequence alignment in BioEdit of cloned *ScIRT1* to full gene sequences generated from *de novo* transcriptome assembly.**

Similar to the result obtained for *ScIREG2*, the cloned sequence perfectly matches the nucleotide sequences from *S. coronatus* some individuals (A3 and C8). The sequence also has a small number of base pair differences when compared to the A1, A2, C7 and C8 plants. These substitutions are non-synonymous and result in numerous amino-acid substitutions displayed in Figure 9B. The perfect match of the cloned fragment to the sequences of *ScIRT1* from the A3 and C8 plants confirms the sequence of *ScIRT1* predicted by the RNA-Seq experiment. The correct and functional sequence of *ScIRT1* was also cloned into *pENTR1A*.

An interesting observation is that the cloned sequences for *ScIREG2* and *ScIRT1* do not both match the same individuals from the same populations from the RNA-Seq experiment. The genes were both amplified from the same cDNA extracted from the same individual in population C (Kaapsehoop region) but the gene version combination does not match those of any of the sequenced individuals in the RNA-Seq experiment. However, this is likely because the cDNA used to amplify the insert was extracted from a different individual from population C than those involved in the RNA-Seq experiment. This individual in population C clearly had a different combination of alleles present than was observed in the individuals used in the RNA-Seq experiment.

3.3 Bioinformatic Analysis of ScIREG2 and ScIRT1 Proteins

Validation of the nucleotide sequences of the genes of interest by direct sequencing justifies the further investigation of the predicted amino acid sequences. A bioinformatic investigation was carried out on the amino acid sequences in an attempt to provide supporting evidence that the genes of interest encode transport proteins. A phylogenetic analysis was generated for both genes to investigate their evolutionary relationship with well characterised metal transporters and to inform their correct annotation as *ScIREG2* and *ScIRT1*. The topology of the encoded proteins was predicted to ascertain if they would likely localize to the membrane which is expected for metal transport proteins. The subcellular localisation of the proteins was also predicted.

3.3.1 Phylogenetics of ScIREG2 and ScIRT1

To construct a phylogenetic analysis, the predicted amino acid sequence generated for *ScIREG2* was compared similar sequences from the Viridiplantae BLAST database from annotated proteins (Figure 10). The well annotated *A. thaliana* IREG proteins were used as a framework to establish if ScIREG2 belongs to this gene family.

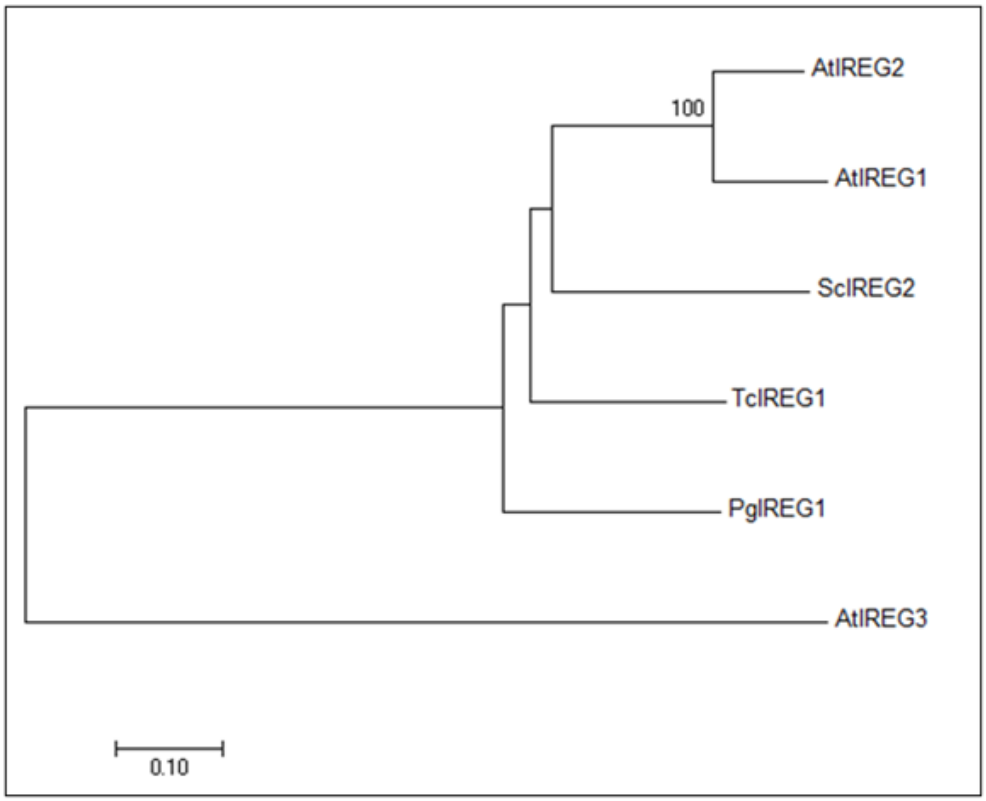

Figure 10**| Phylogenetic analysis of ScIREG2.** The *S. coronatus* IREG2 amino acid sequence is compared to similar annotated genes from *A. thaliana* and other plant species in the Viridiplantae database. The complete amino acid sequences were aligned using ClustalW and was used to generate a phylogenetic tree in MEGA using the Neighbour-Joining method with 1000 bootstrap replications. Significant bootstrap values are shown. Species: *Senecio coronatus* (Sc), *Arabidopsis thaliana* (At), *Theobroma cacoa* (Tc), *Psychotria gabriellae* (Pg). The scale bar relates the length of a branch to the number of amino acid substitutions.

During phylogenetic analysis, the amino acid sequence of ScIREG2 clusters with IREG proteins from a variety of species. AtIREG1 and AtIREG2 appears in a clade with a perfect bootstrap score indicating these *Arabidopsis* genes arose from a recent gene duplication event based on their similarity. ScIREG2 forms a node with AtIREG1 and AtIREG2. The larger clade including this *Arabidopsis* and *S. coronatus* cluster also contains the IREG1 proteins from other plants. The fact that these sequences cluster together so tightly and that ScIREG2 is within this cluster supports the notion that ScIREG2 is correctly annotated as an IREG encoding gene. The differences between these genes and other organisms can be attributable to changes in the same gene over evolutionary time after speciation.

AtIREG3 forms an outgroup to the larger clade indicating that in evolutionary history, it diverged from AtIREG1 and AtIREG2 before *A. thaliana* and *S. coronatus* diverged from their last common ancestor.

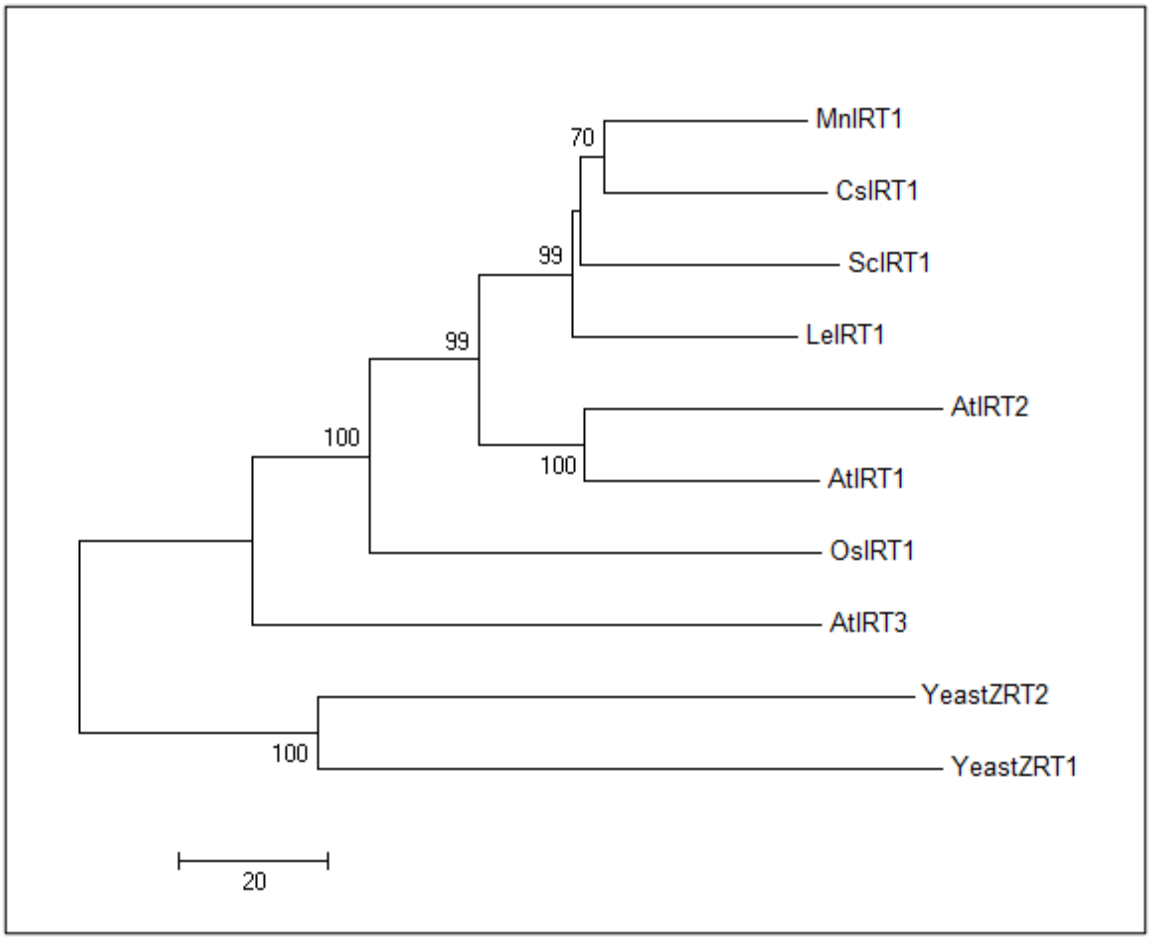

Figure 11**|Phylogenetic analysis of ScIRT1.** The *S. coronatus* IRT1 predicted amino acid sequence is compared to similar annotated genes from *A. thaliana* and other plants in the Viridiplantae database. An outgroup from outside the Viridiplantae database is used. The complete amino acid sequences were aligned using ClustalW and was used to generate a phylogenetic tree in MEGA using the Neighbour-Joining method with 1000 bootstrap replications. Significant bootstrap values are shown. Species: *S. coronatus* (Sc), *Arabidopsis thaliana* (At), *Cucumis sativus* (Cs), *Morus notabilis* (Mn), *Saccharomyces cerevisiae* (Yeast), *Lycopersicon esculentum* (Le), *Oryza sativa* (Os). The scale bar relates the length of a branch to the number of amino acid substitutions.

Phylogenetic analysis of IRT proteins (Figure 11) indicated that the predicted ScIRT1 sequence clusters with IRT proteins from a variety of species. It appeared in a clade with CsIRT1, LeIRT1 and MnIRT1. Again, this analysis supports the correct annotation of ScIRT1 as encoding an IRT gene. The ZRT IRT1 like ZIP family protein from *Morus notabilis* is annotated as a zinc transporter but this family is known to transport a variety of cations. The protein in this project is annotated IRT to mimic the majority of annotations that of the *A. thaliana* homologs as it is the model for the plant system.

Similar to the IREG sequences, AtIRT1 and AtIRT2 form a strong independent node in 98% of bootstrap replicates indicating consistent grouping of ScIRT1 with known IRT1 proteins suggesting it is a true homolog. AtIRT3 forms an outgroup to this clade indicating its gene duplication and divergence from AtIRT1 and AtIRT2 before the speciation of these plant species.

3.3.2 Prediction of ScIREG2 and ScIRT1 Protein Topology

In order to function as a transporter, a protein must be an integral membrane protein, and the different families of transport proteins are characterised by different numbers of transmembrane helices. The likelihood of an amino acid sequence being a membrane protein can be predicted using bioinformatic tools to identify putative transmembrane helices. The hydrophobicity of specific amino acids along the sequence can be used to annotate regions of the sequence that are likely to localize within a membrane. Transmembrane helices were predicted for the proteins of interest by using the Dense Alignment Surface algorithm (http://mendel.imp.ac.at/sat/DAS/DAS.html). The algorithm uses a scoring matrix for the amino acid sequences to compare it to a library of non-homologous membrane proteins. Low stringency dot plots based on the hydrophobicity of the amino acids are then used to predict the number and span of transmembrane domains with a "DAS" profile score.

The accuracy of the DAS algorithm and the degree to which its output is correct was investigated by comparing it to the already well characterised and highly related proteins AtIREG2 for ScIREG2 and AtIRT1 for ScIRT1 (Figure 12 & Figure 13). By comparing the output of the DAS algorithm for the characterised proteins to the annotations described in the literature, the accuracy of the prediction made by this algorithm for the *S. coronatus* proteins in particular can be determined.

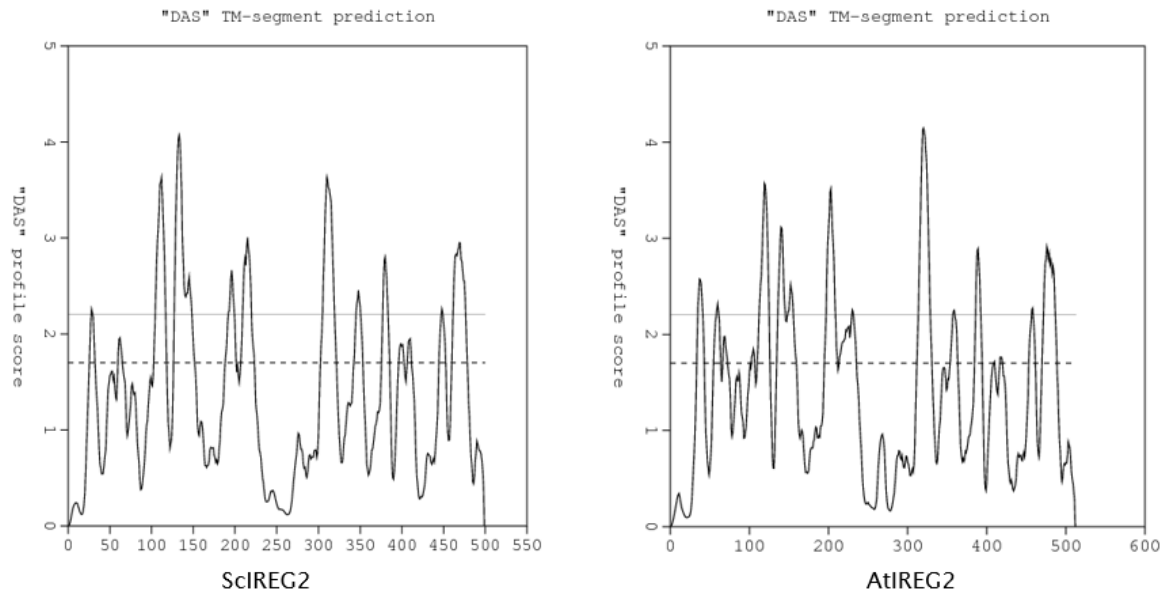

Figure 12**| Dense Alignment Surface algorithm applied to ScIREG2 and AtIREG2 for comparison of predicted transmembrane helices.** The predicted amino acid sequence encoded by ScIREG2 and AtIREG2 based on the output from DAS-TM filter server (http://mendel.imp.ac.at/sat/DAS/DAS.html). Each amino acid along the length of the protein is represented on the X-axis. The dotted line denotes a loose cut-off to define a transmembrane region. The thin solid line denotes a strict cut-off to define a transmembrane region.

AtIREG2 was annotated by Schaaf et al. (2006) to contain 10 putative domains. The strict cut-off using the DAS algorithm predicts 11 transmembrane helices for AtIREG2. The result of the prediction is therefore not perfect but the number of predicted transmembrane helices is very close to the number described in the literature. The nature of the peaks in the DAS profile could provide an explanation of why there is an additional predicted transmembrane

helix. There are some extremely large, clearly defined peaks which greatly exceed the strict cut-off on the DAS profile but there are other smaller peaks which barely intersect the cut-off. Notably, peak 2 in *A. thaliana* is just above the threshold, while the corresponding peak in ScIREG2 is not.

A comparison of the output of the DAS algorithm reveals that the DAS plot is very similar for both ScIREG2 and AtIREG2. This is to be expected given the high degree of sequence similarity between these amino acid sequences. The ScIREG2 plot however only includes 10 peaks which exceed the strict cut-off point predicting 10 transmembrane helices. It is therefore likely to be a membrane protein like AtIREG2 and thus a good candidate for a potential transport protein.

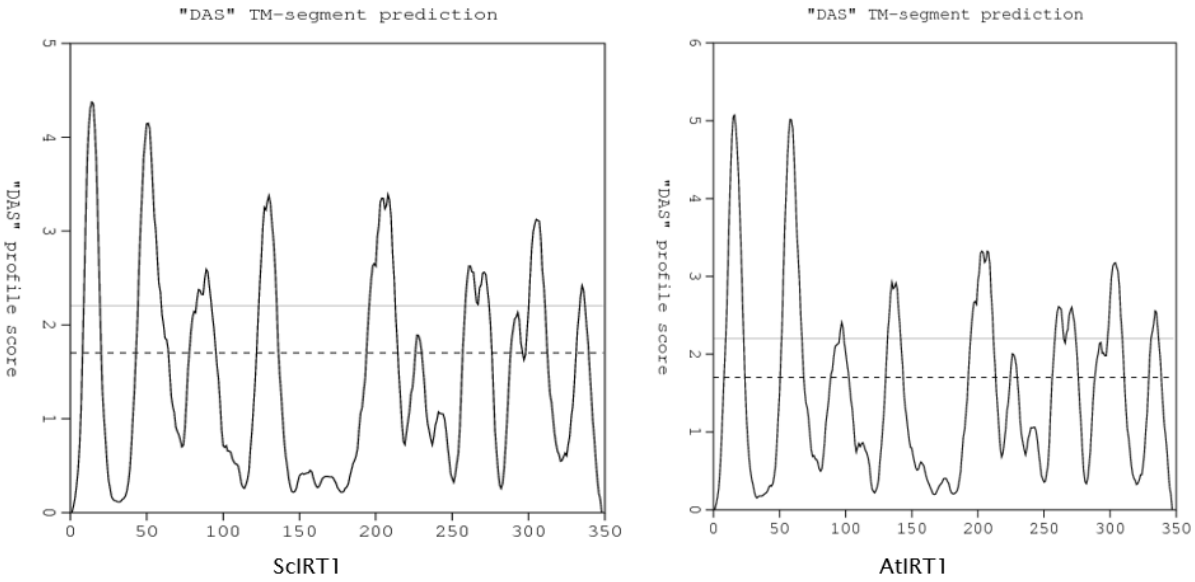

Figure 13**| Dense Alignment Surface algorithm applied to ScIRT1 and AtIRT1 for comparison of predicted transmembrane domains.** The predicted amino acid sequence encoded by ScIRT1 and AtIRT1 based the output from DAS-TM filter server (http://mendel.imp.ac.at/sat/DAS/DAS.html). Each amino acid along the length of the protein is represented on the X-axis. The dotted line denotes a loose cut-off to define a transmembrane region. The thin solid line denotes a strict cut-off to define a transmembrane region.

Eide et al. (1996) described AtIRT1 as a membrane protein containing 8 transmembrane domains. The DAS profile predicts AtIRT to possess 8 transmembrane helices using the strict cut-off so the profile accurately predicts the annotated number. AtIRT1 seems to have much more well defined, evenly spaces peaks in its DAS profile compared to that of AtIREG2. This could be a contributing factor to the number of transmembrane helices being predicted correctly. The DAS profile of ScIRT1 is remarkably similar to that of AtIRT1. It includes the same number of peaks of similar size and shape which exceed the strict cut-off. ScIRT1 is also predicted to include 8 transmembrane helices. Topology analysis of the DAS profiles confirms ScIRT1 is similar to the well characterised membrane metal transporter protein AtIRT1 in both structure and sequence and is therefore also a good candidate for being a transport protein in *S. coronatus*.

3.3.3 Predicted Subcellular Localisation of ScIREG2 and ScIRT1 Proteins

The final objective of the project was to experimentally determine the subcellular localisation of the proteins encoded by the genes of interest using transient expression of C-terminal fluorescent tagged proteins. An attempt

was made to use bioinformatic tools to predict the localisation of ScIREG2 and ScIRT1 based on their amino acid sequences. A plethora of tools is available online which predict the localisation of proteins by identifying localisation features and signals present in the amino acid sequence. These tools all apply different definitions and statistics.

The accuracy of these predictive tools was assessed by comparing the results they generated for the subcellular localisation of the characterised *A. thaliana* homologs with the annotated, experimentally determined descriptions. The Subcellular Proteomic Database (SUBA4) was used to access precompiled bioinformatic predictions for the *A. thaliana* proteins quickly and easily (Figure 14 & Figure 15).

AdaBoost: plasma membrane	BaCelLo: nucleus
MultiLoc: golgi	Plant-mPloc: plasma membrane
PredSL: endoplasmic reticulum	PredSL: extracellular
PredSL: golgi	PProwler: endoplasmic reticulum
PProwler: extracellular	PProwler: golgi
SLPFA: mitochondrion	SLP-Local: cytosol
SLP-Local: nucleus	SubLoc: extracellular
WoLF PSORT: plasma membrane	YLoc: peroxisome

Figure 14**| Prediction of subcellular localisation of AtIREG2 using various predictor tools.** Output of predicted subcellular localisation by various predictor tools accessed through The Subcellular Proteomic Database (SUBA4) for *A. thaliana* proteins.

The various predictive tools compiled for AtIREG2 on SUBA4 predicted a wide range of localisations. AtIREG2 was experimentally demonstrated by Schaaf et al.(2006) to localize to the tonoplast using an AtIREG2-GFP fusion protein. It is also described as localizing to the vacuole by TAIR and AmiGO. Therefore, none of the 16 predictor tools reviewed correctly predicted the proven localisation of AtIREG2. SUBA4 included only 16 precompiled predictor tool results. This is significantly less than the number of tools compiled for other genes such as AtIRT1. It is possible that if more predictor tools were used a correct prediction of tonoplast would have been identified. However, utilizing a significant number (16), none predicted the correct localisation. The accuracy of bioinformatics tools to predict the subcellular localisation of this protein is thus 0%.

AdaBoost: plasma membrane	BaCelLo: endoplasmic reticulum	BaCelLo: extracellular	BaCelLo: golgi
EpiLoc: vacuole	iPSORT: endoplasmic reticulum	iPSORT: extracellular	iPSORT: golgi
MitoPred: mitochondrion	MultiLoc: endoplasmic reticulum	PCLR: plastid	Plant-mPloc: plasma membrane
Predotar: endoplasmic reticulum	Predotar: extracellular	Predotar: golgi	PredSL: endoplasmic reticulum
PredSL: extracellular	PredSL: golgi	PProwler: endoplasmic reticulum	PProwler: extracellular
PProwler: golgi	SLPFA: endoplasmic reticulum	SLPFA: extracellular	SLPFA: golgi
SLP-Local: endoplasmic reticulum	SLP-Local: extracellular	SLP-Local: golgi	SubLoc: extracellular
TargetP: endoplasmic reticulum	TargetP: extracellular	TargetP: golgi	WoLF PSORT: plasma membrane
YLoc: plasma membrane			

Figure 15**| Prediction of subcellular localisation of AtIRT1 using various predictor tools.** Output of predicted subcellular localisation by various predictor tools accessed through The Subcellular Proteomic Database (SUBA4) for *A. thaliana* proteins.

Results had been precompiled by SUBA4 for thirty-three predictor tools, which predicted AtIRT1 to localize to numerous locations in the cell. Using an immunocytochemistry approach and an AtIRT1 specific antibody Barberon et al. (2011) demonstrated experimentally that AtIRT1 dynamically localizes to the plasma membrane and early endosomes. Swissprot has annotated AtIRT1 as occurring in the plasma membrane. Of the 33 precompiled predictor tools, 4 predict the localisation of AtIRT1 to the plasma membrane ,9 predict localisation to the endoplasmic reticulum and 8 predict localisation to the golgi apparatus.

The plasma membrane is thus not the most frequently predicted localisation of AtIRT1. The accuracy of prediction of the subcellular localisation was very low for both IRT1 and IREG2 from *A. thaliana*. Even for AtIRT1, which did have some predictor tools correctly predicting its subcellular localisation, the correct result was not the most frequent prediction. Utilization of these predictor tools to predict the subcellular localisation of the *S. coronatus* genes of interest was deemed futile because a large number of bioinformatic predictors were consistent incorrectly predicting the subcellular localisation. Even if some tools made correct predictions there would be no precedent to expect the most frequent prediction to be a reflection of the true subcellular localisation. No further attempts to use bioinformatic tools to provide an expected result for subcellular localisation experiments of ScIREG2 or ScIRT1 were made. Based on the high degree of similarity in sequence and secondary structure, the best approximation possible for the expected result for subcellular localisation experiments for the genes of interest was simply the same as the described localisations for their *A. thaliana*. ScIREG2 was thus expected to localize to the vacuole and AtIRT1 to localize to the plasma membrane.

3.4 Generation of Yeast Expression Constructs for ScIREG2 and ScIRT1

Bioinformatic analysis of predicted ScIREG2 and ScIRT1 amino acid sequences suggested that putative transporter proteins are encoded and thus warranted experimental investigation into their Ni transport activity. Heterologous expression in yeast and exposure to exogenous Ni was identified as the ideal method to test the capability of the proteins of interest to transport Ni. This required the expression of the genes of interest in *S. cerevisiae*. The yeast expression gateway vector and mutant yeast strain to perform the Ni sensitivity assay was acquired from our collaborator, Sylvain Merlot (French National Centre for Scientific Research). The *pDR195* gateway compatible yeast constitutive expression vector and the yeast *zrt1zrt2* mutant strain are the tools his research group used in his published research on *Psychotria gabriellae* Ni transport proteins (Merlot et al., 2014). The identity of the *pDR195 GTW* vector was confirmed by subjecting it to a diagnostic digestion with *Eco*RI and *Hin*dIII (Figure 16).

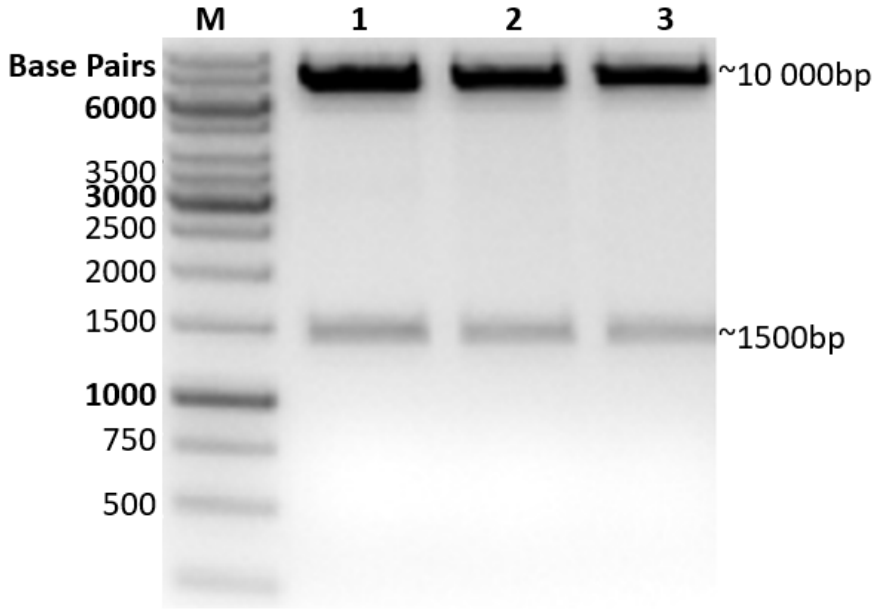

Figure 16**| Confirmation of identity of *pDR195 GTW* Destination Vector.** Double digest of 500 ng purified *pDR195 GTW* vector with *Eco*RI and *Hin*dIII. Products were visualized on a 1% agarose gel and sized with Thermo Scientific O'GeneRuler 1kb DNA Ladder.

The bands visible after digestion correspond with the expected band sizes of *pDR195 GTW*: 8000 base pairs and 1500 base pairs. The banding pattern was consistent with the expected sizes from the vector map (Appendix, Supplementary Figure 2). This result provided confidence in the plasmid's identity as *pDR195 GTW*.

3.4.1 Gateway Cloning of *ScIREG2* and *ScIRT1* into *pDR195* and Confirmation of Presence of Insert Using an Insert Specific PCR

Gateway cloning reactions were performed using the *pENTR1A:ScIREG2* and *pENTR1A:ScIRT1* vectors generated above with *pDR195 GTW* to generate *pDR195:ScIREG2* and *pDR195:ScIRT1*. PCRs were conducted on the purified plasmids after LR clonase reactions with gene specific primers to ensure the presence of the genes of the *ScIREG2* and *ScIRT1* open reading frames (Figure 17 & Figure 18).

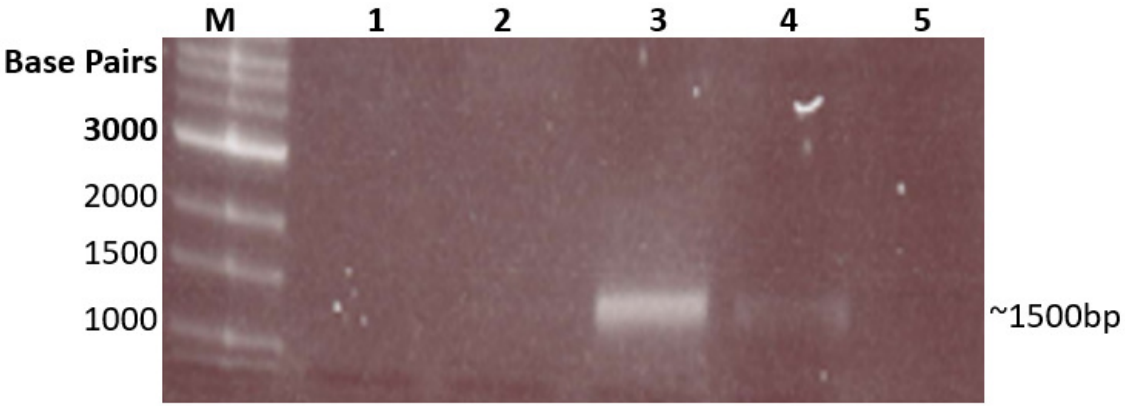

Figure 17**| Amplification of *ScIREG2* from extracted *pDR195* plasmids after Gateway cloning.** PCR conducted using Supertherm polymerase with the *ScIREG2* specific primers: *IREG FOR NOTI* and *IREG FOR SALI*. Lanes **1 to 4** utilized extracted plasmid as template. The plasmids were extracted from *E. coli* after transformation with the Gateway cloning reaction of *pENTR1A:ScIREG2* into *pDR195*. Lane **5** contains a negative PCR control using water as template. Products were visualized on a 1% agarose gel and sized with New England Biolabs 1kb DNA Ladder.

PCR amplification of *ScIREG2* on extracted plasmids resulted in the expected product (approximately 1500 base pairs) forming in lane 3 and potentially in lane 4. The presence of *ScIREG2* after gateway cloning indicates the reaction was a success and *ScIREG2* was transferred to *pDR195*. The plasmid from lane 3 was used in further cloning because it generated a strong gene-specific PCR product.

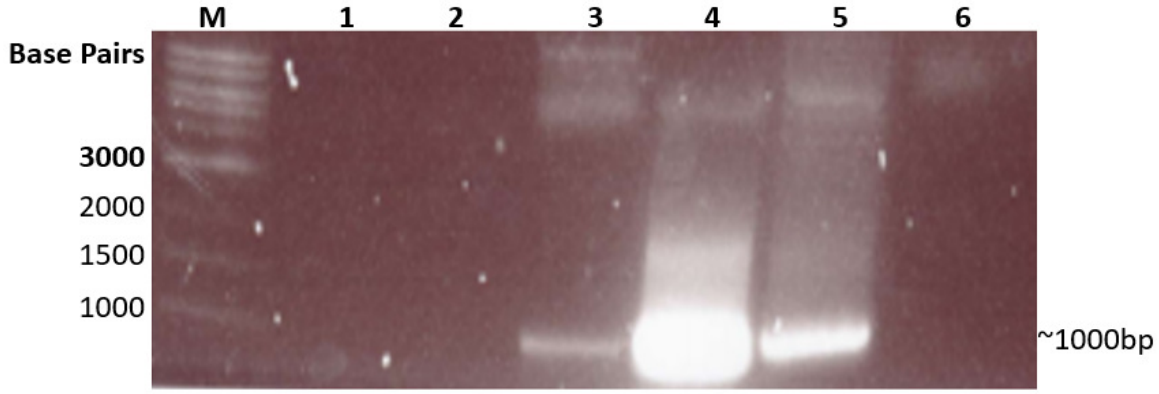

Figure 18**| Amplification of *ScIRT1* from extracted *pDR195* plasmids after gateway cloning.** PCR conducted using Supertherm polymerase with the *ScIRT1* specific primers: *IRT1 FOR* and *IRT1 ECO rev*. Lanes **1 to 5** utilized extracted plasmid as template. The plasmids were extracted from *E. coli* after transformation with the Gateway cloning reaction of *pENTR1A:ScIRT1* into *pDR195*. Lane **5** contains a negative PCR control using water as template. Products were visualized on a 1% agarose gel and sized with New England Biolabs 1kb DNA Ladder.

PCR amplification with *ScIRT1* specific primers on purified plasmids after gateway cloning amplified strong products of the expected size, approximately 1000 base pairs (*ScIRT1* is 1046 base pairs) in lanes 3, 4 and 5. The presence of *ScIRT1* after Gateway cloning indicates the reaction was a success and *ScIRT1* was transferred to *pDR195*. The plasmid DNA used in the PCR reaction run in lane 4 was used for yeast transformation because it demonstrated the strongest amplification of *ScIRT1*.

3.5 Yeast Transformation with *pDR195* Expression Vectors

3.5.1 Confirmation of *zrt1zrt2* Uracil Auxotrophy

Prior to its use in heterologous protein expression experiments, it was necessary to confirm that *zrt1zrt2* was indeed an uracil auxotroph (the strain is a *ura3* mutant) as this is the basis for selection of cells successfully transformed with *pDR195* (which contains the *URA3* gene). Yeast transformed with *pDR195 GTW* should be capable of surviving on uracil deficient media because they can now synthesize uracil while untransformed yeast will not. The efficacy of

this selection method, and the ability of pDR195 to complement the *ura3* mutation, was assessed by culturing untransformed *zrt1zrt2* and *zrt1zrt2* transformed with *pDR195 GTW* on solid media with no uracil present (YNB CSM-uracil) (Figure 19). The lithium acetate transformation method was used to transform yeast competent cells with empty *pDR195 GTW*. Furthermore, the question of whether cells revived from a glycerol stock or cells transferred from another agar plate were the most suitable inoculum source for downstream experiments, was also assessed. This was determined by plating both types on selective media.

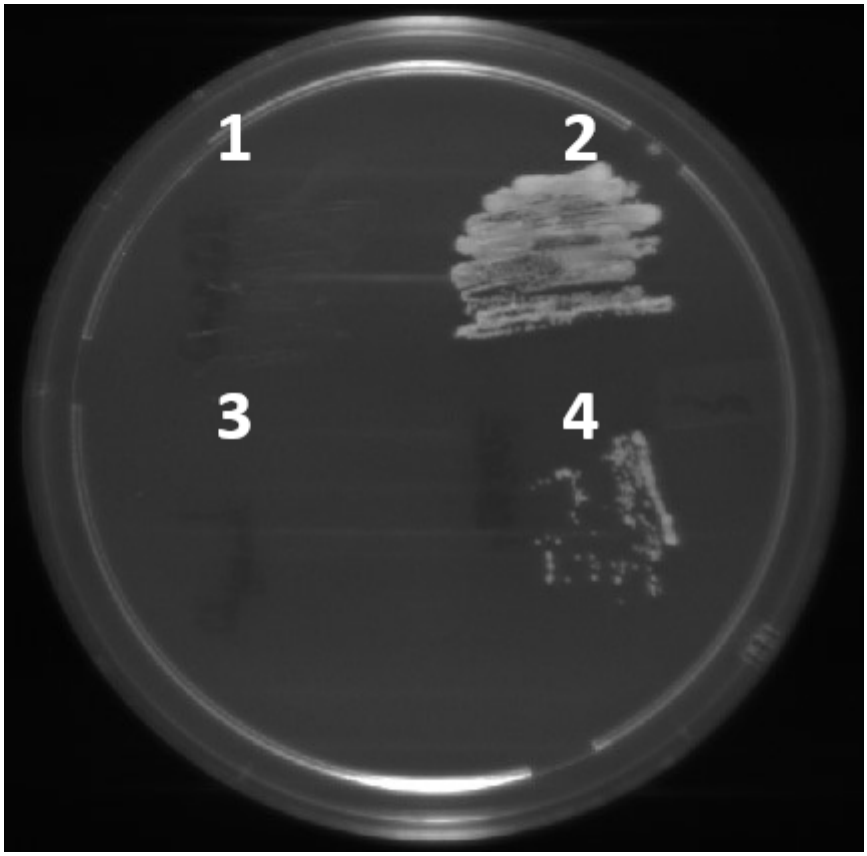

Figure 19**| Growth of *zrt1zrt2* under uracil selection to confirm functionality of selection marker and ability of pDR195 to complement the *ura3* mutation.** Growth on YNB CSM-uracil selective plate after 48 hours after streaking of *zrt1zrt2* inoculum is shown. Section **1** is the growth of untransformed cells streaked from a YPD plate. Section **2** is the growth of cells transformed with *pDR195 GTW* streaked from an YNB CSM-uracil plate. Section **3** is the growth of untransformed cells streaked from a glycerol stock. Section **4** is the growth of cells transformed with *pDR195 GTW* from a glycerol stock.

Analysis of the growth pattern revealed that there is no growth or ability to survive for the untransformed *zrt1zrt2* mutant when plated on uracil deficient media regardless of the inoculum used. In contrast, both inoculum types of the transformed *zrt1zrt2* were capable of growth on the uracil deficient media. The streak for the transformed strain from the solid source exhibits stronger growth than that of the streak from glycerol stock. This may reflect the fact that cells plated from another agar plate are able to grow straight-away while those from a glycerol stock have a longer lag time. Alternatively, the result may just be due to the fact that different numbers of cells were plated. This experiment confirmed the uracil auxotrophy of the *zrt1 zrt2* strain, and the ability of the *pDR195* vector to complement the *ura3* mutation.

3.5.2 Yeast Transformation with *pDR195* Expression Vectors Containing *ScIREG2* and *ScIRT1*

Competent *zrt1zrt2* cells were transformed with *pDR195:ScIREG2* or *pDR195:ScIRT1* (Figure 20). The strain containing the empty *pDR195 GTW* vector was also used to act as a negative control establishing that any changes in Ni sensitivity in the experimental transformants are as a result of activity of the gene of interest and not due simply to the presence of the expression vector. Making use of an untransformed strain as a negative control in the Ni sensitivity assays is not possible because the media used is selective (uracil deficient) to ensure that the experimental transformants retain their expression constructs, so an untransformed strain would perish as shown above (Figure 19). Nevertheless, an untransformed control was used in order to establish the extent of any potential background after transformation. The number of colonies forming for the untransformed control gives an indication of how many false positive colonies will be present in the transformation plates.

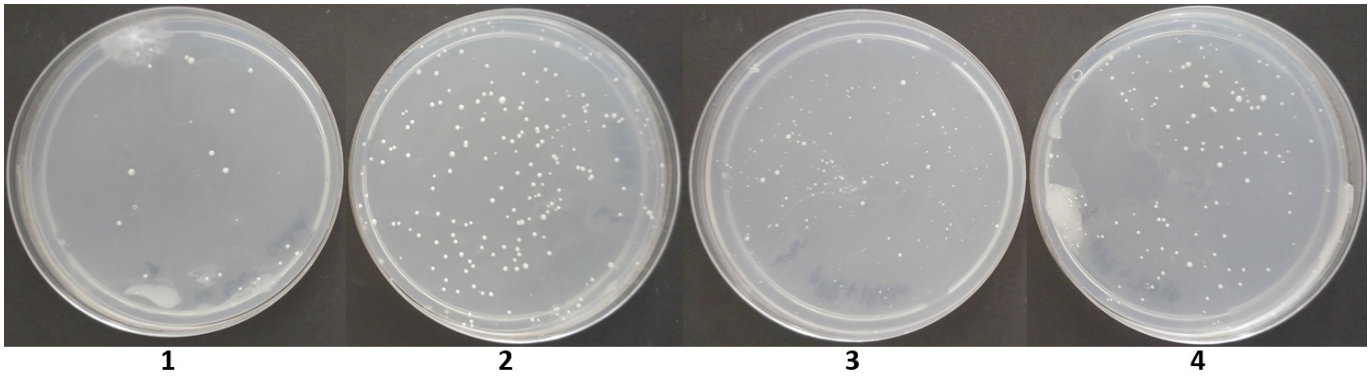

Figure 20**| *zrt1zrt2* transformation plates.** Growth on YNB CSM -uracil selective plates after 48 hours of growth with transformed yeast cells. Plate **1** is a negative control being plated with untransformed yeast. Plate **2** is plated with yeast transformed with the empty vector *pDR195 GTW*. Plate **3** is plated with yeast transformed with the expression vector *pDR195:ScIREG2*. Plate **4** is plated with yeast transformed with the expression vector *pDR195:ScIRT1*.

Transformed colonies are clearly visible as being sharp, discrete, white colonies. The size of the colonies of the transformation with *pDR195:ScIREG2* appear smaller, which might indicate a negative effect of this protein on yeast growth. The number of colonies on each selective plate after inoculation with a *pDR195* vector (with or without insert) is much greater than the number of colonies on the untransformed control plate. This provides evidence that the yeast cells in the colonies were successfully transformed with the respective expression vectors. However, given the presence of a small number of colonies on plate 1, additional confirmation of the presence of the expression constructs in colonies from plates 2-4 was required prior to their use in Ni sensitivity assays.

3.5.3 Yeast Colony PCR to Confirm the Presence of *pDR195* Expression Vectors

In order to confirm the presence of the expression constructs in the transformed yeast, several methods for colony PCR were trialed. The thick cell wall of yeast cells made accessing the expression vector to perform diagnostics problematic. A physical method of denaturation was attempted. This made use of small glass beads and a series of vortex and centrifugation steps to crush the cell walls. However, the resulting extracts were never successfully amplified when used as template in a PCR. It was theorized that even with the use of the glass beads, an insufficient proportion of the transformed yeast cells were lysed to release DNA for PCR amplification. A chemical denaturation

method was investigated and optimized. The method dissolves the yeast cell walls by incubating the cells at high temperatures (95^{o}C) for a long duration (45 minutes) in 40 mM NaOH. The resulting extracts were then used as template in a PCR. In order to confirm the presence of *pDR195 GTW* in the yeast transformants containing the empty vector a set of primers was designed 100 base pairs 5' of the *PMA* promoter and 3' of the *ADH1* terminator, which yielded a product of approximately 2 kb (Figure 21, Lane 1).

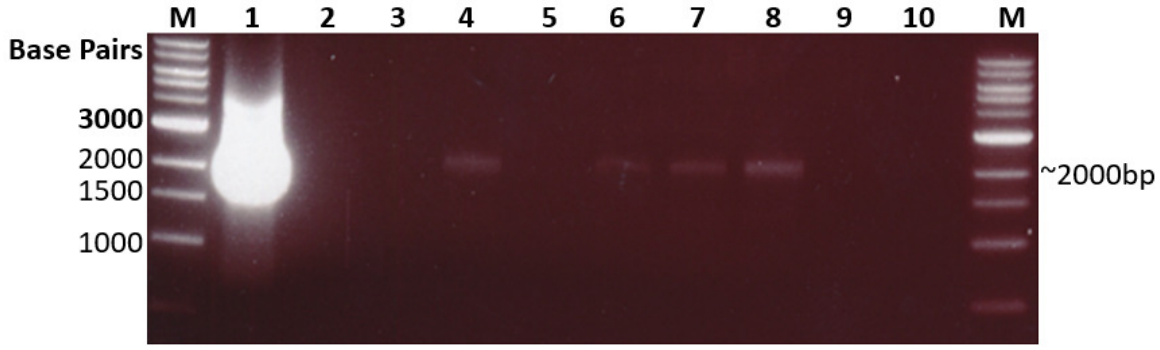

Figure 21**| Amplification of *pDR195* in a yeast colony PCR on transformed *zrt1zrt2* cells.** Supertherm polymerase used for yeast colony PCR using the *pDR195 GTW* specific primers: *pDR195 GTW for* and *pDR195 GTW rev*. Lane **1** is a PCR positive control utilizing purified *pDR195* as template. Lanes **2 to 9** contain yeast colony PCRs where 1 µL of sodium hydroxide digested yeast cells was used as template and each lane represents a different colony. Lane **10** contains a negative PCR control using water as template. Products were visualized on a 1% agarose gel and sized with New England Biolabs 1kb DNA Ladder.

Amplification of the extract after NaOH digestion of yeast *pDR195 GTW* transformants using *pDR195* specific primers resulted in a product being formed at approximately 2000 base pairs in lanes 4, 6, 7, and 8. The size of this product matches the product that is amplified in the positive control which was a PCR directly on the *pDR195 GTW* plasmid (which produced a much stronger product as a result of the template being at a higher concentration and less contaminated than the yeast extract). These results indicated that at least yeast colonies 4, 6, 7 and 8 had been successfully transformed and did contain *pDR195 GTW*. Similar PCR experiments were then carried out on putative *pDR195:ScIREG2* and *pDR195:ScIRT1* yeast transformants (Figure 22 & Figure 23).

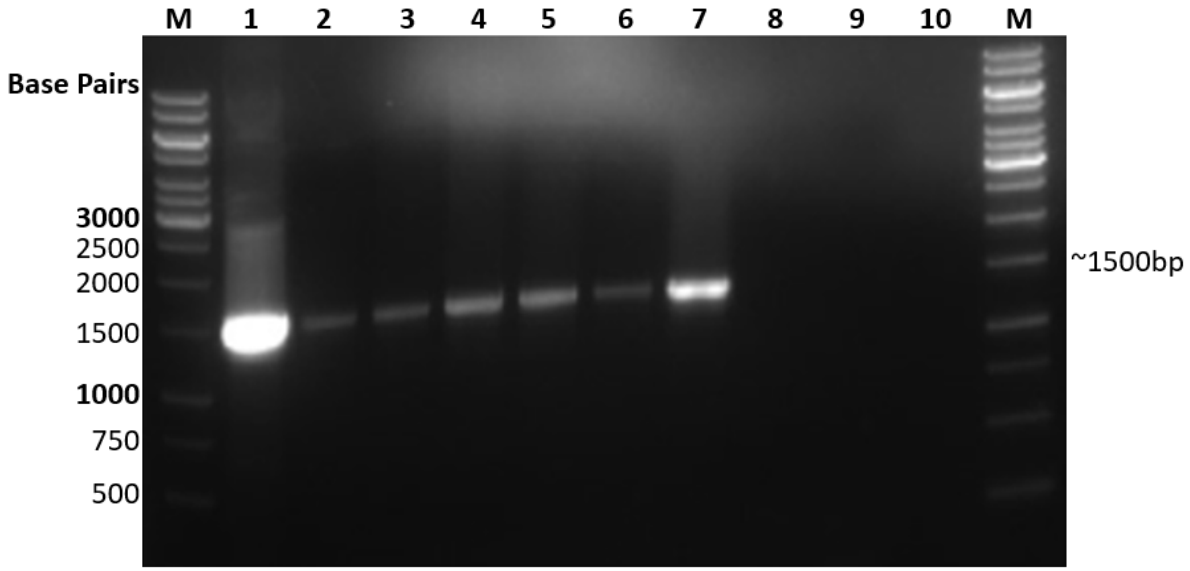

Figure 22**| Amplification of *ScIREG2* in a yeast colony PCR on transformed *zrt1zrt2* cells.** Supertherm polymerase used for yeast colony PCR using the *ScIREG2* specific primers: *IREG FOR NOTI* and *IREG FOR SALI*. Lane **1** is a PCR positive control utilizing dilute purified *pDR195:ScIREG2* as template. Lanes **2 to 9** contain yeast colony PCRs where 1 µL of sodium hydroxide digested yeast cells was used as template and each lane represents a different colony. Lane **10** contains a negative PCR control using water as template. Products were visualized on a 1% agarose gel and sized with Thermo Scientific O'GeneRuler 1kb DNA Ladder.

Amplification of the extract after sodium hydroxide digestion of yeast *pDR195:ScIREG2* transformants using *ScIREG2* gene specific primers resulted in a product being formed that was approximately 1500 base pairs in lanes 2 to 7. The size of the product corresponds with the expected size of *ScIREG2* (1500 base pairs). The colony extracts used in these lanes therefore contain *pDR195:ScIREG2*. These colonies (2 to 7) were thus confirmed to be transformants, and could therefore be used in downstream Ni sensitivity assays.

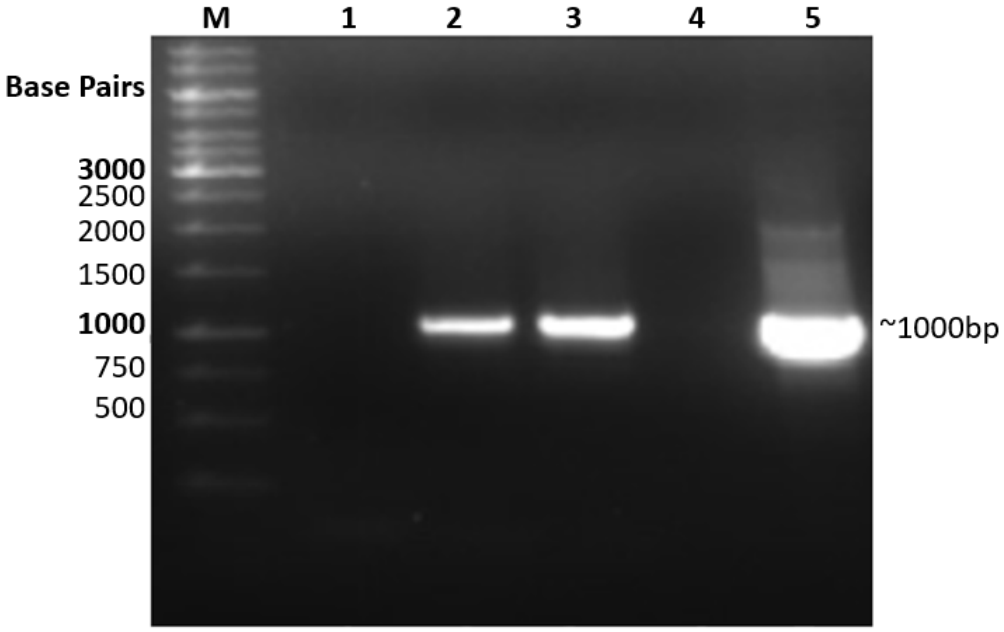

Figure 23**| Amplification of *ScIRT1* in a yeast colony PCR on transformed *zrt1zrt2* cells.** Supertherm polymerase used for yeast colony PCR using the *ScIRT1* specific primers: *IRT1 FOR* and *IRT1 ECO rev*. Lane **1** contains a negative PCR control using water as template. Lanes **2 to 4** contain yeast colony PCRs where 1µL of sodium hydroxide digested yeast cells are used as template and each lane represents a different colony. Lane **5** is a PCR positive control utilizing dilute purified *pDR195:ScIRT1* as template. Products were visualized on a 1% agarose gel and sized with Thermo Scientific O'GeneRuler 1kb DNA Ladder.

Amplification of the extract after NaOH digestion of yeast *pDR195:ScIRT1* transformants using *ScIRT1* gene specific primers resulted in a product being formed that was approximately 1000 base pairs in lanes 2 and 3. The size of the product corresponds with the expected size of *ScIRT1* (1047 base pairs). The colony extracts used in these lanes therefore contain *pDR195:ScIRT1*. These colonies were thus confirmed to be transformants, and so could be used in Ni sensitivity assays.

3.6 Optimization of Ni Sensitivity Assays

Having successfully generated the transgenic yeast containing *pDR195-ScIRT1* and *pDR195-ScIREG2*, the next step was to design an appropriate experimental set-up in which to determine whether this leads to altered susceptibility of the transgenic yeast to exogenous Ni. A critical first step was to determine the Ni sensitivity profile of the control yeast transformed with the empty *pDR195* vector, as this is the baseline against which to determine whether heterologous expression of the transport proteins does indeed have any effect. The optimal experimental setup was researched by examining the literature to determine the common experimental parameters used for Ni sensitivity assays. Particular consideration was given to the published experiments for the Ni transporters *AtIREG2*, *PgIREG* and *AtIRT1* (Merlot et al., 2014; Nishida et al., 2011; Schaaf et al., 2006). Examination of these experiments led to the selection of minimal media (to reduce chelation of Ni by amino acids, especially histidine, a well-known Ni-binding ligand) and a pH of 5 (shown to be necessary to see a Ni transport effect with AtIREG2, consistent with its role as a vacuolar Ni/proton antiporter). It was however necessary to include adenine and tryptophan in the media as the *zrt1zrt2* strain is an auxotroph for these two metabolites in additional to its uracil auxotrophy.

The concentrations of Ni to be used in the sensitivity assays was the most important parameter to consider. This had to be sufficient to ensure that the yeast was exposed to a stressful concentration of Ni to the extent that a visible difference in ability to survive was observable, but could not be excessive to the point at which growth is restricted regardless of yeast genotype. The Ni concentrations used in the published Ni sensitivity assays vary greatly. This suggests that there is no standard experimental setup and that optimization of Ni concentrations is required to generate observable phenotypic differences between transformed and control strains. For example, Schaaf et al. (2006) made use of a concentration gradient of 0 to 1.3mM $NiCl_2$ to demonstrate that AtIREG2 functions as a Ni exporter, however an observable difference between strain survivability was only present at the highest Ni concentration of 1.3mM $NiCl_2$. In contrast, Nishida et al. (2011) simply made use of a 0 µM $NiCl_2$ plate and a plate containing 500 µM $NiCl_2$ to demonstrate that AtIRT1 functions as a Ni importer, while Merlot et al. (2014) observed uptake and export phenotypes at 200 µM and 400 µM $NiCl_2$ for several *Psychotria gabriellae* metal transporters.

3.6.1 Preliminary Ni Sensitivity Assay

The lack of consensus between the published Ni sensitivity assays indicated that the optimum conditions for the assay needed to be determined independently. A preliminary experiment was thus conducted to identify the optimum Ni concentrations to observe a phenotypic difference in Ni sensitivity by plating out yeast transformed with the empty pDR195 GTW vector on minimal media (YNB + Ade + Trp) supplemented with 250, 500 or 750 µM $NiCl_2$ (Figure 24).

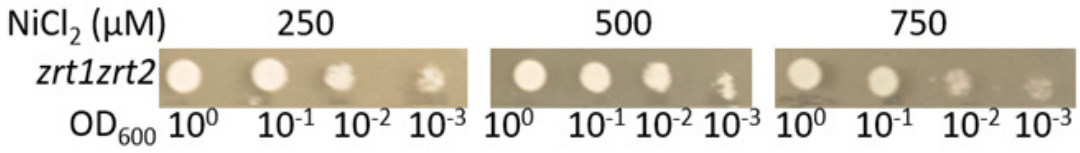

Figure 24**|Ni sensitivity of yeast on minimal media.** *S. cerevisiae zrt1zrt2* transformed with pDR195 GTW were spotted in a serial dilution on MM plates supplemented with 250, 500 or 750 µM $NiCl_2$. Images were taken 28 hours post inoculation after incubation at 30^{O}C.

No apparent difference in the growth was visible when comparing the 250 and 500 µM $NiCl_2$ plates but the growth of

the strain noticeably decreases on the 750 µM $NiCl_2$ plate particularly at the 10^{-2} and 10^{-3} dilutions. Based on this, it was decided that 500 and 750 µM $NiCl_2$ were appropriate Ni concentrations to utilize for Ni initial sensitivity assays on transgenic yeast. These conditions were chosen because heterologous expression of the transgene was expected to change the growth phenotype of *zrt1zrt2* observably. The expression of a Ni importer would increase *zrt1zrt2* susceptibility to Ni toxicity causing retarded growth of the yeast at the lower 500 µM $NiCl_2$ concentration when compared to the growth of the negative control. In contrast, an expressed Ni exporter would result in the transgenic yeast demonstrating resistance to Ni toxicity and so stronger growth on the higher 750 µM $NiCl_2$ concentration than the negative control strain.

Due to the difference in growth being negligible when comparing the 250 and 500 µM $NiCl_2$ plates, the 250 µM $NiCl_2$ concentration was not used in subsequent Ni sensitivity assays. Rather, a 0 µM $NiCl_2$ plate was included as a control to determine whether the expression of the transgene had a deleterious effect on survivability of the strain irrespective of Ni toxicity. The growth on the 0 µM $NiCl_2$ plate should be identical between all the transgenic yeast so differences in growth indicate a problem with the expression of the gene or inconsistencies in the inoculum.

While differences in growth were visible in this preliminary Ni sensitivity assay, an investigation was undertaken to determine if a change in the incubation duration post-inoculation would cause a more discernable difference in survivability being observed. To achieve this, a Ni sensitivity assay was set up using the transgenic yeast on uracil deficient, Ni supplemented media and images of the growth were taken after 24 and 48 hours (Figure 25). Additionally, the experiment was scaled up with triplicates of each inoculated strain being included. The triplicates were independent biological repeats, being cultured from different colonies on the transformation plate (additional transformants having been obtained for *ScIRT1*). The use of replicates allowed for more certainty when comparing different sensitivity phenotypes between the strains, providing all three independent transformants display the same phenotype.

3.6.2 Ni Sensitivity Assays in Triplicate

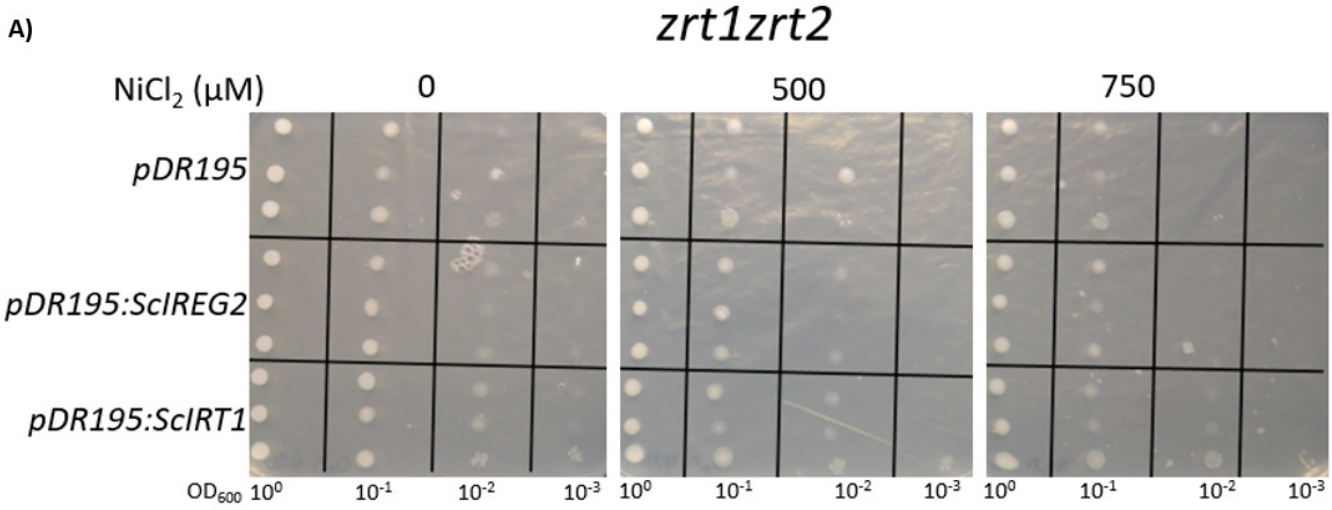

B)

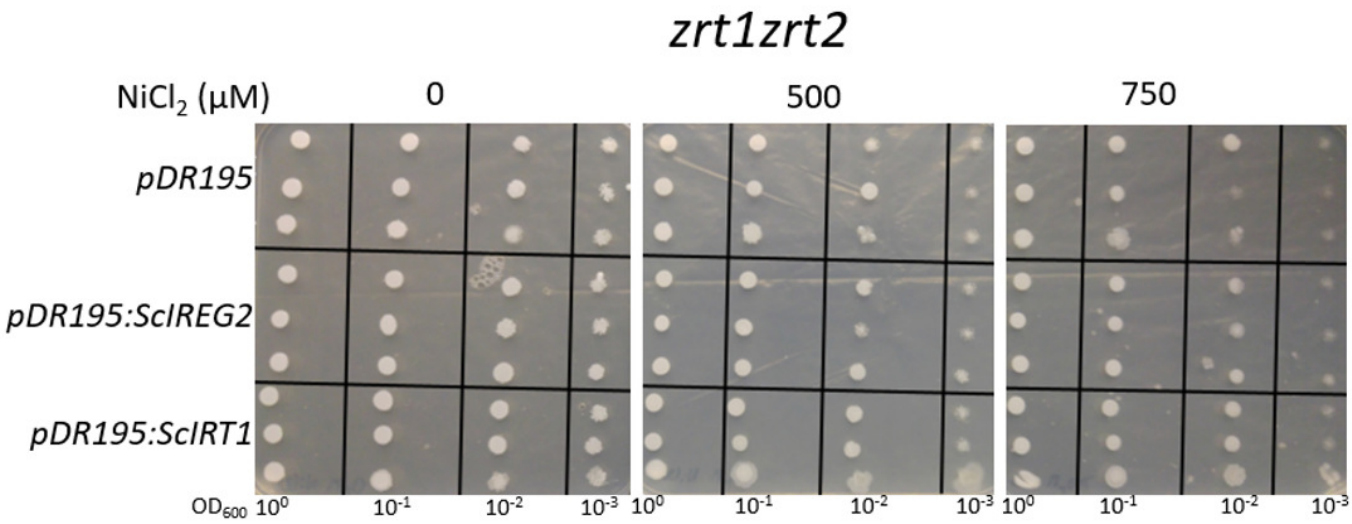

Figure 25**|Ni sensitivity of transformed *zrt1zrt2* on minimal media in triplicate.** *S. cerevisiae zrt1zrt2* strains transformed with *pDR195 GTW*, *pDR195:ScIREG2* and *pDR195:ScIRT1* spotted in a serial dilution on MM YNB + Ade + Trp - ura plates supplemented with 0, 500 or 750 µM $NiCl_2$. Inoculum was generated using 3 independent transformants. Images were taken 24 hours post inoculation in **A** and 48 hours post inoculation in **B** after incubation at 30^{O}C.

The transgenic yeast survivability in the Ni sensitivity assay over the time course was examined. The growth of the strains at both time points was comparable at the lowest dilutions on the 0 µM $NiCl_2$ plates which suggests that expression of the transgenes was not interfering with the ability of *zrt1zrt2* to survive when no Ni was present. The growth of all the strains appeared saturated after 48 hours because growth was visible at all dilutions even on the 750 µM $NiCl_2$ plate. No difference in growth between the strains was discernable after this incubation time.

An inspection of the yeast growth after 24 hours of incubation showed clear effects of Ni toxicity on all strains because all dilutions of the strains form visible growth on the 0 µM $NiCl_2$ plate and their ability to survive gradually decreased with the increasing Ni concentration. There was no significant difference in the observed ability to survive of the *pDR195:ScIREG2* strain compared to the negative control. However, there is no growth observed at the 10^{-3} dilution for any of the strains on the Ni supplemented plates except for the 3rd replicate of the *pDR195:ScIRT1* transformed strain. This observation provided initial evidence that the *ScIRT1* transgene might confer a Ni resistance phenotype to *zrt1zrt2* which was also supported by observing the growth of this strain at the 10^{-2} dilution on the 750 µM $NiCl_2$ plate. Here all three independent *pDR195:ScIRT1* showed clear growth, while faint growth was only observed at this dilution for one of the empty vector controls.

However, the observation of the resistance phenotype of the *pDR195:ScIRT1* was marred by general inconsistencies in growth patterns of all of the strains. These confounding variabilities interfered with the identification of a convincing result. Only one of the *pDR195:ScIRT1* transformed replicates survived at the 10^{-3} dilution on the 500 µM $NiCl_2$ plate and some of the plasmid-only control replicates exhibited growth at the 10^{-2} dilution on the Ni supplemented plates. It was deduced that the source of the inconsistencies in growth patterns between the replicates could have been as a result of technical error in plating causing variable amounts of inoculum being used. This theory was supported by the fact that there was also variation in colony size and opacity between the replicates

of each strain at the higher dilutions on the 0 µM $NiCl_2$ plate. This experiment produced an encouraging observation about the activity of ScIRT1 but the failure to produce an undisputable result caused by technical error necessitated a repeat of the experiment with greater emphasis on ensuring consistency in the inoculation steps (Figure 26).

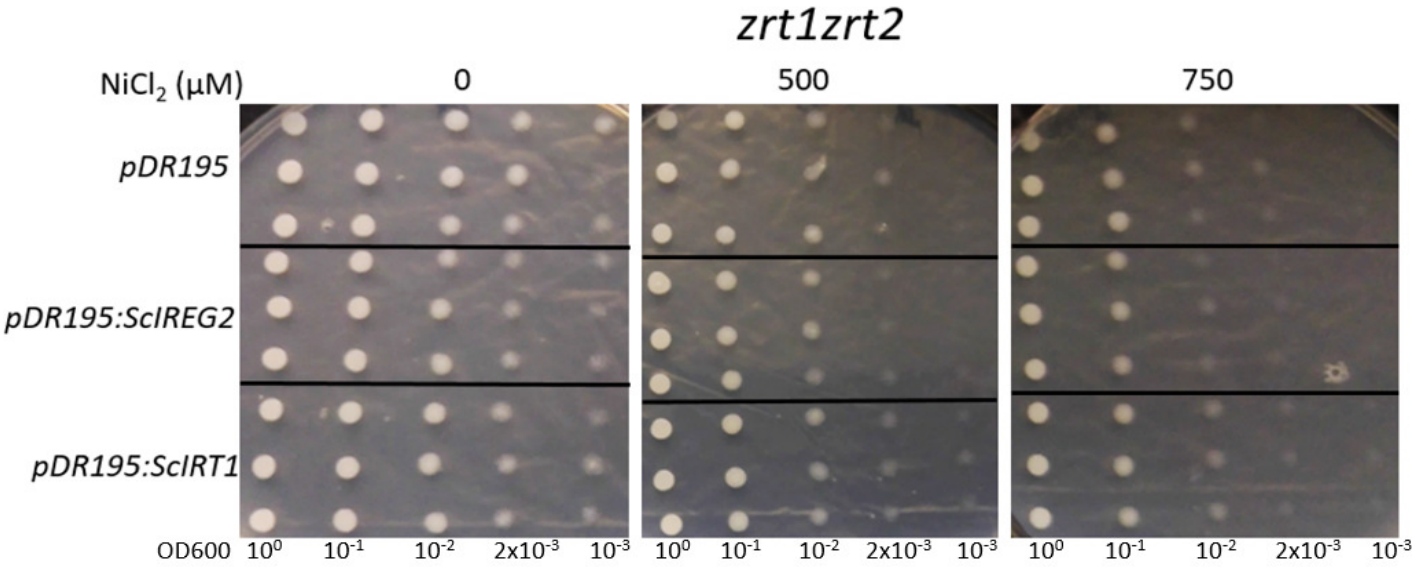

Figure 26**|Ni sensitivity of transformed *zrt1zrt2* on minimal media in triplicate repeated.** *S. cerevisiae zrt1zrt2* strains transformed with *pDR195 GTW*, *pDR195:ScIREG2* and *pDR195:ScIRT1* spotted in a serial dilution on MM YNB + Ade + Trp - ura plates supplemented with 0, 500 or 750 µM $NiCl_2$. Inoculum was generated using 3 independent transformant colonies from each transformation plate. Images were taken **48** hours post inoculation after incubation at 30^{O}C.

Observation of the yeast growth in this experiment after 48 hours revealed that there was a clear effect of Ni toxicity on replicates of all strains because the growth at the higher dilutions was strongest on the 0 mM $NiCl_2$ control plate and gradually decreased as the Ni concentration increased. The incubation time and Ni concentration of the sensitivity assay appeared ideal because there was a clear effect of Ni toxicity and the growth was not saturated. The consistency of growth between replicates of the same yeast genotypes was far superior to that in the previous experiment because the growth patterns were very similar between replicates. The growth of all replicates of all strains on the 0 mM $NiCl_2$ plate was remarkably similar providing confidence the transgenes caused no effect on yeast growth of in the absence of Ni. There was no obvious difference between the growth patterns of the *pDR195:ScIREG2* transformed replicates and the empty vector controls. It was possible that there was a small amount of visible growth at the 10^{-3} dilution on the 500 µM $NiCl_2$ plate for the *pDR195:ScIREG2* transformants where none was visible at this dilution for the empty vector controls but this difference was not convincing. Therefore, making confident conclusions about the activity of ScIREG2 using this data is difficult.

In contrast, there appeared to be a visible, consistent difference in growth pattern between the *pDR195:ScIRT1* transformed strains and the empty vector replicates. The *pDR195:ScIRT1* replicates were capable of forming visible growth at the 10^{-3} dilution on the 500 µM and 750 µM $NiCl_2$ plates when no growth was visible for this dilution on these plates for the empty vector controls. This is consistent with the results obtained in Figure 25 and suggest that heterologous expression of *ScIRT1* results in reduced susceptibility to Ni, consistent with it

acting as a Ni export protein or as a vacuolar importer when expressed in yeast.

To obtain further evidence that ScIRT1 does reduce Ni sensitivity in yeast, it was decided to compare the effect of heterologous expression of this gene with that of a transport protein previously demonstrated to reduce Ni sensitivity, AtIREG2 (Schaaf et al. 2006) (Figure 27). In order to do this, it was necessary to clone *AtIREG2* to generate a *pDR195-AtIREG2* vector for heterologous expression in yeast.

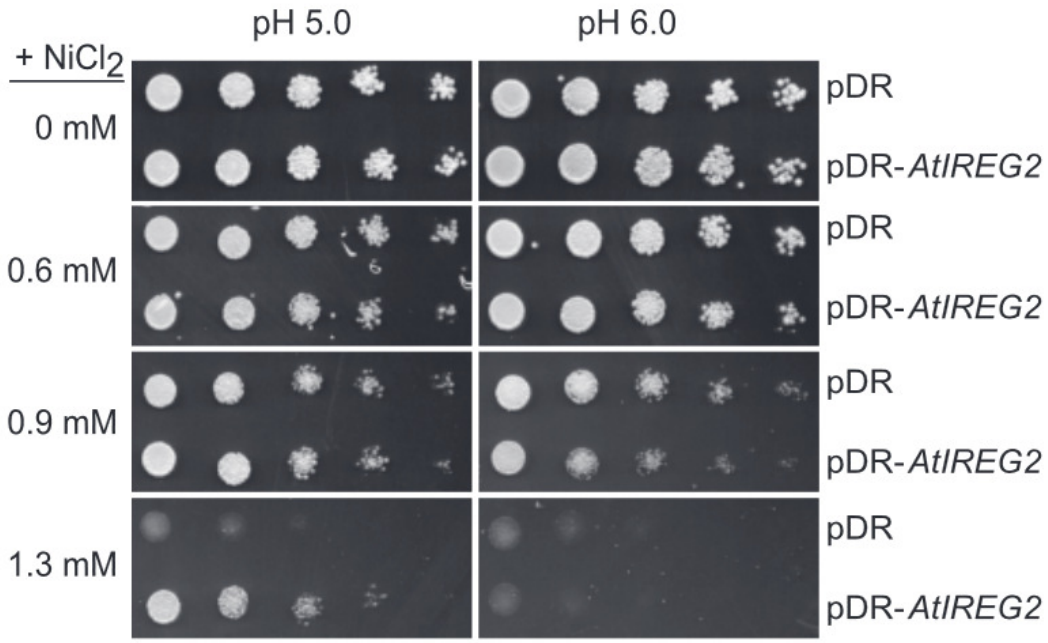

Figure 27**|Schaaf et al. (2006) Ni sensitivity assay of AtIREG2.** *cot1 S. cerevisiae* strains transformed with *pDR195* and *pDR195:AtIREG2* spotted in a serial dilution on a uracil-free yeast nutrient medium supplemented with $NiCl_2$.

3.7 Generation of *pDR195:AtIREG2* Expression Vector

Initial cloning attempts for *AtIREG2* proved problematic because PCRs failed under various conditions to amplify the product using *AtIREG2* specific primers on *A. thaliana* cDNA received from colleagues. Analysis of the annotations for *AtIREG2* on The *Arabidopsis* Information Resource revealed that the one channel array for RNA data of *AtIREG2* had an average signal intensity of 100.203 with a standard deviation of 2.873. According to colleagues with experience in working with *A. thaliana*, this is a relatively low expression level compared to other *Arabidopsis* genes. An experiment was therefore designed to induce the expression of *AtIREG2* in *A. thaliana* so that RNA could be extracted to acquire cDNA with a significantly higher amount of *AtIREG2* transcript for use as template in a PCR for cloning purposes. An Electronic Fluorescent Pictograph was retrieved for *AtIREG2* to inform on the tissue type best suited for extraction of high concentrations of *AtIREG2* (Figure 28).

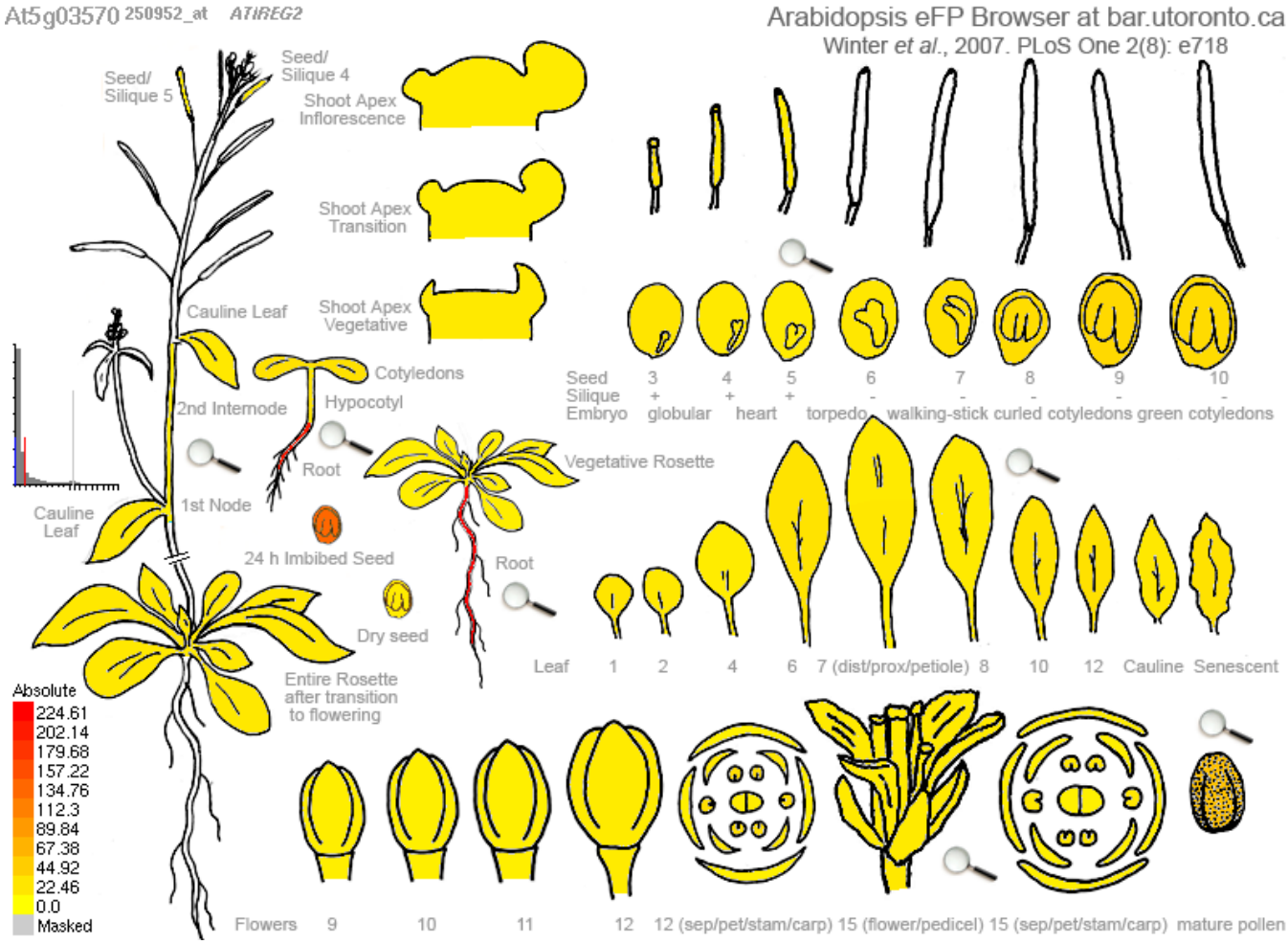

Figure 28|**Electronic Fluorescent Pictograph for AtIREG2 expression. Graphical representation of *A. thaliana* expression of *AtIREG2* based off microarray data (http://www.bar.utoronto.ca/).**

The eFP Browser result showed that *AtIREG2* is expressed at low levels throughout the plant's life cycle in most tissue types but is only expressed at high levels in seedling roots and imbibed seed. For optimum concentrations of *AtIREG2* template to be isolated, RNA was extracted from seedling root tissue after the plants were exposed to iron deficiency stress. This is because *AtIREG2* is upregulated in response to iron deficiency for vacuolar sequestration of Ni inadvertently taken up by AtIRT1 (Schaaf et al., 2006). The Col-0 seedlings were exposed to iron deficiency stress by germinating them on complete plant nutrient media for 3 weeks and then transferring them to plant nutrient media lacking supplemental iron as described in the methods. RNA was then extracted from the root tissue of the induced seedlings and cDNA was synthesized. The integrity of the extracted cDNA was then determined by doing a PCR using primers to an *A. thaliana* house-keeper gene, *SAND* (AT2G28390) that is expressed at a constant level in *Arabidopsis* tissue regardless of the conditions (Figure 29).

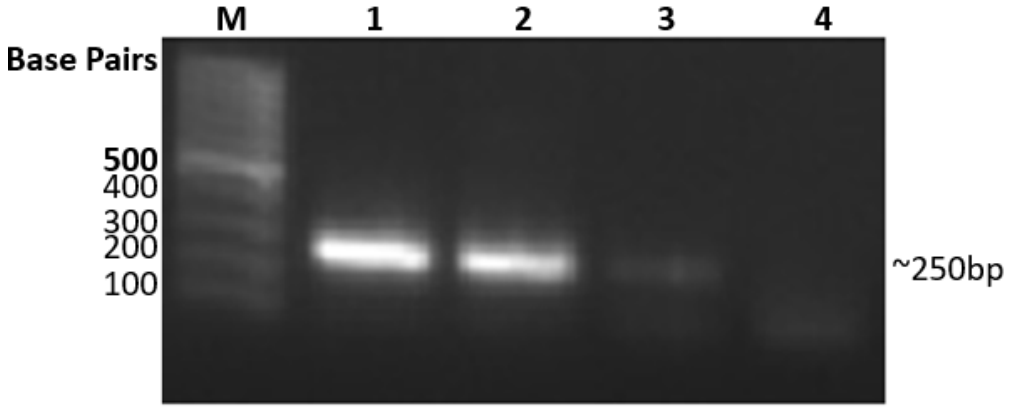

Figure 29**| Confirmation of integrity of synthesized *A. thaliana* cDNA.** A PCR was conducted using *SAND* primers (housekeeper) and Supertherm polymerase to check for successful synthesis of cDNA. Lane **1** contained a positive PCR control using known cDNA from Lee Cacket (University of Cape Town) as template. Lane **2** contained synthesized cDNA undiluted as template. Lane **3** contained diluted cDNA 1:10 as template. Lane **4** contains a negative PCR control using water as template. Products were visualized on a 2% agarose gel and sized with Thermo Scientific O'GeneRuler 100bp DNA Ladder.

Analysis of the amplification of *SAND* from the synthesized *AtIREG2*-induced cDNA revealed that the expected product of a 244 base pair fragment was produced at comparable intensity to the known high quality, undiluted cDNA of a peer. The amplification of SAND from the synthesized cDNA revealed that the cDNA was intact and an attempt could be made to amplify *AtIREG2* from this cDNA (Figure 30).

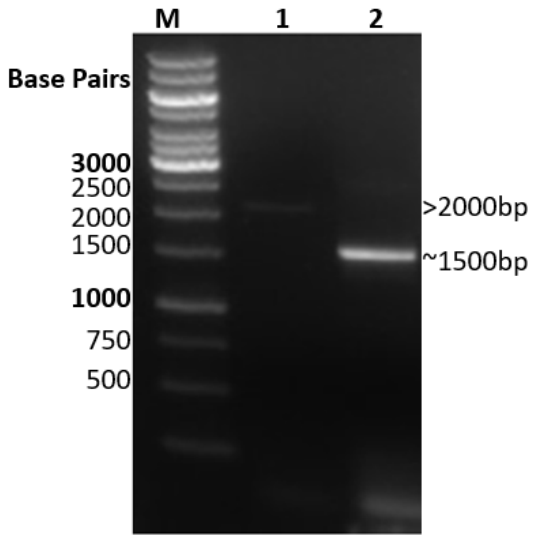

Figure 30**| Amplification of *AtIREG2* from *A. thaliana* DNA.** A PCR amplification of *AtIREG2* using Supertherm polymerase using the *AtIREG2* specific primers: *A.IREG BAM for* and *A.IREG ECO rev* on various templates. In lane **1** *A. thaliana* genomic DNA was used as template. In lane **2** *A. thaliana* cDNA was used as template. Products were visualized on a 1% agarose gel and sized with New England Biolabs 1kb DNA Ladder.

The PCR using Supertherm polymerase using *A. thaliana* genomic DNA as template in lane 1 amplified a faint fragment which is slightly larger than 2000 base pairs. This corresponds to the predicted 2080 base pair size of genomic *AtIREG2*. The primers were therefore capable of amplifying *AtIREG2*. The reaction in lane 2 formed a product at approximately 1500 base pairs which corresponds to the predicted size of the coding sequence of *AtIREG2* (1539 base pairs).

3.7.1 Cloning of *AtIREG2*

The *AtIREG2* was amplified from cDNA using high fidelity polymerase and was cloned into pENTR1A using *Bam*HI and *Eco*RI and the transformants were subjected to colony PCR (Figure 31).

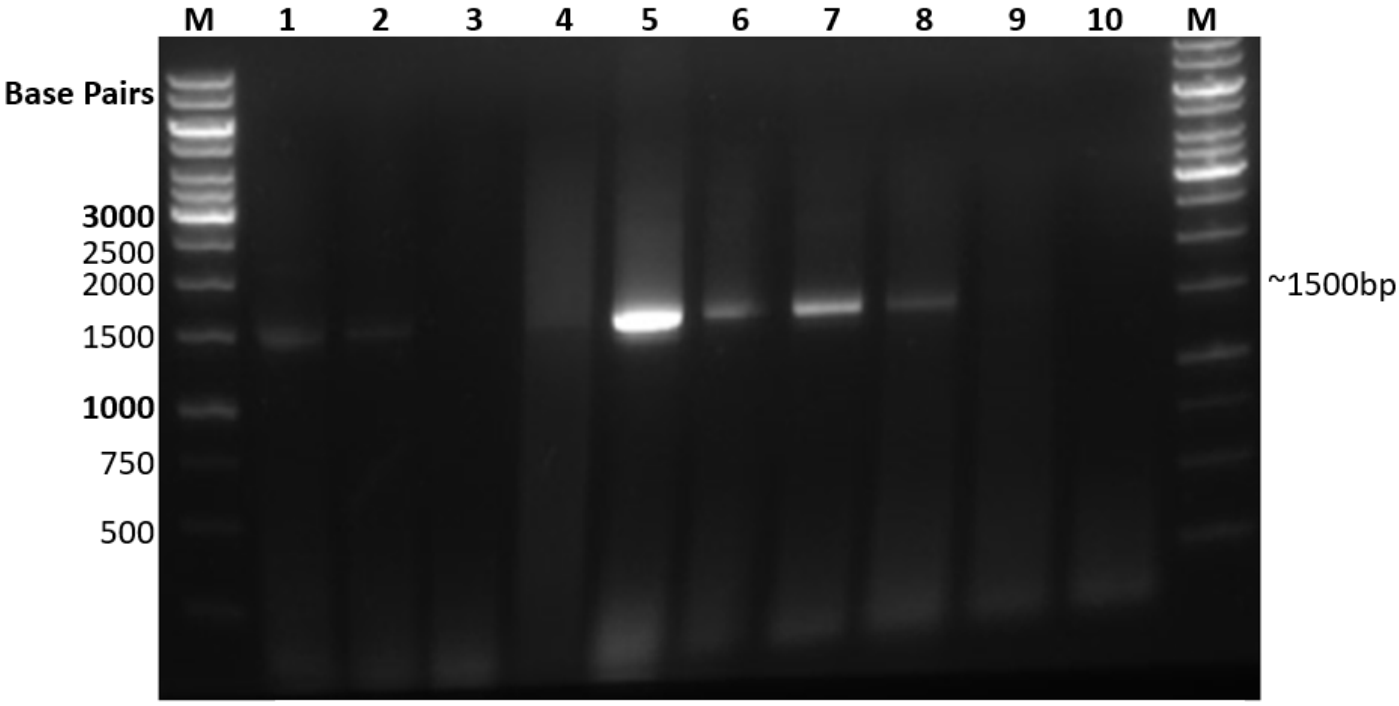

Figure 31**| Amplification of *AtIREG2* from *E. coli* colonies transformed with an *AtIREG2* and *pENTR1A* ligation.** PCR conducted using Supertherm polymerase using the *AtIREG2* specific primers: *A.IREG BAM for* and *A.IREG ECO rev* on *E. coli* colonies as templates. Lane **1** contains a PCR positive control using 1:1000 diluted *AtIREG2* PCR product as template. Lanes **2 to 9** contain *E. coli* colony PCR reactions. Lane **10** contains a negative PCR control using water as template. Products were visualized on a 1% agarose gel and sized with Thermo Scientific O'GeneRuler 1kb DNA Ladder.

The colony PCR resulted in amplification of a fragment of approximately 1500 base pairs being produced for the majority of colonies tested. This matches the 1539 base pair expected size of *AtIREG2.* The ligation and transformation was therefore successful for the colonies in lane 2, 5, 6, 7, and 8 with 5 and 7 exhibiting particularly strong positive results. A diagnostic digest using *Bam*HI and *Eco*RI was performed on the extracted plasmids (Figure 32).

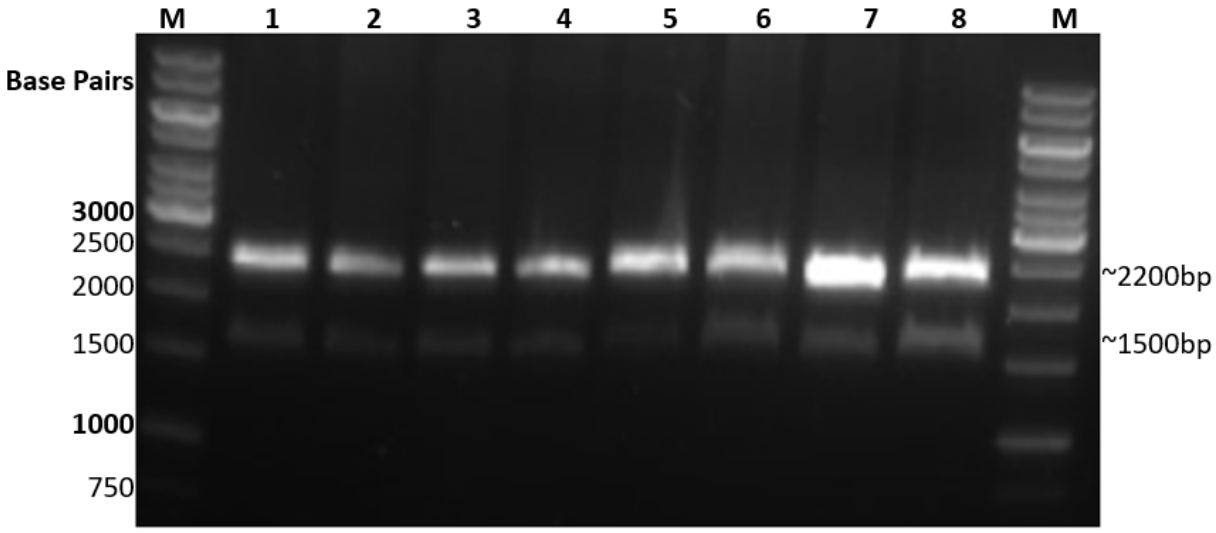

Figure 32**| Double digest of extracted *pENTR1A:AtIREG2* from *E. coli.*** Lanes **1 to 8** contain 0,5µg extracted plasmid from *E. coli* transformation with *pENTR1A:AtIREG2* subjected to complete digestion with *Bam*HI and *Eco*RI. Products were visualized on a 1% agarose gel and sized with New England Biolabs 1kb DNA Ladder.

It is clear in all the digests that a banding pattern of approximately 2200 and 1500 base pair fragments results. This pattern is consistent with the expected size for the backbone (slightly larger than 2200 base pairs) and the 1539 base pair insert of *AtIREG2*. This result provides evidence that the ligation and transformation were successful.

3.7.2 *pENTR1A:AtIREG2* Sequencing

To confirm that no *Taq* errors had been introduced into the sequence, the extracted plasmid from lane 6 of the double digestion was sequenced using *M13* primers (Figure 33).

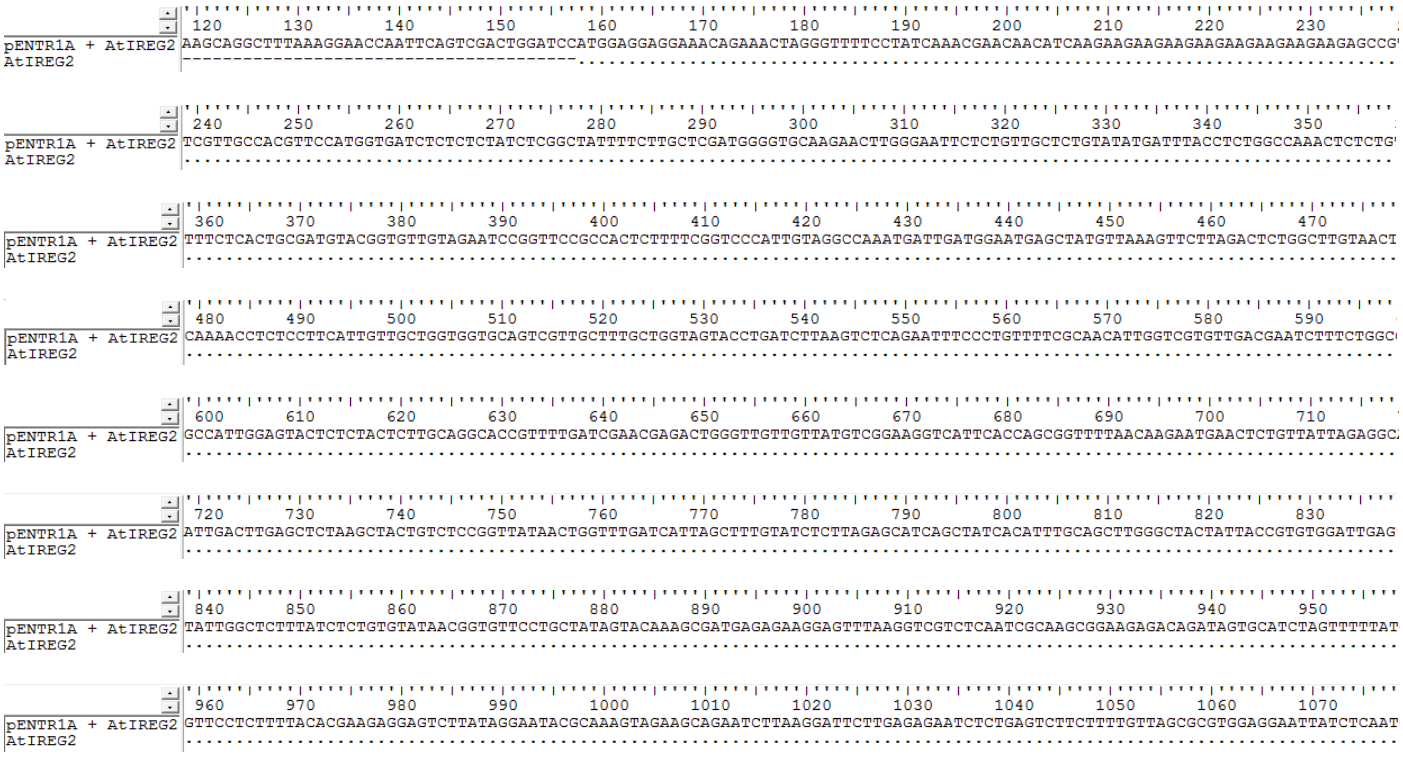

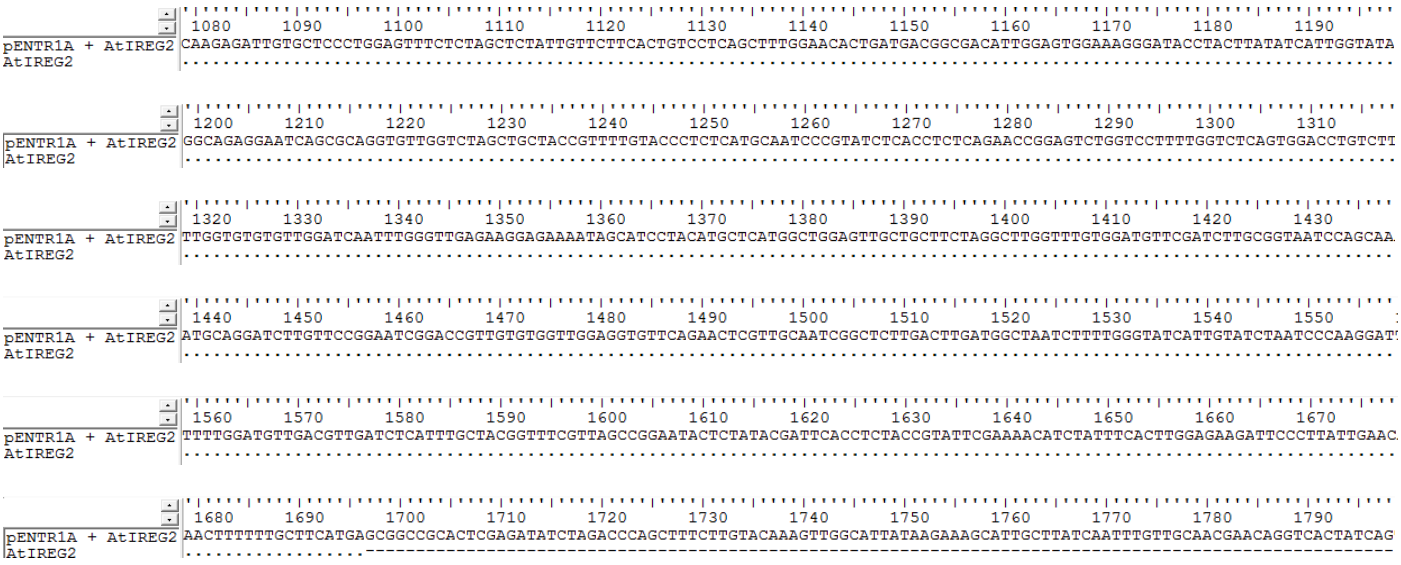

Figure 33**|ClustalW nucleotide multiple sequence alignment in BioEdit of cloned *AtIREG2* to the full length *AtIREG2* sequence acquired from The *Arabidopsis* Information Resource.**

The generated sequencing reads provided a 100% nucleotide identity to the annotated *AtIREG2* coding sequence on The *Arabidopsis* Information Resource. *AtIREG2* was therefore definitively cloned into *pENTR1A* without the introduction of any sequence errors, and so this plasmid was used in a gateway cloning reaction to transfer *AtIREG2* to *pDR195 GTW* for expression analysis.

3.7.3 *pENTR1:AtIREG2* Gateway Cloning

AtIREG2 was gateway cloned into *pDR195 GTW* and the presence of *AtIREG2* after gateway cloning was determined by using the extracted plasmids as template in a PCR using *AtIREG2* specific primers (Figure 34).

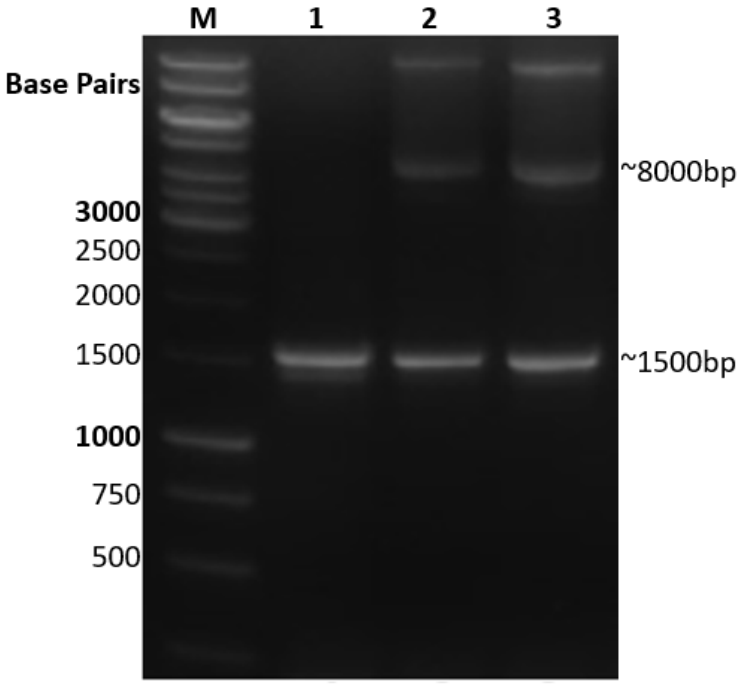

Figure 34**| Amplification of *AtIREG2* from extracted *pDR195* plasmids after gateway cloning.** PCR conducted using Supertherm polymerase using the *AtIREG2* specific primers: *A.IREG BAM for* and *A.IREG ECO rev*. Lane **1** contains a PCR positive control using 1:100 diluted *pENTR1A*:*AtIREG2* as template. In lanes **2** and **3** extracted, 1:10 diluted plasmid was used as template. The plasmids were extracted from *E. coli after* transformation with the Gateway cloning reaction of *pENTR1A:AtIREG2* into *pDR195*. Products were visualized on a 1% agarose gel and sized with Thermo Scientific O'GeneRuler 1kb DNA Ladder.

The amplification of the extracted plasmids after gateway cloning of *pENTR1A:AtIREG2* into *pDR195 GTW* using *AtIREG2* specific primers yielded a product at approximately 1500 base pairs which corresponds to the expected size of the 1539 base pair *AtIREG2* coding sequence. Other very large bands appear at approximately 8 kilo-bases in the experimental reactions. These are likely to be the template plasmids visible on the gel because only a minor dilution of 1:10 of the extracted plasmids was used. This experiment confirmed that *pDR195:AtIREG2* had been successfully generated and so could be used to transform *S. cerevisiae zrt1zrt2* for use as a positive control in the yeast Ni sensitivity assays.

The *pDR195:AtIREG2* construct was transformed into *S. cerevisiae zrt1zrt2* for use in Ni sensitivity assays. Attempts to conduct the full-scale experiment were made but it became clear that in the time taken to clone *AtIREG2*, it was no longer possible to grow the yeast strains on yeast nutrient broth minimal media supplemented with Ade and Trp. The untransformed strain had also become incapable of surviving on this media when it was supplemented with uracil proving that the failure to survive was as a result of the yeast growth requirements not being met and not as a result of activity of the expression vector or uracil selection. Attempts to restore growth by changing water supply, pH and preparing new Ade and Trp supplements were made but to no effect, and no satisfying explanation for the change in yeast growth found.

Time constraints necessitated that an alternative experimental setup be investigated that did not involve the culturing of yeast on minimal media because this had become problematic. Eide et al. (1996) assayed *AtIRT1* on complete media (CSM) plates, and we confirmed that our strains were able to grow on CSM-Ura plates. However, the presence of amino acids, especially His, which can bind to Ni, meant that it was necessary to determine a suitable Ni concentration for these assays on such plates.

3.8 CM Ni Sensitivity Assays

An initial investigation into the optimum Ni concentrations for use in Ni sensitivity assays on CSM was conducted by plating untransformed *zrt1zrt2* on a very broad Ni concentration range of 200 µM, 1.5 and 8 mM $NiCl_2$ (Figure 35). These concentrations were selected because intuitively the Ni concentration used in complete media should be higher than the concentrations used on minimal media due to the inclusion of histidine (and other potential Ni-binding ligands).

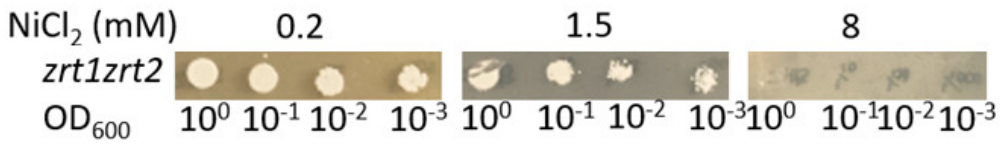

Figure 35**|Ni sensitivity of untransformed yeast on complete media.** Untransformed *S. cerevisiae zrt1zrt2* strains spotted in a serial dilution on CSM + Ura plates supplemented with Ni. Images were taken 48 hours post inoculation after incubation at 30^{O}C. Scratches in colonies are as a result of picking done for further culture after Ni sensitivity assay.

There was no observable growth at any dilution after being plated on the 8mM $NiCl_2$ plate, while growth was clearly viable at the lower concentrations of Ni. It was clear that it was possible to observe the Ni sensitivity phenotype on the complete media despite the presence of histidine achieved by utilizing a sufficiently high concentration of Ni. There does appear to be an effect of Ni toxicity when comparing the 0.2 mM and 1.5 mM $NiCl_2$ plates because the size of the growth formed at the 10^{-1}, 10^{-2} and 10^{-3} dilutions on the 1.5 mM $NiCl_2$ plate was smaller than the growth at the same dilution on the 0.2 mM $NiCl_2$ plate. 1.5 mM $NiCl_2$ is therefore a good candidate for a Ni concentration to be used in Ni sensitivity assays on complete media because it causes a decrease in the strains' survivability but does not cause complete cell death, ensuring that both the sensitivity and resistance phenotypes would be visible at this concentration. A 0 mM $NiCl_2$ plate was used to replace the 0.2 mM $NiCl_2$ plate to control for toxicity of the transgene in the absence of Ni. Based on the growth of the untransformed strain at 1.5 mM $NiCl_2$ it was decided that the slightly higher Ni concentrations of 2 and 2,5 mM $NiCl_2$ were to be included in the range to increase the Ni toxicity and its effects.

3.8.1 Complete Media Ni Sensitivity Assay Utilizing Positive and Negative Control Strains

An experiment was conducted to compare the positive (*pDR195:AtIREG2*) and negative (*pDR195*) transformed strains over this Ni range to establish if a change in yeast Ni sensitivity could be detected (Figure 36). The positive control expressing *AtIREG2* was expected to exhibit increased resistance to Ni toxicity. The observable difference in phenotype needed to be detected in order to confirm that the experimental setup was correct and that conducting the full-scale experiment with the experimental strains was worthwhile.

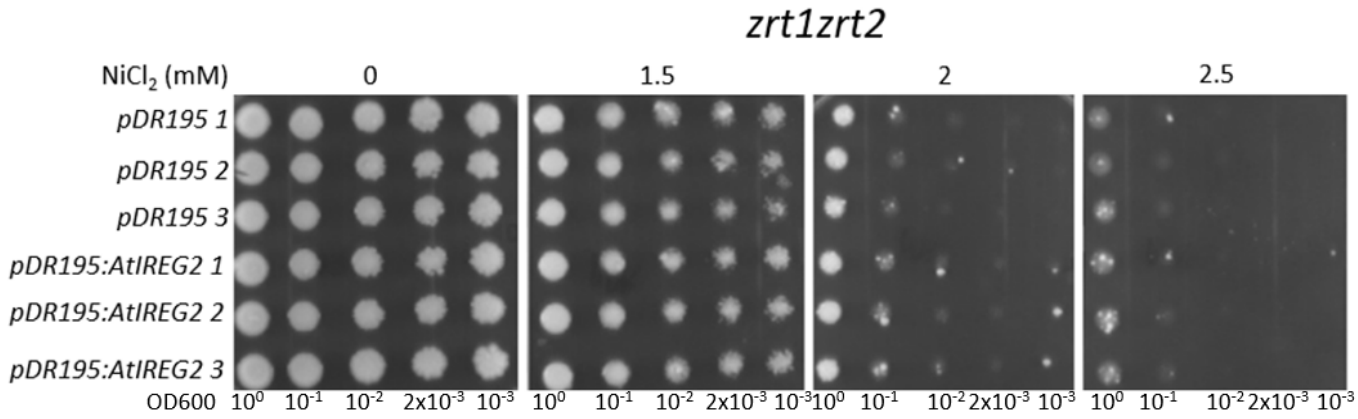

Figure 36**|Ni sensitivity of transformed *zrt1zrt2* on complete media in triplicate.** *S. cerevisiae zrt1zrt2* strains transformed with *pDR195 GTW* (negative control) and *pDR195:AtIREG2* (positive control) spotted in a serial dilution on CSM -ura supplemented with Ni. Inoculum was generated using 3 independent transformants. Images were taken using a Syngene Gbox with a Cybertech 220 V 50 MHz Camera with optics using an upper white light 4 days' post inoculation after incubation at 30^{O}C.

The growth of the yeast strains in the Ni sensitivity assay was observed over a period. It was found that there was minimal difference in the growth pattern between the positive and negative controls after the usual 48-hour incubation period. After 4 days of incubation the growth on the 0 mM $NiCl_2$ plate was exactly the same for all the replicates of both the positive and negative control strains. The colonies were saturated resulting in them appearing a similar size throughout the dilution series but the dilution effect was clear on the Ni supplemented plates. All *pDR195:AtIREG2* transformed replicates at the 10^{-3} dilution on the 2 mM $NiCl_2$ plate consistently formed visible growth while the empty *pDR195 GTW* transformed controls did not have any detectable growth under these conditions. This is a promising experimental result for the setup of the Ni sensitivity assay because it is the expected result for a yeast strain expressing *AtIREG2*. However, it is marred by the fact that no growth is visible for the *pDR195:AtIREG2* replicates at the lower dilution of 1/500 on the 2 mM $NiCl_2$ plate. This is problematic because the inoculum at this dilution is double the concentration used at the 10^{-3} dilution where growth is consistently seen but no growth is detectable for any of the replicates at 1/500 despite this increase in concentration. In the undiluted spots on the 2.5 mM $NiCl_2$ plate it can be argued that the visible growth for the *pDR195:AtIREG2* replicates is also generally larger and more visible than the growth demonstrated by the empty vector control replicates.

Based on the results of this experiment it was determined that it would be worthwhile to conduct the Ni sensitivity assay in full-scale with the experimental strains and the controls in triplicate despite the problems in detecting a significant difference in growth pattern between the positive and negative controls (Figure 37). It was also decided that the inclusion of an intermediate Ni concentration would be appropriate between the 1.5 mM and 2 mM $NiCl_2$ plates because the growth pattern of both strains goes from saturated (largely unaffected by Ni toxicity) on the 1.5 mM $NiCl_2$ plate to very stressed on the 2 mM $NiCl_2$ plate where growth was minimal for both strains. It was believed that the inclusion of a 1.75 mM $NiCl_2$ plate might fill this gap of extreme change in visible growth and enable the convincing detection of Ni sensitivity.

3.8.2 Full-Scale CM Ni Sensitivity Assay Using All Transformed Strains

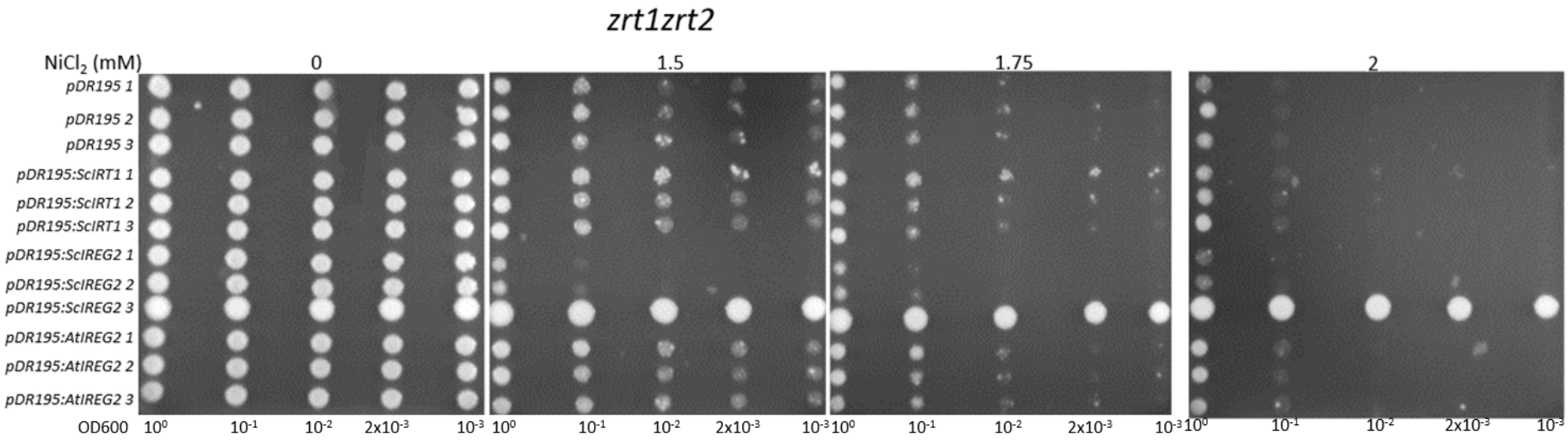

Figure 37**|Ni sensitivity of all transformed *zrt1zrt2* strains on complete media in triplicate.** *S. cerevisiae zrt1zrt2* strains transformed with *pDR195 GTW*, *pDR195:ScIRT1*, *pDR195:ScIREG2* and *pDR195:AtIREG2* spotted in a serial dilution on CSM -ura supplemented with Ni. Inoculum was generated using 3 independent transformants. Images were taken using a Syngene Gbox with a Cybertech 220 V 50 MHz camera with optics using an upper white light 4 days post inoculation after incubation

The 3rd *pDR195:ScIREG2* replicate exhibited exceptional survivability at all concentrations of Ni and at all dilutions displaying complete immunity to the effects of Ni toxicity. This growth was significantly different from the other *pDR195:ScIREG2* replicates and was far beyond what could be attributable to the activity of a strong Ni exporter. No such activity was observed for the known strong Ni transporter AtIREG2 here or in the literature. For these reasons, this *pDR195:ScIREG2* replicate was considered an outlier possibly containing a contaminant and was omitted from further analysis.

After omission of the outlier a comparison of the growth pattern of all plated strains on the 0 mM $NiCl_2$ plate shows that the growth is very similar for all strains indicating that there are no toxic effects of the transgenes. No apparent difference between the growth pattern of the positive (*pDR195:AtIREG2*) and negative (*pDR195*) control strains was observed which was unexpected because the strain expressing AtIREG2 is expected to display resistance to the effects of Ni toxicity. A possible reason for the failure to generate a distinguishable difference in growth pattern between the positive and negative controls might be that the strain containing *pDR195:AtIREG2* is not expressing *AtIREG2* at a level that causes a significant change in phenotype. A qPCR using *AtIREG2* specific primers would confirm if this transgenic yeast strain is expressing *AtIREG2* but this was not conducted in the timespan of the project. This could be a starting point for future work into troubleshooting of the Ni sensitivity assays to generate the expected results of the positive and negative controls. It could also be the case that the *pDR195:AtIREG2* transgenic yeast are successfully expressing *AtIREG2* but it is not functional under these conditions perhaps because it has not localized correctly to a membrane and therefore does not change the yeast Ni sensitivity.

The positive and negative control strains exhibiting the same growth pattern posed problems for analysing the growth patterns of the experimental strains. The *pDR195:ScIREG2* strains which were not omitted appeared to be demonstrating increased susceptibility to Ni toxicity on the Ni supplemented plates. This was inconsistent with what was observed for this strain in YNB minimal media Ni sensitivity assays (Figure 26). Therefore, conclusions cannot be made about the activity of ScIREG2 from this project because of the variation in results between minimal and CSM, and the presence of a confounding outlier in this experiment.

In contrast, the *pDR195:ScIRT1* transformants again exhibited enhanced growth relative to the negative controls which was particularly evident at high dilutions on the 1,75 and 2,0 mM $NiCl_2$. This result was consistent with the observations made about ScIRT1 with the Ni sensitivity assays conducted on minimal media (Figure 26) and coupled together, these results provide convincing evidence that *ScIRT1* encodes a protein functional in the transport of Ni, exporting Ni from yeast or sequestering Ni in the vacuole, enhancing survivability on Ni supplemented media. This observed result is unexpected because Nishida et al. (2011) demonstrated AtIRT1 conferred a Ni sensitivity phenotype when transformed into yeast cells and plated onto a Ni supplemented media. ScIRT1 therefore exhibited the opposite directionality of Ni transport to AtIRT1. However, there is precedent in the literature for homologs of a single transport protein exhibiting opposite apparent directionality of metal ion transport when expressed in yeast; heterologous expression of the *N. caerulescens* Ni transporter NRAMP4 in yeast by Wei et al. (2009) resulted in a decrease in yeast sensitivity due to reduced metal uptake while expression of NRAMP4 from *Noccaea cochleariforme* by Mizuno et al. (2005) caused an increase in yeast sensitivity to Ni as a result of greater uptake. It may be inadvisable to infer transporter functionality *in planta* solely from yeast expression experiments. For example, heterologous expression of an IREG2 homologue from *Psychotria gabriellae* led to reduced sensitivity to and accumulation of Ni i.e. Ni export across the plasma membrane, yet *in planta*, PgIREG1 localizes to the tonoplast and transports Ni into the vacuole (Merlot et al. 2014).

3.9 Determination of the Subcellular Localisation of ScIREG2 and ScIRT1

The final aim investigated in this Masters project was to determine the subcellular localisation of the proteins encoded by the genes of interest *in planta*. ScIREG2 and ScIRT1 were cloned into the expression vector (p*EarlyGate101*) generating C-terminal YFP fusion proteins (Appendix, Supplementary Figure 3). The expression constructs for the fusion proteins were then transformed into *A. tumefaciens* which were used to agro-infiltrate plant cells for expression and visualization of the subcellular localisation of the fluorescent proteins using fluorescence microscopy. The use of the *pEarlyGate101* destination vector necessitated a repeat of the entry cloning process because the previously generated vectors contained a stop codon at the 3' end which would cause the ribosome to stop protein synthesis before the YFP open reading frame. To generate the new entry vectors, new reverse primers were designed and synthesized for *ScIREG2* and *ScIRT1* which omitted the stop codon.

3.9.1 *pENTR1A:ScIREG2-noSTOP* Cloning

The newly synthesized *ScIREG2* reverse primer excluding the stop codon was used in tandem with the *ScIREG2* forward primer to amplify *ScIREG2* from *S. coronatus* cDNA to obtain the full CDS of *ScIREG2* with the stop codon removed. The insert was cloned into *pENTR1A* using *Bam*HI and *Eco*RI and the then used to transform *E. coli.* The resulting colonies were then checked for the presence of *ScIREG2* by using the extracted plasmid as template in a PCR using the *ScIREG2* specific primers (Figure 38).

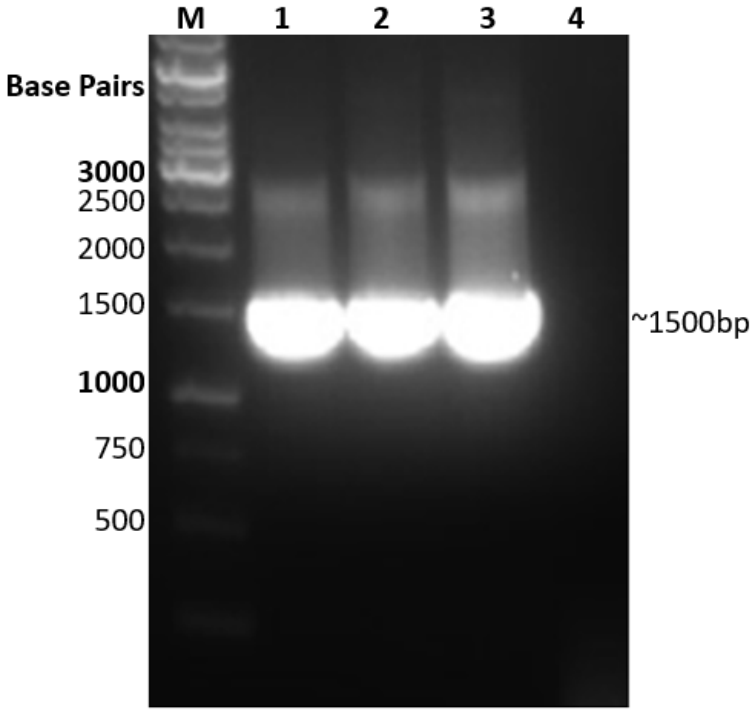

Figure 38**| Amplification of Sc*IREG2-noSTOP* from extracted plasmids from *E. coli* colonies after transformation with Sc*IREG2-noSTOP* and *pENTR1A* ligation.** PCR conducted using Supertherm polymerase using the *ScIREG2* specific primers: *IREG BAM for* and *IREG YFP rev2*. Lane **1** is a PCR positive control using 1:100 diluted, purified *pENTR1A:ScIREG2* from previous cloning as template. Lanes ***2*** and ***3*** use 1:100 diluted, extracted plasmids from *E. coli* transformed with a pENTR1A and ScIREG2-noSTOP variant ligation. Lane **4** contains a negative PCR control using water as template. Products were visualized on a 1% agarose gel and sized with Thermo Scientific O'GeneRuler 1kb DNA Ladder.

Examination of the products after the PCR reveals that both of the extracted plasmids from the *E. coli* transformation with the *pENTR1A* and *ScIREG2-noSTOP* ligation amplified a strong fragment at approximately 1500 base pairs. The size corresponds to the expected size of *ScIREG2* (1500 base pairs). The PCR provides evidence that *pENTR1A:ScIREG2-noSTOP* was successfully synthesized but further confirmation was attained by performing a diagnostic digest (Figure 39).

3.9.2 *pENTR1A:ScIREG2-noSTOP* Diagnostic Digest

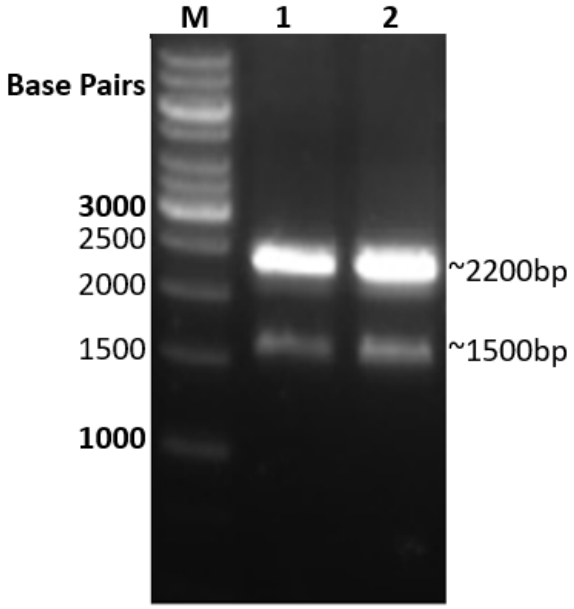

Figure 39**| Diagnostic double digest of extracted *pENTR1A:ScIREG2-noSTOP* from *E. coli.*** Lanes **1 and 2** contain 0,5 µg extracted plasmid from *E. coli* transformed with a *pENTR1A* and *ScIREG2-noSTOP* variant ligation subjected to complete digestion with *Bam*HI and *Eco*RI. Products were visualized on a 1% agarose gel and sized with New England Biolabs 1kb DNA Ladder.

The double digest of the extracted plasmid results in two visible fragments of approximately 2200 and 1500 base pairs in both lanes. The band sizes correspond to the expected sizes for the *pENTR1A* backbone and *ScIREG2*. The 2nd extracted plasmid was selected to be sent for sequencing analysis.

3.9.3 pENTR1A:ScIREG2-noSTOP Sequencing

The extracted plasmid was sequenced using the *M13* forward and reverse *pENTR1A* specific sequencing primers. The internal *ScIREG2* sequencing primer *IREG SEQ int*, was also used to generate a sequencing read of the internal region of the gene. The sequencing reads were compiled and compared to the known *ScIREG2* nucleotide sequences from the RNA-Seq experiment and the previous cloning into *pENTR1A* in a ClustalW multiple sequence alignment seen in Figure 7.

The sequencing reads confirmed that the *ScIREG2* insert was present in *pENTR1A*. The sequence has a perfect match to the *ScIREG2* nucleotide sequences from the A2, C7 and C9 individuals from the RNA-Seq experiment and also perfectly matches the *ScIREG2* cloned into *pENTR1A* previously. The stop codon is absent as required.

3.9.4 Failure to Gateway Clone *ScIREG2-noSTOP* into *pEarlyGate101*

At this point in the cloning process of the *IREG2-YFP* variant difficulties were encountered with gateway cloning of the insert in *pENTR1A* into *pEarlyGate101*. Both *pENTR1A* and *pEarlyGate101* make use of kanamycin as the selection marker which interferes with the gateway cloning process. Simple use of kanamycin selection after gateway cloning of any insert from *pENTR1A* to *pEarlyGate101* would yield completely indistinguishable colonies, successfully transformed with *pENTR1A* containing the insert and *pEarlyGate101* containing the insert. An additional step was therefore devised which involved linearization of *pENTR1A:ScIREG2-noSTOP* by digestion with *Nhe*I before conducting the LR clonase reaction as described in the methods to prevent transformation with the entry vector. *Nhe*I was chosen as the restriction enzyme for linearization because it had only one restriction site in the *pENTR1A* backbone.

This linearization step necessitated the inclusion of an additional transformation control after the gateway cloning reaction. The linearized *pENTR1A:ScIREG2-noSTOP* needed to be transformed into competent *E. coli,* followed by kanamycin selection to determine the level of background of successful transformation with intact *pENTR1A:ScIREG2-noSTOP* which would interfere with the isolation of *pEarlyGate101:ScIREG2-noSTOP* after gateway cloning. During the course of the project *pENTR1A:ScIREG2-noSTOP* was subjected to digestion with *Nhe*I numerous times under a variety of conditions and used in a control transformation of competent *E. coli* cells. Despite the digestion with *Nhe*I, many transformant colonies formed on kanamycin selection media indicating an extremely high level of background. It was clear that *Nhe*I was not functioning in digesting and linearizing the entry vector. This resulted in intact vector persisting which successfully transformed the bacteria at high efficiency. The cloning of the *ScIREG2-noSTOP* variant was therefore abandoned.

3.9.5 *pENTR1A:ScIRT1-noSTOP* Cloning

ScIRT1 was amplified from *S. coronatus* cDNA using the gene-specific forward primer *IRT1 for*, and the gene specific reverse primer designed with the stop codon removed *IRT YFP rev2*. The amplified product then cloned into *pENTR1A* using *Bam*HI and *Eco*RI. For confirmation of the presence of the *ScIRT1-noSTOP* variant after cloning, a diagnostic double digest was performed (Figure 40).

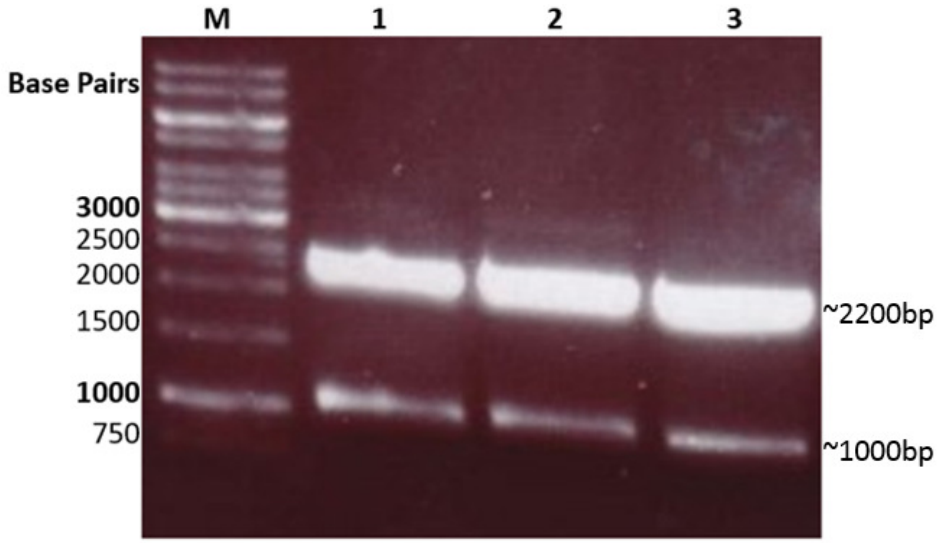

Figure 40**| Diagnostic double digest of extracted *pENTR1A:ScIRT1-noSTOP* from *E. coli.*** Lanes **1 to 3** contain 0,5 µg extracted plasmid from *E. coli* transformation with *pENTR1A:ScIRT1-noSTOP* subjected to digestion with *Bam*HI and *Eco*RI. Products were visualized on a 1% agarose gel and sized with New England Biolabs 1kb DNA Ladder.

After digestion two strong bands were visible for each extract at approximately 2200 and 1000 base pairs corresponding to the predicted size of the *pENTR1A* backbone and *ScIRT1-noSTOP* (1045 base pairs) respectively. The digest provided evidence that *pENTR1A:ScIRT1-noSTOP* had been cloned into pENTR1A.

3.9.6 *pENTR1A:ScIRT1-noSTOP* Sequencing

For further confirmation of the identity of the extracted plasmids, the plasmid from lane 1 was sequenced using the *M13 pENTR1A* sequencing primers. The reads were compiled into a complete sequence and compared to the *ScIRT1* nucleotide sequences from individuals in the RNA-Seq experiment and the previous successful *ScIRT1* clone in a ClustalW multiple sequence alignment in Figure 9. The multiple sequence alignment reveals that *ScIRT1-noSTOP* was successfully inserted into *pENTR1A* and the gene sequence perfectly matches the *ScIRT1* sequence from the A3 and C8 individuals from the RNA-Seq experiment and the *ScIRT1* clone sequenced previously. The sequencing also demonstrated that the stop codon was not present.

3.9.7 Gateway Cloning *ScIRT1-noSTOP* into *pEarlyGate101*

A gateway cloning reaction of *pENTR1A:ScIRT1-noSTOP* into *pEarlyGate101* was attempted (Figure 41) but the extent of background transformation with the intact entry vector needed to be limited because of the problems associated with using both *pENTR1A* and *pEarlyGate101*. To eliminate the possibility of *pENTR1A:ScIRT1-noSTOP* transforming competent bacteria after the LR clonase reaction, it was digested with *Nhe*I to linearize the vector before being introduced into the gateway cloning reaction for recombination into *pEarlyGate101*.

A) 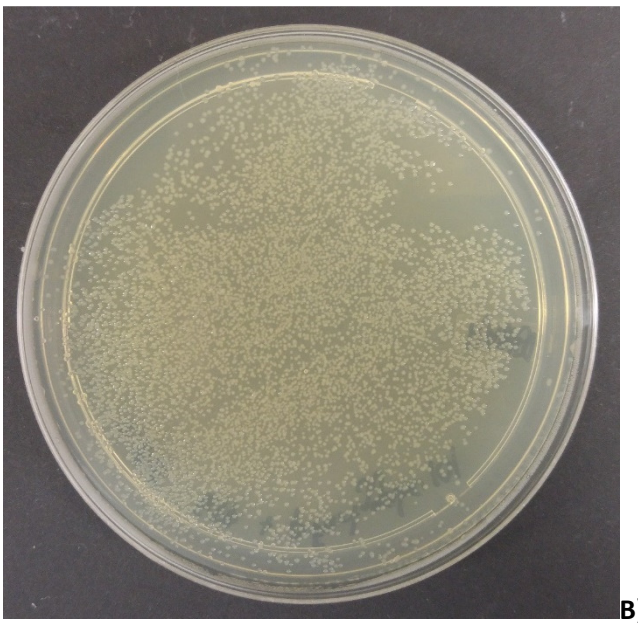 **B)** 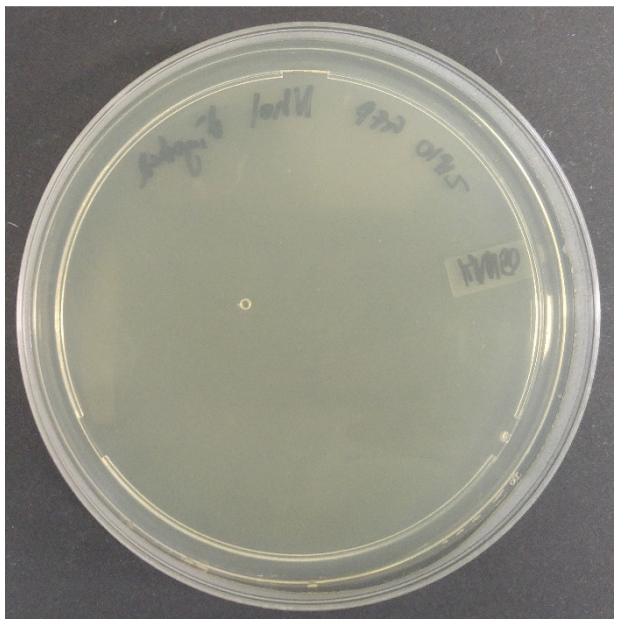

Figure 41**| *E. coli growth* after transformation with gateway cloning reaction of *pDR195:ScIRT1-noSTOP* into *pEarlygate101* (A) and *pENTR1A:ScIRT1-noSTOP* after *Nhe*I digestion (B).** Plate **A** is an LB kanamycin plate inoculated with an *E. coli* transformation with the product of gateway cloning

reaction of *Nhe*I linearized *pENTR1A:ScIRT1-noSTOP* and *pEarlyGate101*. Plate **B** is an LB kanamycin selective plate inoculated with competent *E. coli* cell transformation with *Nhe*I linearized *pENTR1A:ScIRT1-noSTOP*.

In stark contrast to the situation with *pENTR1A:ScIREG2-noSTOP* described above there were no colonies formed for the *E. coli* transformation with the *Nhe*I digested *pENTR1A:ScIRT1-noSTOP* indicating that the entry vector was successfully linearized and was not able to transform *E. coli*. The reason for this difference is unknown but suggests that the *Nhe*I site in *pENTR1A:ScIREG2* may possibly have been lost through mutation. Numerous colonies formed when transformed with the gateway cloning reaction of *ScIRT1-noSTOP* into *pEarlyGate101*. This indicated that the reaction and transformation were successful and took place with high efficiency. A further experimental diagnostic was performed to confirm that the plasmid DNA extracted from these colonies was *pEarlyGate101:ScIRT1-noSTOP* and not undigested *pENTR1A:ScIRT1-noSTOP*. This was done by designing a set of PCR primers which would only be capable of amplifying a product from *pEarlyGate101:ScIRT1-noSTOP* and not *pENTR1A*. The reverse primer used was simply the *ScIRT1-noSTOP* reverse primer that amplified ScIRT1-noSTOP initially which was selected to ensure specificity to *ScIRT1-noSTOP*. A new forward primer was designed which anneals specifically to the *35S* promoter present in *pEarlyGate101* (and not *pENTR1A*) upstream of the *attR* sites to which the insert is transferred by LR clonase. A product can thus only be amplified using these primers if the template is *pEarlyGate101:ScIRT1-noSTOP*. A PCR was conducted on all the extracted plasmids using this primer pair to confirm their identity as *pEarlyGate101:ScIRT1-noSTOP* (Figure 42).

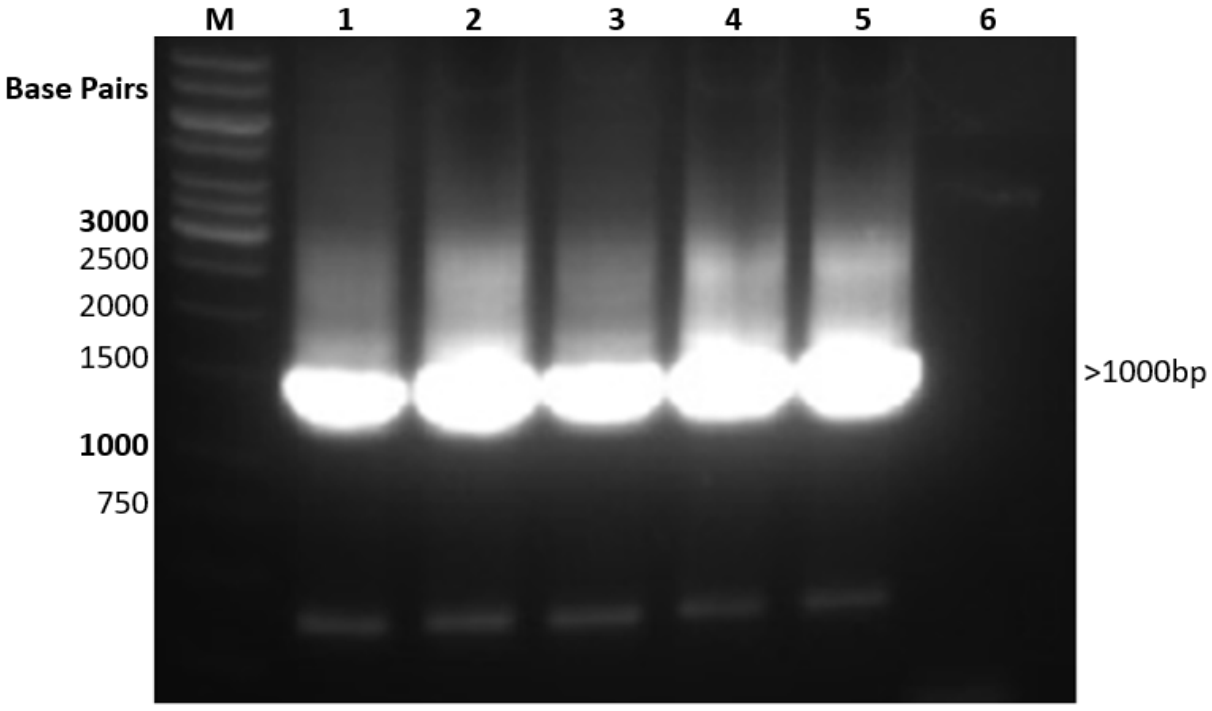

Figure 42**| Amplification of *ScIRT1-noSTOP* from extracted plasmids from *E. coli* colonies after transformation with Gateway cloning reaction of *pDR195:ScIRT1-noSTOP* into *pEarlygate101*.** PCR conducted using Supertherm polymerase with 35S promoter forward primer and the gene specific reverse primer *IRT1 YFP rev2*. Lanes **1 to 5** use 1:10 diluted, extracted plasmids as template. The plasmids were extracted from *E. coli* after transformation with the Gateway cloning reaction of *pDR195:ScIRT1-noSTOP* into *pEarlyGate101*. Lane **6** contains a negative PCR control using water as template. Products were visualized on a 1% agarose gel with Thermo Scientific O'GeneRuler 1kb DNA Ladder.

All extracted plasmids when used as template in a PCR with the 35S forward primer and *ScIRT1-noSTOP* specific reverse primer amplified an extremely bright product at approximately 1500 base pairs. The size of the amplified product corresponded to what would be expected of these primers amplifying from *pEarlyGate101:ScIRT1-noSTOP*. This is because the product would include the full length of *ScIRT1* (1045 base pairs), the *attR1* site (120 base pairs) and the 35S promoter (343 base pairs). The fact that there is amplification using these primers which are specific to *pEarlyGate101:ScIRT1-noSTOP* and the size of the product provides evidence that these plasmids are indeed *pEarlyGate101:ScIRT1-noSTOP*.

3.9.8 DNA Sequencing of *pEarlyGate101:ScIRT1-noSTOP*

The PCR diagnostic provides evidence that the extracted plasmids are indeed *pEarlyGate101:ScIRT1-noSTOP* but it is not conclusive proof. Confirmation of the plasmid identity was attained by DNA sequencing. A new reverse sequencing primer was designed specific to *YFP* in *pEarlyGate101* (*YFP rev*) which would generate a sequencing read from *YFP*, through the *att* site, and into the region where *ScIRT1-noSTOP* would have been transferred by a successful gateway cloning reaction. A sequencing read of this nature would provide conclusive proof if *ScIRT1-noSTOP* is present in *pEarlyGate101*. A further objective was achieved with the design of this sequencing primer for determining whether the *ScIRT1-noSTOP* insert was inserted into the expression vector by LR clonase in-frame to allow for read-through by the ribosome during translation thus generating the ScIRT1-YFP fusion protein.

The first extracted plasmid was sequenced using this YFP reverse sequencing primer and the resulting read was translated to amino acid sequence by inputting into ExPASy. The single longest frame without a stop codon was identified and aligned to *ScIRT1* by ClustalW to confirm the presence of the insert and the known amino acid sequence of YFP to ensure that *ScIRT1* and YFP were in the same reading frame (Figure 43).

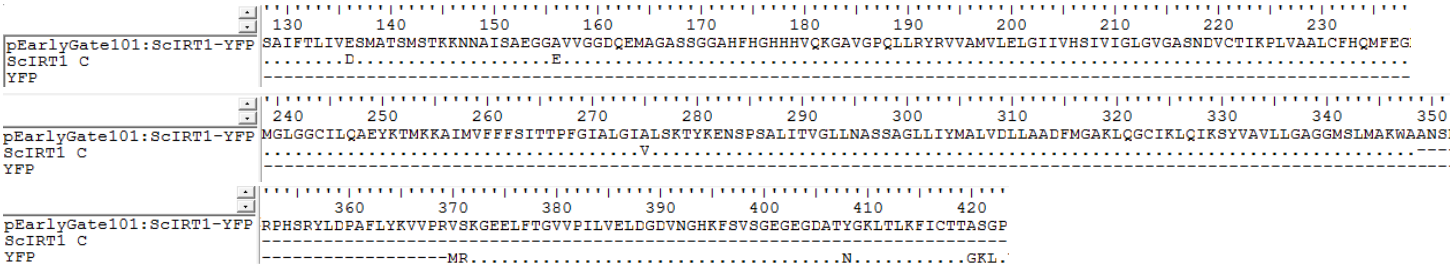

Figure 43**| Multiple sequencing alignment of translated sequence of *pEarlyGate101:ScIRT1-noSTOP* sequencing read from the *YFP* specific reverse primer *YFP rev*.** ClustalW multiple sequence alignment showing an amino acid match of the ExPASy translated portion of the *pEarlyGate101:ScIRT1-noSTOP* sequencing read to approximately 220 amino acids from the end of the translated *ScIRT1* sequence from the C8 individual from the RNA-Seq data and to a YFP amino acid sequence from Uniprot.

The terminal end of the sequencing read (the sequence in the alignment is reverse complimented) demonstrated a near perfect amino acid match to the translated ScIRT1 sequence from the RNA-Seq experiment. The changes in amino acid sequence are a result of poor sequencing quality towards the 3' end of the sequence. The 5' end of the sequencing read also clearly matches to the annotated amino acid sequence of YFP with some amino acid substitutions again explained by poor read quality at the beginning of the sequence. The same frame of the

translated sequencing read matched to both ScIRT1 and to YFP with no stop codon present confirming that *ScIRT1* was successfully inserted into *pEarlyGate101* in-frame so expression of this construct would result in a transcript coding for ScIRT1 which would continue to be translated into the YFP sequence by the ribosome. The expression construct was therefore suitable for further cloning and expression analysis in plants to fulfil the objective of discovering the subcellular localisation of *ScIRT1*.

3.9.9 A. tumefaciens Transformation with *pEarlyGate101:ScIRT1-noSTOP*

pEarlyGate101:ScIRT1-noSTOP was transformed into competent *A. tumefaciens* as described in the methods. An agrobacterium colony PCR was performed on the resulting colonies after transformation using *ScIRT1* specific primers to confirm the presence of *ScIRT1*, thus providing further evidence that the cells were successfully transformed with *pEarlyGate101:ScIRT1-noSTOP* (Figure 44).

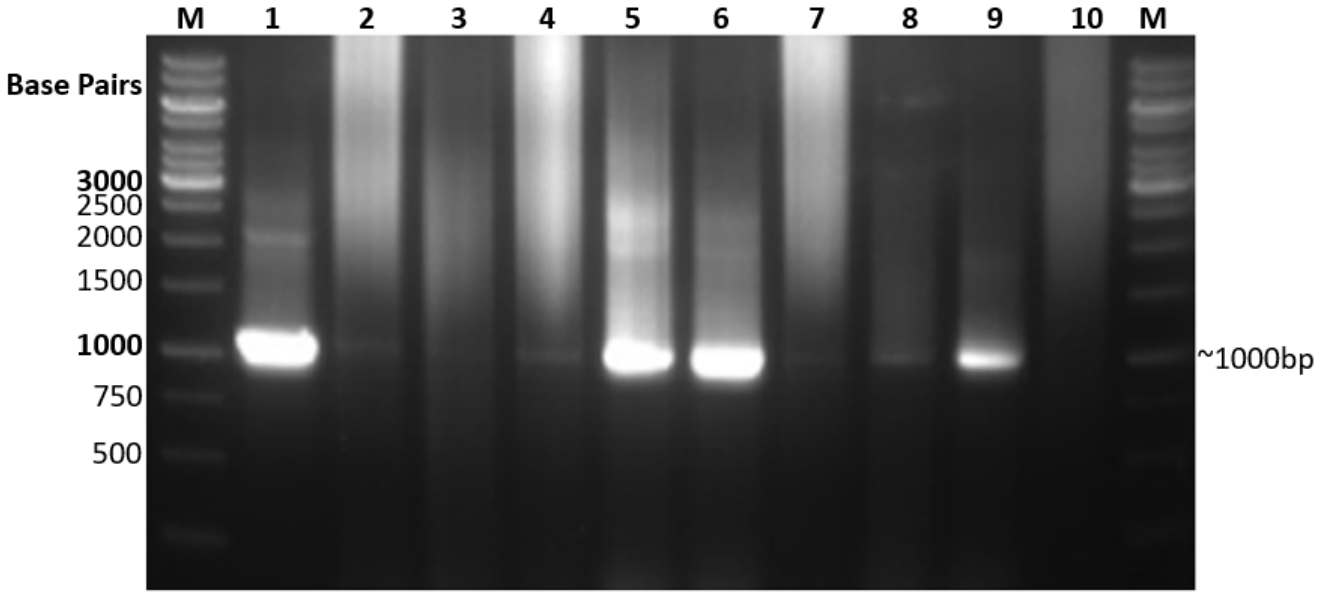

Figure 44**| Amplification of *ScIRT1* in an *A. tumefaciens* colony PCR.** Supertherm polymerase used for *Agrobacerium* colony PCR using the *ScIRT1* specific primers: *IRT1 FOR* and *IRT1 YFP rev2*. Lane **1** is a PCR positive control using purified, 1:100 diluted *pEarlyGate101:ScIRT1-noSTOP*. Lanes **2 to 9** used single colonies of *A. tumefaciens* as template after transformation with *pEarlyGate101:ScIRT1-noSTOP*. Lane **10** contains a negative PCR control using water as template. Products were visualized on a 1% agarose gel and sized with Thermo Scientific O'GeneRuler 1kb DNA Ladder.

All colony PCR experimental lanes generated a product approximately 1000 base pairs in length which corresponds with the expected size of *ScIRT1-noSTOP* (1047 base pairs). There was no amplification from the negative control PCR so the amplification of this product is as a result of the template used in each lane. The size and intensity of the products formed provide evidence that the colonies used as templates in lanes 5, 6 and 9 are likely candidates for successful transformations of *A. tumefaciens* with *pEarlyGate101:ScIRT1-noSTOP*.

3.9.10 Onion Cell Transfection with *A. tumefaciens* and Determination of Subcellular Localisation of ScIRT1 by Fluorescence Microscopy

In order to transiently express the construct in plant tissue, the protocol for onion cell (*Allium cepa* L) transfection devised and published by Xu et al. (2014) was adopted. This method was selected because it is described as having an extremely high transformation efficiency, takes comparatively less time than other transfection methods and makes use of readily available reagents. Onion cells were also considered to be the ideal tissue type for this experiment due to the large, transparent plant cells. This would facilitate the detection of the fluorescent proteins in the tissue by fluorescence microscopy and enable characterization of the subcellular localisation of the protein of interest. Optimization of this research method to agro-infiltrated onion cells had begun by colleagues allowing the application of it to the *pEarlyGate101:ScIRT-noSTOP* expression construct with a system that was already in place.

The experimental setup of the agro-infiltration of onion cells involved the pre-treatment of onion bulbs before introduction of agrobacterium. The bulbs were incubated at 37^{o}C for 72 hours with limited exposure to light which was described by Xu et al. (2014) as the optimum conditions for pre-treatment before agro-infiltration. *Agrobacterium* transformed with *pEarlyGate101:ScIRT1-noSTOP* was selectively cultured and resuspended in agro-infiltration liquid at an OD of 0.1. Agro-infiltration of the onion bulb then took place using a small needle and syringe to inject 200 µL of agro-infiltration liquid into the tissue between the adaxial epidermis and mesophyll of the onion scales which was accessed by partially dissecting the bulb using a scalpel. The infiltrated onions were then incubated for a further 72 hours with no exposure to light.

3.9.11 Preliminary Fluorescence Microscopy of ScIRT1-YFP *in planta*

After the incubation period, the transfected onion bulbs were retrieved and prepared into wet mounts for fluorescence microscopy to detect YFP fluorescence (Figure 45).

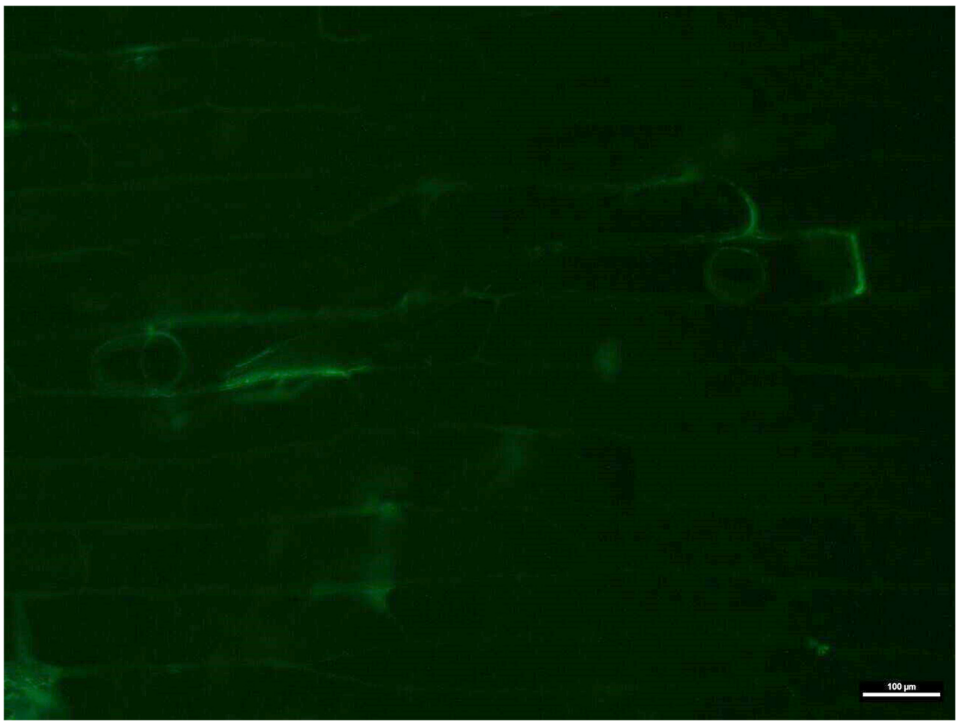

Figure 45**| Digital images of cell layer of *Allium cepa* L transfected with *A. tumefaciens* transformed with *pEarlyGate101:ScIRT1-noSTOP* using a fluorescence microscope.** Cell layers were injected with agro-infiltration liquid containing *Agrobacterium* containing *pEarlyGate101:ScIRT1-noSTOP* and incubated at 30^{O}C for 72 hours then prepared into single layer wet mounts. Imaging done using a darkfield fluorescence

microscope (Nikon Eclipse T*i*-E) using the YFP filter and 10X objective. No bright field image of this frame was taken.

The digital image of the onion cell layer transfected with *A. tumefaciens* containing *pEarlyGate101:ScIRT1-noSTOP* using the YFP filter was inspected for fluorescence. There appeared to be zones of bright YFP fluorescence associated with some of the cells. Strong, straight lines of fluorescence lit up between cells and two circular structures within the cells fluoresce. The intensity and shape of the observed YFP fluorescence was encouraging because it suggested that YFP was being expressed and it was possible to identify cellular structures in these images. The method of onion cell transfection appeared to be functional. However, the experimental setup of this investigation was flawed because no controls were included to identify any auto-fluorescence caused by the onion cells or *A. tumefaciens* and no supplementary images were taken that may have assisted in identifying cellular structures.

An optimized experiment to determine the subcellular localisation of ScIRT1 was designed that would make use of the same method but included untransfected onion cells and onion cells transfected with untransformed *A. tumefaciens* to identify any auto-fluorescence caused by the onion cells or *A. tumefaciens*. The inclusion of bright field images is also necessary to allow for the identification of cellular structures in the YFP filter images. In order to confirm the identity of the organelles fluorescing in the previous experiment, it was decided that a nuclear stain should be included. This would make the nucleus easily identifiable using the fluorescent microscope. Hoescht stain, which fluoresces under UV, was used for this purpose.

The experiment was conducted using these parameters (Figure 46). When making observations of the generated specimens using the fluorescent microscope, the bright field filter was used to focus and orientate the sample and the YFP filter was used to identify regions of interest where specific YFP fluorescence was visible. Once a digital image of the region of interest was taken using the YFP filter, additional images were taken of the exact same field using the bright field filter and the UV filter to visualize the Hoescht stain. Once a digital image of the same frame was acquired using all three filters, a composite image of all three images was made using ImageJ. This allowed for direct comparison of the images using the different filters by showing the fluorescing regions overlaid on the bright field image.

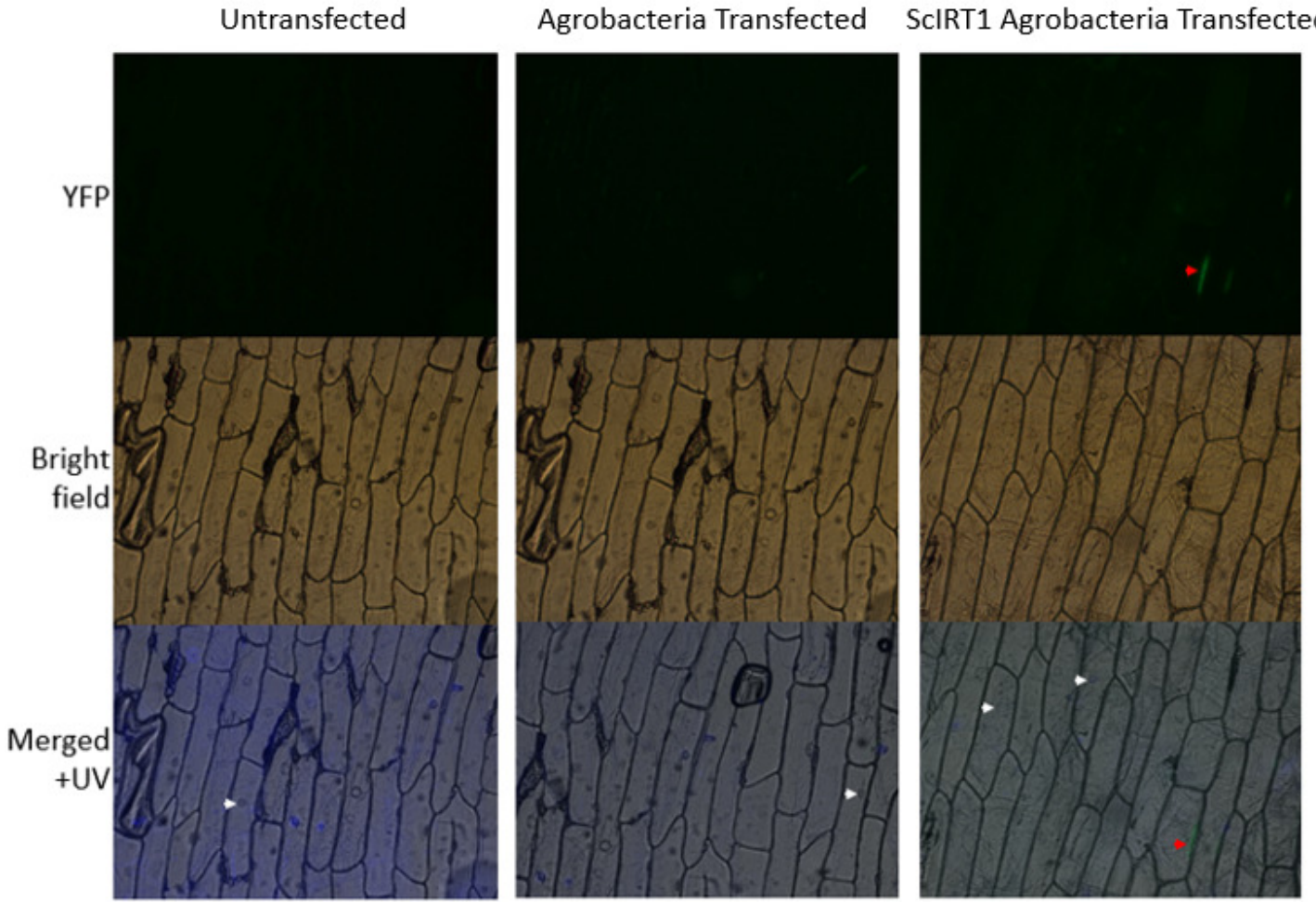

Figure 46**| Fluorescence microscopy digital images of cell layers of *Allium cepa* L. to identify the subcellular localisation of exogenous ScIRT1-YFP.** Fluorescence microscopy 10X magnification images of untransfected red onion cells, cells transfected with *A. tumefaciens* and cells transfected with *A. tumefaciens* containing *pEarlyGate101:ScIRT1*. Cell layers were injected with agroinfiltration liquid and incubated at 30^{O}C for 72 hours then prepared into single layer wet mounts. Hoecht's stain was then applied to the wet mounts for 15 minutes and washed off with PBS. Imaging done using a darkfield fluorescence microscope (Nikon Eclipse T*i*-E) using the YFP, bright field and UV filter. YFP and bright field images are shown in the figure as well as a merged image using ImageJ of the bright field, UV (nuclear Hoechts stain) and YFP images. Arrows included in the images label visible fluorescence such that ▶ denotes Hoechst stained nucleus and ▶ denotes YFP fluorescence.

The digital images using the various filters of the transfected and untransfected onion cells were analysed to identify YFP fluorescence specific to the cells that could be as a result of fluorescence of ScIRT1-YFP. The Hoechst stain appeared to stain the nucleus inconsistently such that some of the samples had visible, stained nuclei while others did not. The YFP images for the untransfected negative control displayed a very faint green signal giving an indication of what background YFP fluorescence could be expected in the transfected samples. The green signal seemed to be associated with the outline of the cells indicating that the onion cells were auto-fluorescing but at a very low intensity.

A single cell layer of onion cells transfected with untransformed *A. tumefaciens* was examined using the bright field and YFP filters. As in the untransfected negative control, the cells generally displayed a faint background of green signal which can be attributable to auto-fluorescence. The inclusion of untransformed *A. tumefaciens* therefore does not influence the intensity of the background YFP signal.

The onion cells transfected with *Agrobacterium* transformed with *pEarlyGate101:ScIRT1-noSTOP* were examined using the YFP filter. Bright fluorescence was visible as two straight, parallel lines labelled with a red arrow. This fluorescence was distinctive from the background signal and was strongly associated with the border of two onion cells outlined in the bright field image. This strong association was clearly visible in the merged image. The fluorescence was also in-focus with the onion cells and blurred when the sample became out of focus indicating that the fluorescence originated from the sample. This result was consistent with the observed localisation of ScIRT1-YFP seen in Figure 45.

This result suggests that these two onion cells were successfully transfected with *A. tumefaciens* containing *pEarlyGate101:ScIRT1-noSTOP* and expressed the ScIRT1-YFP fusion fluorescent protein. The fluorescence consistently appeared to localize inside the cells and on the boarder of the cell wall which is the expected location of the plasma membrane. The cellular membrane was not stained in these mounts which would have been a valuable adjustment to the experimental setup. The use of propidium iodide staining to stain the cell wall as done by Merlot et al. (2014) may have granted greater clarity in determining the exact subcellular localisation of the fusion protein. Nevertheless, this strong observed fluorescence suggests that ScIRT1 may localize to the plasma membrane when expressed *in planta*.

4. Conclusion

An experimental investigation was conducted into the candidate *Senecio coronatus* Ni transporter genes, *ScIREG2* and *ScIRT1*. Both genes were successfully amplified from *S. coronatus* cDNA and cloned. Sanger-based sequencing of the clones confirmed that the amplified sequences matched the *ScIREG2* and *ScIRT1* sequences derived from the RNA-Seq experiment conducted by Meier et al. (2017). This result validated the RNA-Seq data confirming that *ScIREG2* and *ScIRT1* are real genes expressed in *S. coronatus*.

A bioinformatic investigation of the gene sequences was performed to ensure that these genes are consistent with the role of metal transporters. A phylogenetic analysis of the genes and closely related homologs was carried out to inform on the correct annotation of the gene names and to suggest, through sequence homology to known metal transporters, that the genes of interest encode metal transporters. A bioinformatics algorithm (Dense Alignment Surface algorithm) was used to predict the number of transmembrane helices in the genes of interest. ScIREG2 was predicted to contain 10 transmembrane helices while ScIRT1 predicted to contain 8, the same number that has been experimentally discovered for the *A. thaliana* homolog AtIRT1. The high number of transmembrane helices and similarity to membrane proteins supports the notion that these genes are also membrane proteins which is typical of metal transporters. An attempt was made to predict the subcellular localisation of the proteins encoded by the genes of interest using bioinformatic tools but the available algorithms were found to be too unreliable in predicting the correct localisation for the characterised homologs, to warrant their use as predictors for the *S. coronatus* proteins.

The genes of interest were expressed in *S. cerevisiae zrt1zrt2* mutant using an appropriate, constitutive yeast expression vector, *pDR195*. Uracil biosynthesis complementation was successfully used to identify transformed yeast on uracil deficient media. The ability of the expressed *Senecio* genes to transport Ni was assessed using Ni sensitivity assays. The effects of Ni toxicity on the transformed yeast strains were determined by plating a dilution series of yeast culture on Ni supplemented media to give an indication if the proteins encoded by the *S. coronatus* genes were causing a change in the Ni sensitivity of the strain. Optimized Ni sensitivity assays conducted on minimal and complete media were inconclusive for ScIREG2 because no significant difference in survivability was seen between the transformed and control strains on Ni supplemented media. The experiments conducted on CSM were also confounded by an outlier replicate which exhibited exceptional resistance to Ni toxicity. The inconsistent results for the ScIREG2 expressing yeast strains made it impossible for a conclusion to be drawn about its activity as a Ni transporter, necessitating further investigation.

The well characterised Ni transporter *AtIREG2* was successfully transformed into *zrt1zrt2* and made use of as a positive control for the Ni resistance phenotype. It appeared possible to detect a discernible difference in strain survivability between the strain expressing *AtIREG2* and the negative control strain in a preliminary Ni sensitivity assay on CSM testing the control strains. However, use of the *pDR195:AtIREG2* transformed strain in full-scale Ni sensitivity assays produced an inconsistent and minor change in phenotype compared to the negative control strain making it an inappropriate positive control and necessitating further optimization.

The strain *zrt1zrt2* expressing *ScIRT1* consistently demonstrated a modest increase in resistance to exogenous Ni that was greater than that of the positive control expressing *AtIREG2*. This result and its consistency across all conducted Ni sensitivity assays on YNB and YNB CSM-ura provide convincing evidence that *ScIRT1* encodes a protein

functional in transporting Ni, specifically in export of Ni out of the cell or vacuolar sequestration of Ni, improving its resistance to Ni toxicity. *ScIRT1* was expected to encode a Ni transport protein based on its homology to the characterised Ni transporter AtIRT1. However, it was expected to cause an increase, rather than a decrease, in Ni sensitivity when expressed in yeast as AtIRT1 did when investigated by Nishida et al. (2011). Determination of the intracellular Ni content of the transgenic yeast would be a worthwhile future experiment to confirm these findings. The opposite directionality of Ni transport between AtIRT1 and ScIRT1 was found to have precedent in the literature from investigations into the Ni transporter, NRAMP4 proteins.

Further cloning of *ScIREG2* and *ScIRT1* took place to obtain an expression construct that would fuse these proteins to YFP for direct observation of their subcellular localisation in plants. A *ScIREG2* variant with the stop codon removed was successfully cloned into the entry vector *pENTR1A* but the cloning process was incomplete because it was not successfully transferred to the expression vector *pEarlyGate101* due to technical difficulties. The *ScIRT1* variant with the stop codon removed was successfully cloned into the *pEarlyGate101* expression vector and it was confirmed to be inserted in the same frame as *YFP* by sequencing analysis. The *ScIRT1-YFP* expression construct was successfully transformed into *A. tumefaciens* which was used transfect onion cells using a method developed by Xu et al. (2014). Cell layers of the transfected onion cells transiently expressing *ScIRT1-YFP* were observed using a fluorescence microscope with a YFP filter. Negative control samples consisting of untransfected onion tissue and onion tissue transfected with untransformed *Agrobacterium* displayed a low level of background signal but no specific YFP fluorescence. Bright, specific YFP fluorescence was observable in onion cells expressing ScIRT1-YFP which localized to the periphery of the plant cells, alongside the cell wall, which is the expected location of the plasma membrane.

5. Future Work

Efforts should be made to provide a more conclusive result for the subcellular localisation of ScIRT1 by generating more images of transformed cells demonstrating YFP fluorescence. Additional fluorescence microscopy should also make use of propidium iodide staining to label the cell wall and membrane to make these structures clearer when assessing the origin of the fluorescence of YFP. Gateway cloning of the *ScIREG2* variant with removed stop codon into *pEarlyGate101* is required to create a construct capable of expressing ScIREG2 fused to YFP. The expression construct can then be expressed in plant tissue and the YFP fluorescence of *ScIREG2-YFP* can be visualized using fluorescence microscopy to determine the subcellular localisation of ScIREG2, which is predicted to localise to the vacuole based on homology to AtIREG2.

Further investigation into *ScIREG2* and *ScIRT1* is necessary to characterize these genes and establish if they encode Ni transport proteins playing a significant role in causing the Ni hyperaccumulation phenotype in *S. coronatus*. Optimization of the Ni sensitivity assays is required. The problems with culturing the yeast strains on minimal media need to be resolved so that the Ni sensitivity assays can continue to be conducted on minimal media to make the assay comparable to those in the literature. Full-scale Ni sensitivity assays need to be conducted under these conditions with greater consistency between replicates and no growth outliers present to confound results. The experimental conditions of Ni concentration and growth medium pH need to be optimized further to generate a more significant difference in growth particularly between the positive *AtIREG2* expressing and negative empty vector strains. The strong positive result published by Schaaf et al. (2006) seemed to be dependent on optimized pH conditions. pH is known as a significant factor in determining the availability of metal for uptake in growth media. A clear positive result in the positive control would enable more meaningful description of the yeast sensitivity phenotype of the experimental strains. An alternative approach to yeast complementation would be to attempt to complement the *A. thaliana irt1* and *ireg2* mutants with the *S. coronatus* homologs to determine whether wild-type transport of Ni is restored in these plants under conditions of iron-deficiency (Nishida et al., 2011; Schaaf et al., 2006).

Future work into *S. coronatus* transporters can then make use of this method to conduct Ni sensitivity assays on other candidate genes which have been identified as potential Ni transporters to confirm their activity. In total, 22 *S. coronatus* differentially expressed genes from the RNA-Seq data have been identified as potential transport proteins based on sequence homology to known metal transporters. *S. coronatus* exhibits an extreme Ni hyperaccumulation phenotype which is surely as a result of the activity of many genes. In order to fully understand the system, all proteins functional in managing acquired Ni must be identified.

Once the Ni transport proteins in *S. coronatus* have been identified, the mechanism of their upregulation in hyperaccumulating sub-populations must be established. Analysis of the *S. coronatus* genome must be conducted to determine the features that lead to an abundance of these transcripts. Investigations into other metal hyperaccumulating plants suggests that the two major causes for increased transcript abundance are gene duplication events and changes in the strength of their promoters due to mutation (Courbot et al., 2007; Hanikenne et al., 2008; Hussain et al., 2004). Gene duplication events of the genes encoding metal transport proteins can be identified using qPCR of an absolute quantity of genomic DNA. qPCR primers can be designed to the genes of interest and to a housekeeper gene that is known to only being represented a single time in the genome. qPCR amplification using these primers on a known concentration of gDNA will allow comparison of the template abundance of the

gene of interest relative to the housekeeper and this will give an indication of the presence of gene duplication events.

Promoter enhancements have the potential to cause an increase in tissue specific transcriptional activity from the genes of interest by increasing the affinity of the site for transcription factor binding. This in turn will improve the efficiency of RNA polymerase recruitment and transcription. The transcription factor binding sites in the promoter therefore need to be characterised. The 5' untranslated regions of the Ni transport candidates can be acquired from the transcriptome assembly by Meier et al. (2017). The promoter sequence upstream of the transcriptional start site then needs to be generated so it can be scrutinized for any features that may enhance its activity in hyperaccumulator versus non-accumulator populations. The unknown sequence upstream of the transcriptional start site can be amplified using a technique called splinkerette PCR. The process involves digesting the entire genome with a series of restriction enzymes and ligating an adaptor which possesses the corresponding digested end to the enzyme used. The adaptor is an oligonucleotide which consists of two sites to which adaptor specific, forward PCR primers can bind. Two 5' UTR specific reverse primers can then be designed downstream of the transcriptional start site and used in a nested PCR in conjunction with the adaptor primers to amplify a product. Probability suggests that one of the restriction enzymes will cut the genome within range, upstream of the transcriptional start site to form a PCR product. Using splinkerette PCR, the unknown region between the likely digestion site and the transcriptional start site, which includes the promoter, can be amplified and sequenced.

An alternative method to identify these features may be facilitated by the improvement of next generation sequencing technology making full genome sequencing of *S. coronatus* more viable. This would allow for direct comparison to the genomes of non-accumulators to identify the molecular basis of upregulation of transporter proteins. However, *S. coronatus* possesses a 3 gigabase genome which is not a trivial size to sequence and assemble even with access to next generation sequencing technology. This problem is exacerbated by the fact that the acquisition of a full genome sequence from a hyperaccumulator and non-accumulator would be ideal for comparative studies, doubling the amount of assembly required. Therefore, an experimental approach to characterizing *S. coronatus* genomic features is likely necessary for the foreseeable future.

Bioinformatic analysis can be performed on acquired promoter sequences to identify transcription factor binding sites. However, this may not fully elucidate the most significant features in the promoter. Experimental investigation into the activity of transcription factors on the promoters of the identified Ni transporters in *S. coronatus* is likely to form a bulk of the future work necessary to characterize the system of Ni hyperaccumulation in this species. This characterization will be necessary whether or not the genome is sequenced because simply knowing the sequence of the promoter does not completely describe how transcription factors will act. Additionally, it is also hypothesized that the basis of the Ni hyperaccumulation traits in *S. coronatus* may occur through overexpression of transcription factors, which regulate a plethora of metal transporters simultaneously rather than via alterations directly to the promoters of specific Ni transporter genes.

Transcription factors that act upon the promoter region of genes of interest can be identified experimentally by conducting a yeast-one-hybrid screen. This would involve creating a reporter construct which utilizes the known promoter of candidate Ni transport genes to drive the expression of a reporter gene such as β-galactosidase. The expression construct can then be co-expressed with an expression construct containing a fragment from a cDNA library, generated from *S. coronatus*. Colonies which are exhibiting activity for the reporter gene can then be easily

identified by activity of the reporter gene indicating that the library fragment expressed in that colony encodes a transcription factor that is active on the promoter. This encoded transcription factor can then be isolated for sequencing and further analysis from the colony expressing the reporter gene. In this way, the transcription factors driving the expression of Ni transporters in *S. coronatus* can be identified and characterised to generate a complete model of how transcription factors and Ni transport proteins are expressed to cause Ni hyperaccumulation traits in *S. coronatus*. Utilization of the yeast-one-hybrid screen to identify transcription factors may become the basis for explaining how the system of Ni hyperaccumulation occurs in *S. coronatus*.

6. References

Anderson, C. W. N., Brooks, R. R., Chiarucci, A., Lacoste, C. J., & Leblanc, M. (1999). Phytomining for nickel , thallium and gold. *Journal of Geochemical Exploration*, 67, 407–415.

Assunção, A. G. L., Herrero, E., Lin, Y. F., Huettel, B., Talukdar, S., Smaczniak, C., Immink, R. G., van Eldik, M., Fiers, M., Schat, H. & Aarts, M. G. (2010). *Arabidopsis thaliana* transcription factors bZIP19 and bZIP23 regulate the adaptation to zinc deficiency. *Proceedings of the National Academy of Science*, 107, 10296–10301.

Assunção, A. G. L., Martins, P. D. A. C., Folter, S. D., Vooijs, R., Schat, H., & Aarts, M. G. M. (2001). Elevated expression of metal transporter genes in three accessions of the metal hyperaccumulator *Thlaspi caerulescens*. *Plant, Cell and Environment*, 3, 217–226.

Baker, A. J. M., & Brookes, R. R. (1989). Terrestrial higher plants which hyperaccumulate metallic elements , A review of their distribution, ecology and phytochemistry. *Biorecovery*, 1, 81–126.

Baker, A. J. M., McGrath, S. P., Reeves, R. D., & Smith, J. A. C. (2000). *Metal-hyperaccumulator plants: A review of the ecology and physiology of a biochemical resource for phytoremediation of metal-polluted soils*. Terry N, Banuelos G, Vangronsveld J (Ed.), Phytoremediation of contaminated soil and water. Boca Raton: Lewis Publishers, 85-107.

Barker, A. V., & Pilbeam, D. J. (2015). *Handbook of Plant Nutrition.* 2 (Ed.), Boca Raton: CRC Press, 1–26.

Barberon, M., Zelazny, E., Robert, S., Conéjéro, G., Curie, C., Friml, J., & Vert, G. (2011). Monoubiquitin-dependent endocytosis of the transporter controls iron uptake in plants. *Proceedings of the National Academy of Sciences*, 108, 450–458.

Becher, M., Talke, I. N., & Krämer, U. (2004). Cross-species microarray transcript profiling reveals high constitutive expression of metal homeostasis genes in shoots of the zinc hyperaccumulator *Arabidopsis halleri*. *The Plant Journal*, 37, 251–268.

Beckett, P. H. T., & Davis, R. D. (1977). Upper critical levels of toxic elements in plants. *The New Phytologist*, 79, 95–106.

Boyd, R. S., Davis, M. A., & Balkwill, K. (2008). Elemental patterns in Ni hyperaccumulating and non-hyperaccumulating ultramafic soil populations of *Senecio coronatus*. *South African Journal of Botany*, 74, 158–162.

Boyd, R. S., & Martens, S. N. (1998). The significance of metal hyperaccumulation for biotic interactions. *Chemocology*, 8, 1–7.

Brookes, R. R., & Wither, E. D. (1977). Nickel accumulation by *Rinorea bengalensis* . *Journal of Geochemical Exploration*, 7, 295–300.

Brooks, R. R., Chambers, M. F., Nicks, L. J., & Robinson, B. H. (1998). Phytomining. *Trends in Plant Science*, 3, 359–362.

Chiarucci, A., & Baker, A. J. M. (2007). Advances in the ecology of serpentine soils. *Plant and Soil*, 293, 1–2.

Chomczynski, P., & Mackey, K. (1995). Substitution of chloroform by bromochloropropane in the single-step method of RNA isolation. *Analytical Biochemistry*, 225, 163–164.

Courbot, M., Willems, G., Motte, P., Arvidsson, S., Roosens, N., Saumitou-Laprade, P., & Verbruggen, N. (2007). A major quantitative trait locus for cadmium tolerance in *Arabidopsis halleri* colocalizes with *HMA4*, a gene encoding a heavy metal ATPase. *Plant Physiology*, 144, 1052–1065.

Dellaporta, S. L., Wood, J., & Hicks, J. (1983) A plant DNA minipreparation, *Plant Molecular Biology Reporter*, 1, 19–21.

Eide, D., Broderius, M., Fett, J., & Guerinot, M. L. (1996). A novel iron- regulated metal transporter from plants identified by functional expression in yeast. *Proceedings of the National Academy of Sciences*, 93, 5624–5628.

Ellis, D. R., & Salt, D. E. (2003). Plants, selenium and human health. *Current Opinion in Plant Biology*, 6, 273–279.

Epstein, E. (1965). *Typical concentra sufficient for plant growth*. J. Bonner and J.E Varner (Ed.), Plant Biochemistry. London: Academic Press, 438–466.

Hall, J. L. (2002). Cellular mechanisms for heavy metal detoxification and tolerance. *Journal of Experimental Botany*, 53, 1–11.

Hanikenne, M., Talke, I. N., Haydon, M. J., Lanz, C., Nolte, A., Motte, P., Kroymann, J., Weigel, D., & Krämer, U. (2008). Evolution of metal hyperaccumulation required cis-regulatory changes and triplication of *HMA4*. *Nature*, 453, 391–395.

Haughn, G. W., Somerville, C. R (1987) *Selection for herbicide resistance at the whole plant level*. HM LeBaron, RO Mumma, RC Honeycutt, JH Duesing (Ed.), Applications of Biotechnology to Agricultural Chemistry. Washington DC: American Chemical Society, 98-108.

Hörger, A. C., Fones, H. N., & Preston, G. (2013). The current status of the elemental defense hypothesis in relation to pathogens. *Frontiers in Plant Science*, 4, 1–11.

Hussain, D., Haydon, M. J., Wang, Y., Wong, E., Sherson, S. M., Young, J., Camakaris, J., Harper, J. F., & Cobbett, C. S. (2004). P-type ATPase heavy metal transporters with roles in essential zinc homeostasis in *Arabidopsis*. *The Plant Cell*, 16, 1327–1339.

Ingle, R. A., Mugford, S. T., Rees, J. D., Malcolm, M., Campbell, M., & Smith, J. A. C. (2005). Constitutively high expression of the histidine biosynthetic pathway contributes to nickel tolerance in hyperaccumulator plants. *The Plant Cell*, 17, 2089–2106.

Korshunova, Y. O., Eide, D., Clark, W. G., Guerinot, M. L., & Pakrasi, H. B. (1999). The IRT1 protein from *Arabidopsis thaliana* is a metal transporter with a broad substrate range. *Plant Molecular Biology*, 40, 37–44.

Krämer, U. (2010). Metal hyperaccumulation in plants. *Annual Review of Plant Biology*, 61, 517–34.

Krämer, U., Cotter-Howells, J. D., Charnock, J. M., Baker, A. J. M., & Smith, J. A. C. (1996). Free histidine as a metal chelator in plants that accumulate nickel. *Nature*, 379, 635–679.

Ma, J. F., Ueno, D., Zhao, F. J., & McGrath, S. P. (2005). Subcellular localisation of Cd and Zn in the leaves of a Cd-hyperaccumulating ecotype of *Thlaspi caerulescens*. *Planta*, 220, 731–736.

Meier, S., Adams, N., Wolf, M., Balkwin, K., Muasya, M., Gehring, C., Ingle, R. (2017). RNA-Seq analysis of *Senecio coronatus* (Asteraceae) suggests that mis-regulation of iron uptake may underlie the evolution of nickel hyperaccumulation in this species. *New Phytologist*, manuscript in preparation.

Merlot, S., Hannibal, L., Martins, S., Martinelli, L., Amir, H., Lebrun, M., & Thomine, S. (2014). The metal transporter *PgIREG1* from the hyperaccumulator *Psychotria gabriellae* is a candidate gene for nickel tolerance and accumulation. *Journal of Experimental Botany*, 65, 1551–1564.

Mills, R. F., Francini, A., Ferreira Da Rocha, P. S. C., Baccarini, P. J., Aylett, M., Krijger, G. C., & Williams, L. E. (2005). The plant P1B-type ATPase *AtHMA4* transports Zn and Cd and plays a role in detoxification of transition metals supplied at elevated levels. *FEBS Letters*, 579, 783–791.

Mizuno, T., Usui, K., Horie, K., Nosaka, S., Mizuno, N., & Obata, H. (2005). Cloning of three *ZIP/NRAMP* transporter genes from a Ni hyperaccumulator plant *Thlaspi japonicum* and their Ni^{2+}-transport abilities. *Plant Physiology and Biochemistry*, 43, 793–801.

Morrey, D. R., Balkwill, K., & Balkwill, M. (1989). Studies on serpentine flora : Preliminary analyses of soils and vegetation associated with serpentinite rock formations in the south-eastern Transvaal. *South African Journal*

of Botany, 55, 171–177.

Morrissey, J., Baxter, I. R., Lee, J., Li, L., Lahner, B., Grotz, N., Kaplan, J., Salt, D., & Guerinot, M. L. (2009). The ferroportin metal efflux proteins function in iron and cobalt homeostasis in *Arabidopsis*. *The Plant Cell*, 21, 3326–3338.

Navari-Izzo, F., Pinzino, C., Quartacci, M. F., & Sgherri, C. L. M. (1999). Superoxide and hydroxyl radicai generation, and superoxide dismutase in PSII membrane fragments from wheat. *Free Radical Research*, 31, 3–9.

Navari-Izzo, F., Quartacci, M. F., Pinzino, C., Vecchia, F. D., & Sgherri, C. L. M. (1998). Thylakoid-bound and stromal antioxidative enzymes in wheat treated with excess copper. *Physiologia Plantarum*, 104, 630–638.

Nishida, S., Tsuzuki, C., Kato, A., Aisu, A., Yoshida, J., & Mizuno, T. (2011). *AtIRT1*, the primary iron uptake transporter in the root, mediates excess nickel accumulation in *Arabidopsis thaliana*. *Plant and Cell Physiology*, 52, 1433–1442.

Noret, N., Meerts, P., Vanhaelen, M., Dos Santos, A., & Escarré, J. (2007). Do metal-rich plants deter herbivores? A field test of the defence hypothesis. *Oecologia*, 152, 92–100.

Oomen, R. J. F. J., Wu, J., Lelièvre, F., Blanchet, S., Richaud, P., Barbier-Brygoo, H., Aarts, M. G. M., & Thomine, S. (2009). Functional characterization of NRAMP3 and *NRAMP4* from the metal hyperaccumulator *Thlaspi caerulescens*. *New Phytologist*, 181, 637–650.

Padmavathiamma, P. K., & Li, L. Y. (2007). Phytoremediation technology: Hyper-accumulation metals in plants. *Water, Air, and Soil Pollution*, 184, 105–126.

Pence, N. S., Larsen, P. B., Ebbs, S. D., Letham, D. L. D., Lasat, M. M., Garvin, D. F., Eide, D., & Kochian, L. V. (2000). The molecular physiology of heavy metal transport in the Zn/Cd hyperaccumulator *Thlaspi caerulescens*. *Proceedings of the National Academy of Sciences*, 97, 4956–4960.

Pollard, A. J., Reeves, R. D., & Baker, A. J. M. (2014). Facultative hyperaccumulation of heavy metals and metalloids. *Plant Science*, 217–218, 8–17.

Quartacci, M. F., Cosi, E., & Navari-Izzo, F. (2001). Lipids and NADPH-dependent superoxide production in plasma membrane vesicles from roots of wheat grown under copper deficiency or excess. *Journal of Experimental Botany*, 52, 77–84.

Rascio, N., & Navari-Izzo, F. (2011). Heavy metal hyperaccumulating plants : How and why do they do it ? And what makes them so interesting ? *Plant Science*, 180, 169–181.

Reeves, R. D., & Adıgüzel, N. (2004). Rare plants and nickel accumulators from Turkish serpentine soils, with special reference to *Centaurea* species. *Turkish Journal of Botany*, 28, 147–153.

Whitney, E., & Rolfes, S. R. (2007). *Understanding Nutrition* (11th ed.). Boston: Cengage Learning, 1–22.

Schaaf, G., Honsbein, A., Meda, A. R., Kirchner, S., Wipf, D., & von Wirén, N. (2006). *AtIREG2* encodes a tonoplast transport protein involved in iron-dependent nickel detoxification in *Arabidopsis thaliana* roots. *Journal of Biological Chemistry*, 281, 25532–25540.

Seregin, I. V., & Kozhevnikova, A. D. (2006). Physiological role of nickel and its toxic effects on higher plants. *Russian Journal of Plant Physiology*, 53, 257–277.

Talke, I. N., Hanikenne, M., & Krämer, U. (2006). Zinc-dependent global transcriptional control, transcriptional deregulation, and higher gene copy number for genes in metal homeostasis of the hyperaccumulator *Arabidopsis halleri*. *Plant Physiology*, 142, 148–167.

Tsonev, T., & Lidon, F. J. C. (2012). Zinc in plants - An overview. *Emirates Journal of Food and Agriculture*, 24, 322–333.

Vacchina, V., Mari, S., Czernic, P., Margués, L., Pianelli, K., Schaumloffel, D., Lebrun, M. & Lobinski, R. (2003). Speciation of nickel in a hyperaccumulating plant by high-performance liquid chromatography-inductively coupled plasma mass spectrometry and electrospray MS/MS assisted by cloning using yeast complementation. *Analytical Chemistry*, *75*, 2740–2745.

van der Mortel, J. E., & Aarts, M. G. M. (2006). Comparative transcriptomics – model species lead the way. *New Phytologist*, 170, 199–201.

Verbruggen, N., Hermans, C., & Schat, H. (2009). Molecular mechanisms of metal hyperaccumulation in plants. *New Phytologist*, 181, 759–776.

Vert, G., Grotz, N., Dédaldéchamp, F., Gaymard, F., Guerinot, M. L., Briat, J., & Curie, C. (2002). IRT1, an *Arabidopsis* transporter essential for iron uptake from the soil and for plant growth. *The Plant Cell*, 14, 1223–1233.

Weber, M., Harada, E., Vess, C., Roepenack-Lahaye, E. V., & Clemens, S. (2004). Comparative microarray analysis of *Arabidopsis thaliana* and *Arabidopsis halleri* roots identifies nicotianamine synthase, a ZIP transporter and other genes as potential metal hyperaccumulation factors. *The Plant Journal*, 37, 269–281.

Wei, W., Chai, T., Zhang, Y., Han, L., Xu, J., & Guan, Z. (2009). The *Thlaspi caerulescens NRAMP* homologue *TcNRAMP3* is capable of divalent cation transport. *Molecular Biotechnology*, 41, 15–21.

Xu, K., Huang, X., Wu, M., Wang, Y., Chang, Y., Liu, K., Zhang, J., Zhang, Y., Zhang, F., Liming, Y., TingTing, R., Tan, G., & Li, C. (2014). A rapid, highly efficient and economical method of *Agrobacterium*-mediated *in planta* transient transformation in living onion epidermis. *PLoS ONE*, 9, 1–7.

Zhang, L., Angle, J. S., & Chaney, R. L. (2007). Do high-nickel leaves shed by the nickel hyperaccumulator *Alyssum murale* inhibit seed germination of competing plants? *New Phytologist*, 173, 509–516.

Zhao, F. J., & McGrath, S. P. (2009). Biofortification and phytoremediation. *Current Opinion in Plant Biology*, 12, 373–380.

7. Appendix

Comments for pENTR1A no ccdB
2294 nucleotides

rrnB T1 transcription termination sequence: bases 106-149
rrnB T2 transcription termination sequence: bases 281-308
attL1:bases 358-457 (complementary strand)
multiple cloning site (MCS): bases 457-522
attL2:bases 522-622
Kanamycin resistance gene: bases 745-1554
pUC origin: bases 1619-2291

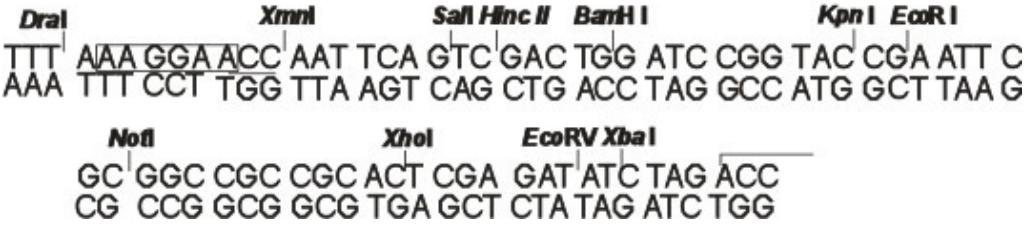

Supplementary Figure 1|**Vector map of the *pENTR1A* vector.** The *Not*I, *Bam*HI, *Eco*RI and *Sal*I sites used for digestion and cloning purposes are mapped.

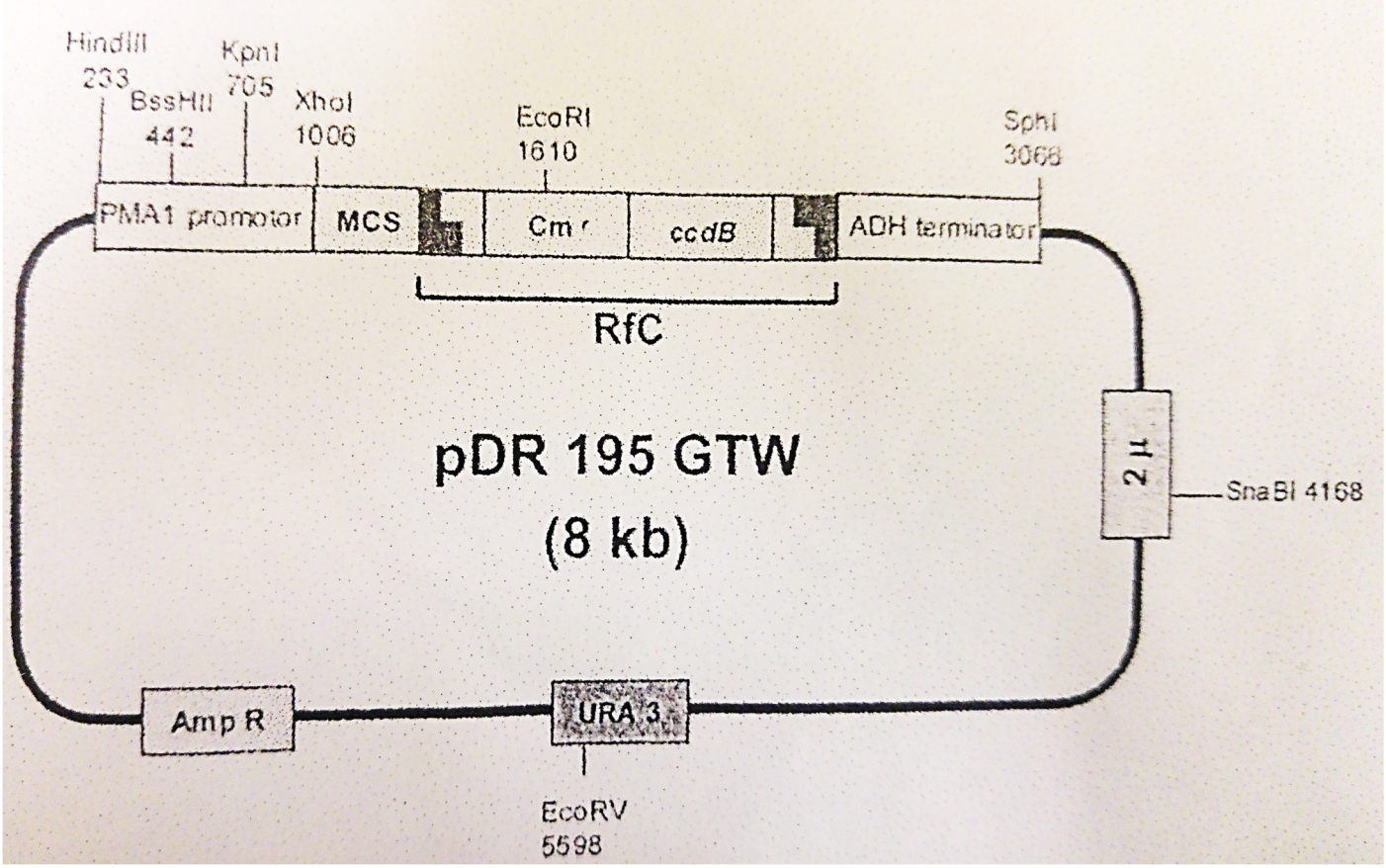

Supplementary Figure 2|**Vector map of the *pDR195 GTW* vector.** The destination vector used to express the genes of interest in yeast.

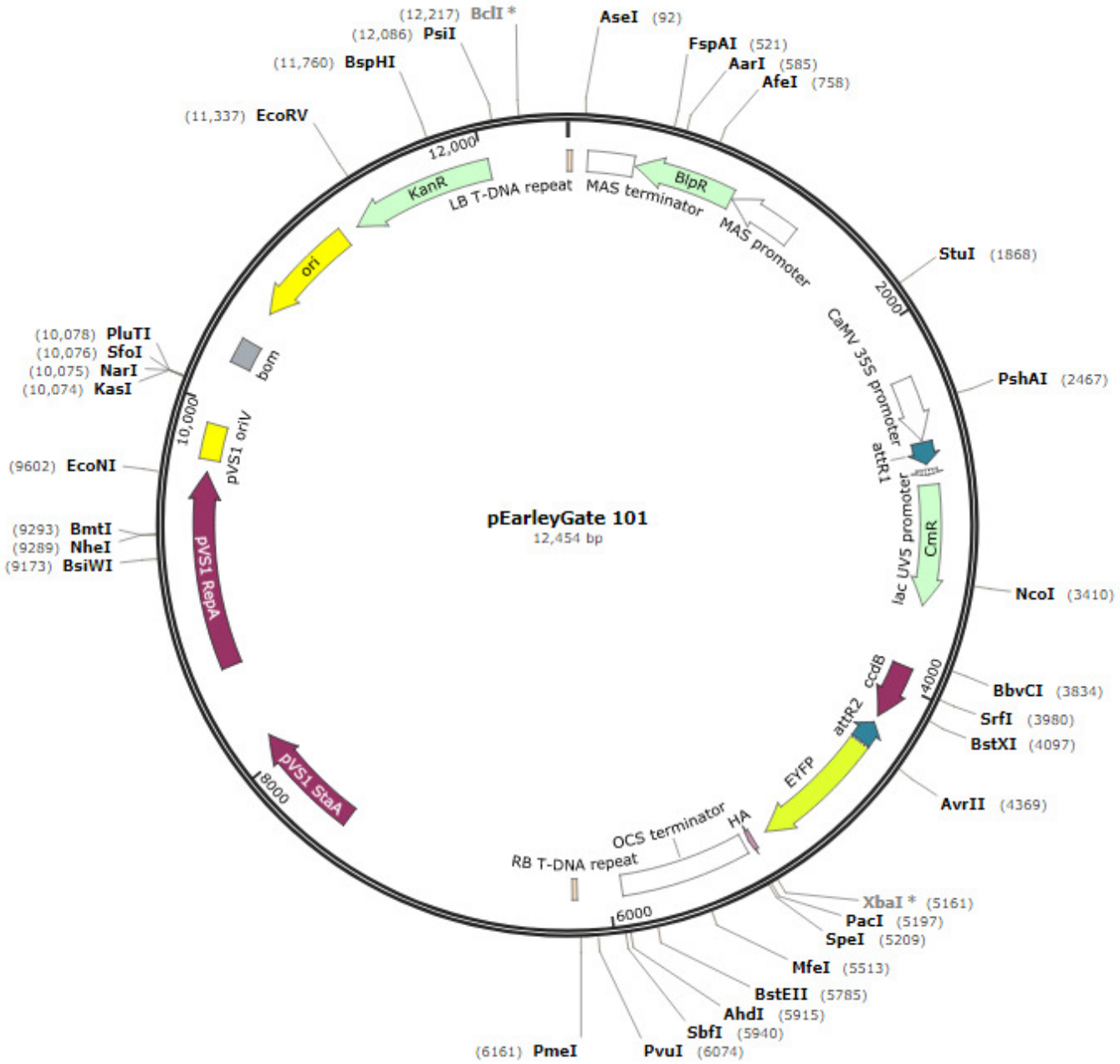

Supplementary Figure 3|**Vector map of the *pEarlyGate101* vector.** The *attR* sites used for gateway cloning purposes are mapped.